Lucchi, R.G., St. John, K.E.K., Ronge, T.A., and the Expedition 403 Scientists
Proceedings of the International Ocean Discovery Program Volume 403
publications.iodp.org

Expedition 403 summary[1]

K.E.K. St. John, R.G. Lucchi, T.A. Ronge, M.A. Barcena, S. De Schepper, L.C. Duxbury, A.C. Gebhardt, A. Gonzalez-Lanchas, G. Goss, N.M. Greco, J. Gruetzner, L. Haygood, K. Husum, M. Iizuka, A.K.I.U. Kapuge, A.R. Lam, O. Libman-Roshal, Y. Liu, L.R. Monito, B.T. Reilly, Y. Rosenthal, Y. Sakai, A.V. Sijinkumar, Y. Suganuma, and Y. Zhong[2]

[1] St. John, K.E.K., Lucchi, R.G., Ronge, T.A., Barcena, M.A., De Schepper, S., Duxbury, L.C., Gebhardt, A.C., Gonzalez-Lanchas, A., Goss, G., Greco, N.M., Gruetzner, J., Haygood, L., Husum, K., Iizuka, M., Kapuge, A.K.I.U., Lam, A.R., Libman-Roshal, O., Liu, Y., Monito, L.R., Reilly, B.T., Rosenthal, Y., Sakai, Y., Sijinkumar, A.V., Suganuma, Y., and Zhong, Y., 2026. Expedition 403 summary. In Lucchi, R.G., St. John, K.E.K., Ronge, T.A., and the Expedition 403 Scientists, Eastern Fram Strait Paleo-Archive. Proceedings of the International Ocean Discovery Program, 403: College Station, TX (International Ocean Discovery Program). https://doi.org/10.14379/iodp.proc.403.101.2026
[2] **Expedition 403 Scientists' affiliations.**

Contents

Keywords
International Ocean Discovery Program, IODP, Expedition 403, *JOIDES Resolution*, Eastern Fram Strait Paleo-Archive, Earth climate system, biosphere frontiers, carbon sequestration, Site U1618, Site U1619, Site U1620, Site U1621, Site U1622, Site U1623, Site U1624, Svalbard-Barents Sea Ice Sheet, North Atlantic Water, West Spitsbergen Current, gas hydrate, sediment drift, Isfjorden drift, Bellsund drift, Vestnesa Ridge, Svyatogor Ridge, mid-Pleistocene transition, mid-Brunhes transition, Last Glacial Maximum, shelf-edge glaciation, trough mouth fan, diamicton, sea ice, meltwater, Northern Hemisphere glaciation, Pleistocene, Late Miocene, Pliocene

Core descriptions

Supplementary material

References (RIS)

MS 403-101
Published 29 January 2026

Funded by NSF OCE1326927, ECORD, and JAMSTEC

Abstract

The North Atlantic and Arctic Oceans are unquestionably major players in the climatic evolution of the Northern Hemisphere and in the history of the Northern Hemisphere overturning circulation of the Atlantic Ocean. The establishment of the modern North Atlantic Water (NAW) transporting heat, salt, and moisture to the Northern Hemisphere has been indicated as one of the main forcing mechanisms for the onset of Northern Hemisphere glaciation. NAW controls the extent and dynamics of circum-Arctic and circum-North Atlantic ice sheets and sea ice in addition to deep water and brine production. How the ocean system and cryosphere worked during past warmer intervals of high insulation and/or high atmospheric CO_2 content is still largely unknown and debated. The required information can only be attained by offshore scientific drilling in high-resolution continuous expanded sedimentary sequences identified on the western continental margin of Svalbard and eastern side of the Fram Strait, along the main pathway and northern penetration of the NAW flowing into the Arctic Ocean. The area around Svalbard is very sensitive to climatic variability and can be considered a sentinel of climate change. Furthermore, the reconstruction of the dynamic history of the marine-based paleo-Svalbard–Barents Sea Ice Sheet is important because it is considered the best available analog to the modern, marine-based West Antarctic Ice Sheet, for which the loss of stability is presently the major uncertainty in projecting future global sea level rise in response to the present global climate warming.

Plain language summary

The Fram Strait is an important gateway for ocean currents to flow between the North Atlantic and Arctic Oceans. The northward-flowing current system plays critical roles in regional and global climate change because of the heat, salt, and moisture it brings to the Arctic region, which influence the formation and melting of ice sheets and sea ice, as well as the overturning circulation of the ocean itself. Thick deposits of ocean sediments (sediment drifts) have accumulated over millions of years under the effect of the warm current flowing along the seafloor in the eastern Fram Strait. Shaped by the bottom current and fed by the input of marine biological activity and sediments delivered by advancing and retreating glaciers on the nearby continental margin, sediment drifts contain the record of the past (paleo) oceanographic and climatic changes that occurred over millions of years. The dynamic history of ocean-ice interactions during global climate transitions, such as the onset of Northern Hemisphere glaciation, and past periods of rapid warming and higher CO_2 levels than today, can be reconstructed from the detailed record contained in these sediment drifts. These paleoclimate data are valuable for groundtruthing climate models of projected future CO_2, temperature, and ice sheet stability.

1. Introduction

The Arctic and North Atlantic Oceans are unquestionably major players in the climatic evolution of the Northern Hemisphere (e.g., Overland et al., 2011, Mahajan et al., 2011). Many uncertainties remain about the establishment, evolution, and role of the northern North Atlantic–Arctic Ocean circulation in relation to the opening of the Fram Strait and its impact on Earth's global climate during the major climatic transitions that occurred since the Late Miocene. Further, the linkage among changes in insolation, atmospheric CO_2 levels, ocean dynamics, and the cryosphere in the past and in the future remains unclear. A present major concern is the impact that meltwater release from Greenland and Antarctic ice sheets under the ongoing global climate warming will have at regional to global scales. The Arctic is currently experiencing temperature changes that are two to four times faster than the global average (Stocker et al., 2013; Rantanen et al., 2022). Numerical simulations of past and current Greenland ice sheet melting have indicated the meltwaters' potential to slow the Atlantic Meridional Overturning Circulation (AMOC) (Rahmstorf et al., 2015; Turney et al., 2020). The weakening of the AMOC was shown to induce a bipolar seesaw by transferring the heat to southern high latitudes, accelerating the demise of the West Antarctic Ice Sheet (WAIS) during the last interglacial (Turney et al., 2020). Antarctic ice sheet melting could then cause a cooling and a drying in the Northern Hemisphere high latitudes due to a reduction of Antarctic Bottom Water formation as one of major drivers of the AMOC (Golledge et al., 2019). Reconstructing the dynamic history of ocean and ice sheet interactions along the western margin of Svalbard and eastern side of the Fram Strait at the gateway to the Arctic is key to understanding the linkage among insolation, atmospheric CO_2 concentration, ocean circulation, and ice sheet dynamics.

International Ocean Discovery Program (IODP) Expedition 403 (Figure **F1**) was motivated by the necessity of retrieving continuous, high-resolution, and datable depositional sequences containing

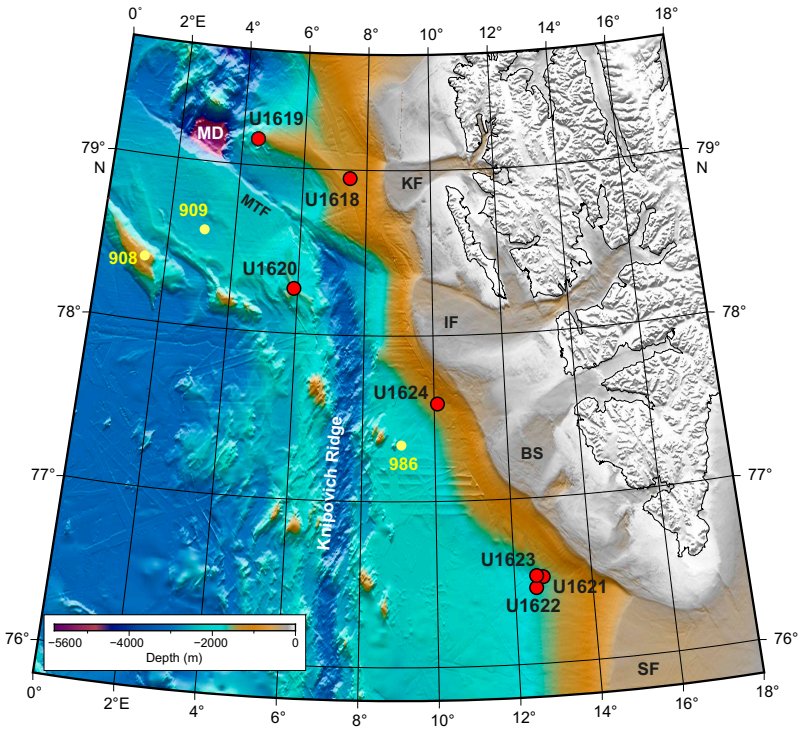

Figure F1. Bathymetric map showing the locations of Expedition 403 sites. Sites U1618 and U1619 are on the eastern and western terminations of the Vestnesa Ridge, respectively; Site U1620 is on the Svyatogor Ridge; Sites U1621 and U1623 are on the Bellsund drift; Site U1622 is on the deeper area of the Storfjorden TMF; and Site U1624 is on the Isfjorden drift. Locations of the Konsfjorden (KF), Isfjorden (IF), Bellsund (BS), and Storfjorden (SF) glacial troughs are shown along the western margin of Svalbard. The Molloy Transform Fault (MTF) is parallel to and south of the Vestnesa Ridge and connects the ultraslow-spreading Knipovich Ridge to the Molloy Ridge. MD = Molloy Deep. Previously drilled ODP Site 909 is located on an abyssal hill south of the MTF, ODP Site 908 on the Hovgaard Ridge, and ODP Site 986 between the Knipovich Ridge and the Svalbard margin.

the record of the paleoceanographic characteristics and cryosphere evolution during past key climatic transitions that followed the opening of the Fram Strait. Such data are greatly needed to generate a frame of information to better constrain global climate connections, forcing mechanisms, and climate models.

2. Background

2.1. Modern oceanography and climate

The Fram Strait is the only deepwater (~2600 m) passage between the Arctic and the subpolar oceans, and it is crossed by two opposite oceanic currents (Figure **F2**). North Atlantic Water (NAW) flows into the Arctic via the West Spitsbergen Current (WSC), which is the northernmost branch of the North Atlantic Current, delivering heat, salt, and moisture to the Arctic Ocean (Teigen et al., 2010; Agarwal and Worster, 2021). The heat from the WSC is the primary control on air temperature over Svalbard and is the primary control enabling nearly sea ice–free conditions in the winter months in the eastern Fram Strait and western Svalbard margin. In contrast, cold, low-salinity water masses are brought southward along the western side of the Fram Strait by the East Greenland Current (EGC), which is responsible for the sea ice coverage along East Greenland and contributes to the stability of the Greenland Ice Sheet.

The WSC is a bathymetrically controlled boundary current that hugs the continental slope of western Svalbard, flowing at an average rate of 30 cm/s approximately along the 1000 m isobath (Beszczynska-Möller et al., 2012; Bensi et al., 2019). The current transports to the north both NAW, which is a subsurface water mass located between 300–400 and 800–1000 m water depth, and the Norwegian Sea Deep Water (NSDW), located below 1200 m water depth. The NAW is a saline (~35.5 psu; Norwegian Polar Institute, 2022) and warm water mass, 2°–6°C in the summer and 2°–4°C in the winter (von Appen et al., 2016; Beszczynska-Möller et al., 2012). It is estimated that the shallow core of the WSC composed of NAW loses ~300 W/m^2 in the summer and 1000 W/m^2 in the winter, having a strong impact on the Arctic Ocean heat balance (Saloranta and Haugan, 2004). In addition to seasonal differences in temperature and heat loss, the WSC also exhibits seasonal cycles of stratification, velocity, and stability. Wintertime cooling and stronger winds lead to weaker stratification (greater convection), stronger flow (at times overshooting 40 cm/s in the shallow area; Bensi et al., 2019), and more vertical shear. These factors create more instability in the current and increase the formation of eddies, as compared to summer conditions (von Appen et al., 2016; Hattermann et al., 2016).

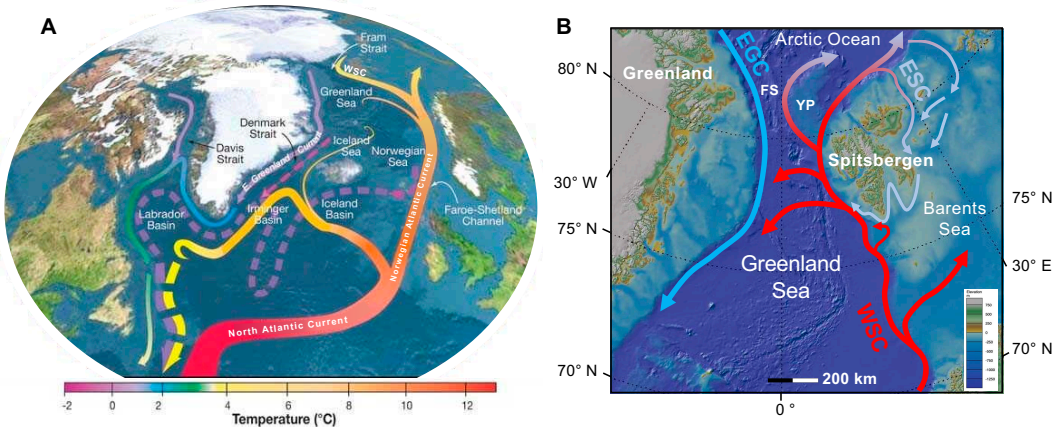

Figure F2. Modern oceanographic configuration of the North Atlantic Ocean. A. Schematic circulation of surface currents (solid curves) and deep currents (dashed curves) that form a portion of the AMOC. The North Atlantic Current, transporting warm and salty NAW, derives from the Caribbean Gulf Stream; its name changes along the European coasts and becomes the WSC at the northernmost tip flanking the western margin of Spitsbergen. Modified after Curry (2010) (permission for use via Creative Common 3.0). B. Details of northernmost Atlantic Ocean current configuration. ESC = East Spitsbergen Current, YP = Yermak Plateau, FS = Fram Strait (Bathymetry IBCAO v. 3; Jakobsson et al., 2012).

The colder (less than –0.9°C) and slightly less saline (~34.91 psu; Norwegian Polar Institute, 2022) NSDW fills the deep marine environment below 1200 m water depth underlying the NAW (Aagaard et al., 1985; Rudels et al., 2000; Langehaug and Falck, 2012). At this depth, the WSC is slower (5–10 cm/s; Bensi et al., 2019) but still steering northward. Although the high-energy shallow core of WSC causes erosion of the upper slope and outer part of the shelf, the slower, deeper core moving within the NSDW allows for greater deposition, contributing to the growth of sediment drifts along the seabed (Figure **F3**). Source water for the NSDW comes from the mixing of Greenland Sea Deep Water and Eurasian Basin Deep Water in the Fram Strait (Bensi et al., 2019) and is modified locally by turbulent mixing along the Barents Sea slope (Swift and Koltermann, 1988).

The proximity of the WSC to the continental shelf of western Svalbard sets up additional interactions that modify physical properties of the water as well as nutrient availability. Cold freshwater from the Svalbard coast and fjords that mix with the warmer, salty NAW contribute to cooling and freshening of the WSC as it flows north (Koenig et al., 2018). Dense water formation from heat loss to the atmosphere, sea ice formation, and related brine rejection can overflow the shelf edge (Quadfasel et al., 1988, 1992; Schauer, 1995; Bensi et al., 2019). Some of this overflow includes sediment-rich gravity plumes (sensu Fohrmann et al., 1998), which cascades downslope, transporting terrigenous sediment, oxygen, and nutrients offshore. Conversely, WSC warm waters can intrude into the shelf waters and in fjords (some at a 200–400 m water depth; Nilsen et al., 2016). The shoreward propagation of Atlantic waters from the WSC occurs both from wind-driven upwelling and from seasonal storms (Koenig et al., 2018). The addition of oceanic heat can increase the melt rate of ocean-terminated glaciers (especially ice shelves) and has been identified as a contributing mechanism leading to accelerating ice flow, thinning, and retreat (Nilsen et al., 2016, and references therein).

Decades of oceanographic monitoring indicate that core temperatures of the WSC are rising. For example, the decadal average temperatures of the WSC between 20 and 200 m water depth rose from 4.4°C in 1963 to 5.3°C in 2021 at monitoring stations at ~79°N (Norwegian Polar Institute, 2022). The influx of warm North Atlantic waters to the Arctic via the WSC flow through the Fram Strait is a primary contributor to modern Arctic sea ice loss. This process, known as "Atlantification" of the Nordic Seas and Arctic (Årthun et al., 2012; Tsubouchi et al., 2018; Tesi et al., 2021; Gamboa Sojo et al., 2024), in turn, furthers heat transfer from the ocean to the atmosphere, as well as reduces regional albedo, resulting in disproportionate air and surface warming of the Arctic region ("Arctic amplification"), such that the Arctic has warmed two to four times faster than the global average since 1979 (Rantanen et al., 2022) and may be transitioning to a new climate state.

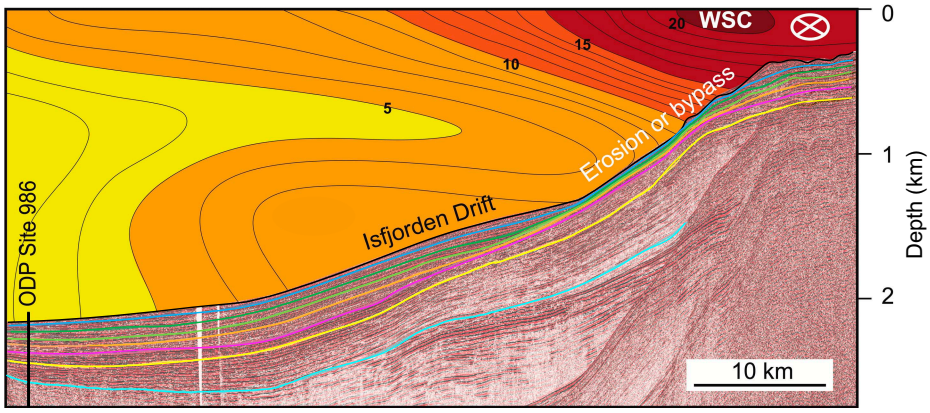

Figure F3. Seismic profile across Isfjorden drift (Figure F1) plotted below the WSC velocity (cm/s) pattern (modified after Rebesco et al., 2013). The velocity profile of WSC presents two cores: a strong shallow core of WSC transporting warm NAW (30–40 cm/s) causes sediment erosion and/or bypass in the upper continental slope and shelf, whereas a low-velocity deep core (~1500 m water depth; 5–10 cm/s) transporting NSDW promotes deposition with growth of the Isfjorden drift. White cross (arrow's tail) = WSC northward-flowing direction.

As the WSC flows north of Svalbard, it splits into two main currents (Figure **F2**). One branch (the North Spitsbergen Current) flows northeast along the Eurasian continental margin, where it divides into a returning current following the eastern and southern margin of Spitsbergen (East Spitsbergen Current; Figure **F2**), and a branch that moves along the north Eurasian margin, ultimately contributing to the counterclockwise current system that encircles the entire Arctic basin and returns to the North Atlantic Ocean via the EGC. The other branch (the Yermak Slope Current) flows more directly north at intermediate depths along the western margin of the Yermak Plateau, transporting relatively warm North Atlantic waters into the central Arctic Ocean interior.

Additionally, branches of the WSC recirculate west within the Fram Strait (Figure **F2**) (Bourke et al., 1988; Carmack et al., 2015). It is estimated that approximately half of the North Atlantic Waters transported in the WSC recirculate westward between 76° and 81°N (Marnela et al., 2013), feeding the southward flowing EGC and thereby ultimately contributing to the AMOC (Hattermann et al., 2016, and references therein). However, changes in the proportion transported north to the Arctic or west (recirculating) are influenced by seasonal climatic and hydrographic cycles (von Appen et al., 2016), as well as longer term regional and global changes, such as the dynamics of the North Atlantic Oscillation (Weijer et al., 2022), weakening of the Atlantic subpolar gyre associated with freshening of waters south of Greenland (Tesi et al., 2021), and anthropogenic global warming. Thus, the WSC is part of a complex oceanographic system that influences and is influenced by atmospheric, sea ice, and shelf water interactions; its connections to regional gyres; and global ocean thermohaline circulation. Therefore, it is important to understand the behavior of the WSC under a range of climate states, transitions, and timescales.

2.2. Geologic setting

The timing and modality of the opening of the Fram Strait are still largely debated (e.g., Thiede and Myhre, 1996; Jokat et al., 2008; Knies and Gaina, 2008; Backman and Moran, 2009; Poirier and Hillaire-Marcel, 2011; Ehlers and Jokat, 2013). Strike-slip movement and oblique ultraslow spreading in this region linked the active ocean ridge systems in the Norwegian-Greenland Sea (to the south) and the Arctic Eurasian Basin (to the north) (Gruetzner et al., 2022). The continental areas were separated by the Early Miocene, but subsidence histories of different parts of the strait are poorly known. However, much evidence indicates a deep ocean circulation was established between the Norwegian-Greenland Sea and the Arctic Ocean since about 6 Ma, during the Late Miocene (Jakobsson et al., 2007; Mattingsdal et al., 2014; Knies et al., 2014; Stärz et al., 2017).

The bathymetry of the eastern Fram Strait is related to its tectonic history as well as its depositional history. Eiken and Hinz (1993) describe several bathymetric regions in this area, three of which are most relevant to the Expedition 403 sites (Figure **F1**):

- The region north of the Molloy Transform Fault (MTF) between the active spreading Molloy Ridge and the western Svalbard continental slope. The northernmost Expedition 403 Sites U1618 and U1619 are in this region at the east and west terminations of an elongate sediment drift deposit (Vestnesa Ridge) that overlies relatively young oceanic crust (<19 Ma).
- The region south of the MTF between the Hovgaard Ridge and the northernmost extension of the Knipovich Ridge. The Hovgaard Ridge is an aseismic (i.e., nonspreading) ridge of uncertain origin (Myhre et al., 1982; Engen et al., 2008; Gruetzner et al., 2022). Ocean Drilling Program (ODP) Leg 151 Site 908 is located on that ridge, and Site 909 is in the Molloy Basin just north of it. Expedition 403 Site U1620 is located on a sediment drift deposit (Svyatogor Ridge) that extends off the western flank of the Knipovich Ridge and overlies very young (<10 Ma) oceanic crust.
- The region between the active spreading Knipovich Ridge and the western Svalbard continental slope. ODP Site 986 (Leg 162) and the southernmost Expedition 403 sites are in this region. The Expedition 403 Sites U1621–U1624 are situated on plastered sediment drifts deposited along the continental slope (Bellsund and Isfjorden drifts) or on the deeper portion of the Storfjorden trough mouth fan (TMF) (Site U1622).

The depositional history along the eastern Fram Strait is influenced by changes in strength of the WSC, as well as the onshore geology, including postbreakup regional tectonic uplift, and the dy-

namics of the paleo-SBSIS complex. The archipelago of Svalbard is the northwest emergent part of the Barents Sea shelf. Western Svalbard is a mountainous terrain of faulted and folded Devonian to Paleogene sedimentary units partially overlying older crystalline basement rocks. Additionally, Quaternary volcanic units occur in the northwest. Western Svalbard experienced multiple episodes of uplift and erosion that occurred both pre- and postrifting (Lasabuda et al., 2021; Patton et al., 2024). Uplift events are associated with a range of tectonic (e.g., rift flank uplift, crustal flexure, and transpressive movement), mantle, and glacio-isostatic processes (Auriac et al., 2016; Minakov, 2018; Lasabuda et al., 2021). The creation of elevated topography may have been one of the necessary preconditions for glaciation at the Miocene–Pliocene transition and for the growth of ice sheets in Svalbard and across the broader Barents Sea shelf in the Late Pliocene and Pleistocene (Knies et al., 2014; Gruetzner et al., 2022).

The Barents Sea covers one of Earth's most extensive continental shelves. It is characterized by a complex morphology of shallow banks (50–100 m water depth) and deep troughs (200–400 m water depth) cutting across the shelf (Nilsen et al., 2016), and it was shaped by multiple advancements and retreats of the paleo-SBSIS in the Pliocene–Pleistocene (Alexandropoulou et al., 2021). Similar to the Antarctic margins, the ice sheet basal ablation and ice mass weight caused deepening of the substrate and differential isostatic subsidence generating retrograde profiles along the main glacial troughs (e.g., Bear Island and Storfjorden Troughs). In the Pleistocene, the paleo-SBSIS complex became marine based (Laberg et al., 2010; Alexandropoulou et al., 2021; Patton et al., 2022; Zieba et al., 2017), and this change potentially subjected the paleo-SBSIS to marine ice sheet instabilities under warm oceanic conditions as outlined by Petrini et al. (2018, 2020) and Sejrup et al (2022). To these extents, the paleomarine-based SBSIS can be considered the best analog to the modern marine-based WAIS, for which the loss of stability is a major concern for future global sea level projections in response to the present global warming (Joughin and Alley, 2011; Jordan et al., 2023; Naughten et al., 2023). The record of the paleo-SBSIS is more easily accessible compared to Antarctica, making it an important laboratory to further investigate the effects of ice-atmosphere-ocean interactions under fast warm climatic oscillations, as well as the Late Miocene and Pliocene–Quaternary transitions that remain poorly constrained.

Recent bathymetric analysis of submarine glacial landforms in the Norwegian Sea provides further evidence that Nordic paleo–ice sheet records can inform scientific understanding about modern WAIS processes and future risks. Batchelor et al. (2023) identified submarine grounding lines along the mid-Norwegian shelf that indicate rapid (55–610 m/day) buoyancy-driven ice sheet retreat during the Late Pleistocene deglaciation. These values exceed previously reported rates of glacial retreat from modern (satellite) and paleo (marine-geologic) records and suggest the possibility for rapid retreat of currently vulnerable glaciers, including those of the WAIS.

2.3. Depositional setting and processes

The sedimentary records that are the focus of Expedition 403 are contained within the contourite drifts that were built and shaped by the WSC flowing along the western margin of Svalbard and eastern side of the Fram Strait into the Arctic Ocean (Figures **F3**, **F4**). Contourite drifts are mounded depocenters generated by persistent (over My) bottom water currents that transport and deposit sediments delivered to the marine depositional system through other processes such as marine biological activity, downslope moving turbidity currents, and glaciogenic processes. They cover large areas of the European North Atlantic margin, including the Norwegian Sea, Barents Sea, western Svalbard, and the eastern side of the Fram Strait (Laberg et al., 2005). Their development has been related to tectonically influenced intensification of the paleocirculation system transporting warm NAW to the North Atlantic and the Arctic Ocean. These influences include the closing of the Central American Seaway in the Pliocene (Coates and Obando, 1996; O'Dea et al., 2016), the subsidence of the Greenland-Scotland Ridge during the Middle Miocene (Bohrmann et al., 1990; Wright, 1998), the opening of the Fram Strait between the Late Eocene and Late Miocene, and the activation of the deep oceanic circulation sometime during the Late Miocene (e.g., Jakobsson et al., 2007; Jokat et al., 2008; Knies and Gaina, 2008; Zachos et al., 2008; Geissler et al., 2011; Thompson et al., 2012; Hegewald and Jokat, 2013; Stärz et al., 2017; Stevenson et al., 2015; Tripati and Darby, 2018).

During times of glacial ice expansion and retreat, terrigenous sediment has been delivered to the western Svalbard continental slope through two main glaciogenic processes (Figure **F4**): (1) gravity mass transport deposition during shelf edge glaciations, forming several tens of meters thick deposits of highly consolidated glaciogenic diamicton (upper slope) and normally consolidated glaciogenic debris flows (middle and low slope) (Solheim et al., 1996; Vorren and Laberg, 1997; Butt et al., 2000; Vanneste et al., 2007; Lucchi et al., 2012, 2013), and (2) sediment-laden meltwater plumes associated with ice sheet melting and retreat during glacial terminations and responsible for the deposition of plumites (sensu Hesse et al., 1997), which have an aerial distribution confined within a few tens of kilometers from the source area (Lucchi et al., 2002, 2013; Shackleton et al., 2020). The thickness of plumites can vary from a few centimeters to several meters in the area proximal to the efflux point. Ice-rafted debris (IRD) can be associated with meltwater deposition (ice sheet decay) and with a highly dynamic growing ice sheet (high calving rates). All these sediment types provide direct information on the ice sheet dynamics that is complementary to the paleoceanographic information and contribute to the reconstruction of the climate history of the area.

During warm interglacials, the sedimentation is dominated by bottom currents (Figure **F4**), generating condensed sequences in the upper slope where the current speed is higher and expanded sequences in the lower slope where drifts of fine-grained and strongly bioturbated sediments build. Presently, and possibly during past interglacials, sediment input from nearshore settings is delivered by downslope cascading of brine-enriched shelf water (BSW), which forms during winter through persistent freezing and brine rejection (Quadfasel et al., 1988; Schauer, 1995; Skogseth et al., 2005). Dense BSW, moving across the shelf, resuspends seafloor sediments that are trans-

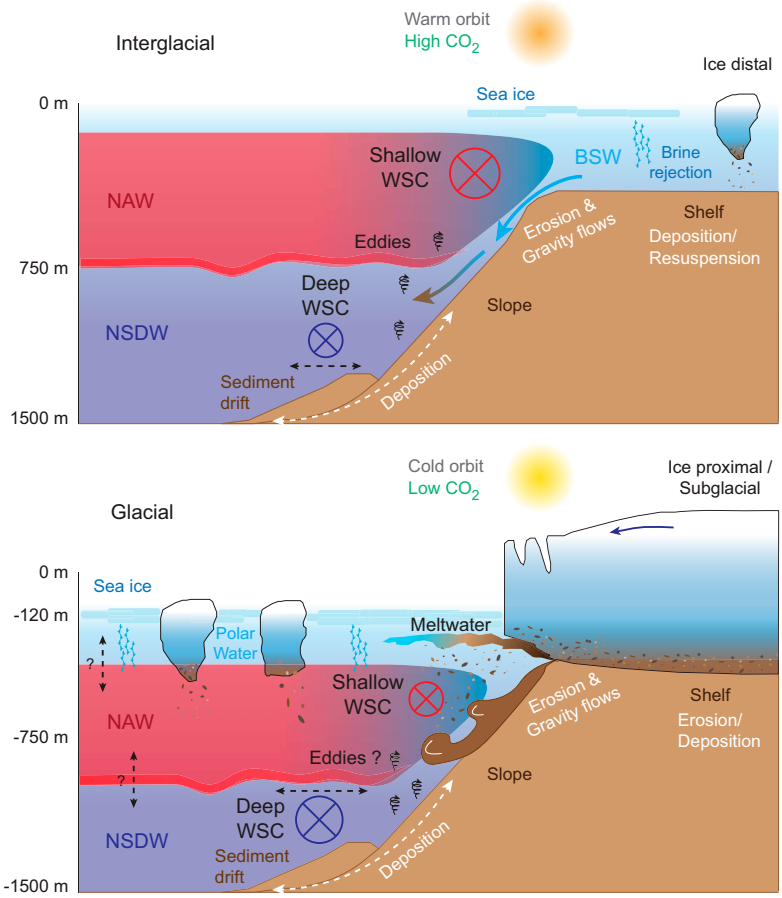

Figure F4. Schematic cross-section views of depositional processes that contribute sediment to contourite depositional system during different climate regimes. Shallow and deep cores of the WSC change depth and strength between glacial and interglacial stages. Crossed circles (arrow's tails) = northward-flowing WSC.

ported to the shelf break and delivered to the deeper environments entering the NSDW and transported northward or deposited in sediment drifts. This process is thought to be the present principal mechanism responsible for initiation of slope convection not only in the Arctic Ocean but all the Arctic areas, including the western margin of Svalbard, contributing significantly to the overall heat and salt balance of the deep Arctic Ocean basins and thus providing ventilation to the deeper environments (Fer et al., 2003; Schauer et al., 2004).

Given these sediment input processes, contourites provide records of marine biogenic and terrestrial/cryospheric variability through time, as well as changes in current intensity. Contourite drifts on the slope close to the outlet troughs of marine-based ice sheets can contain detailed information on ice sheet dynamics through time. Additionally, contourite drifts that develop on the slope between TMF systems can be especially useful for paleoceanographic reconstructions, as these interfan-slope depocenters are mainly under the influence of along-slope currents and hemipelagic deposition but are less directly in the path of debris flows. These settings are characterized by relatively high and continuous accumulation rates. Additionally, because of the continuous supply of oxygen and nutrients through bottom currents, these areas are suitable environments to support the benthic biological community. The high sedimentation rates also result in fast burial of the biological remains, promoting their preservation (Laberg and Vorren, 2004; Knutz, 2008; Rørvik et al., 2010; Rebesco et al., 2014a). The depositional sequences of the contourite drifts that developed along the western margin of Svalbard and eastern side of the Fram Strait, therefore, represented the best location to recover a high resolution high-resolution, mostly continuous sedimentary record since the Late Miocene (Eiken and Hinz, 1993; Howe et al., 2008; Rebesco et al., 2013; Waghorn et al., 2018), with regionally consistent paleoceanographic and paleoclimatic records at least since 1.6–1.3 Ma (Butt et al., 2000; Rebesco et al., 2014b).

2.4. Paleoceanographic and paleoclimatic context

The establishment of the modern NAW circulation has been indicated as one of the main forcing mechanisms for the Late Pliocene–Pleistocene onset of the Northern Hemisphere glaciation (NHG) (Haug et al., 2005; Schmidt, 2007; Lunt et al., 2008), notwithstanding the warming effects of the Middle–Late Pliocene high concentration of atmospheric CO_2. The NAW flux and properties (salinity and temperature) exerted a strong control on the extent and dynamics of circum-Arctic and circum-North Atlantic ice sheets, sea ice formation and distribution, modulating brine production, deep water mass characteristics, and hence climate.

Expedition 403 was designed to target the continuous and expanded (>300 m/My) paleoceanographic records preserved in the contourite drifts developed on the western margin of Svalbard and eastern side of the Fram Strait (Bellsund and Isfjorden drifts and Svyatogor and Vestnesa Ridges; Figure **F1**) since the onset of the NAW circulation in the northern Atlantic and Arctic Ocean (Howe et al., 2008; Rebesco et al., 2013; Waghorn et al., 2018). The regional record of the following key paleoclimatic transitions and events are expected to be present in the Expedition 403 cored sedimentary sequence.

2.4.1. Late Miocene–Early Pliocene transition

The Late Miocene–Early Pliocene transition (7–3.6 Ma; Holbourn et al., 2018) spanned the transition between the Late Miocene cooling (LMC; 7–5.5 Ma) and the Early Pliocene (5.5–3.6 Ma), characterized by temperatures warmer than today. The LMC was the end period of a gradual temperature decrease that initiated at around 13 Ma, after the Middle Miocene Climatic Optimum (17–14.8 Ma). The LMC was characterized by a substantial drop in atmospheric CO_2 (≤300 ppm; Zhang et al., 2013; Mejía et al., 2017). Proxy-based global sea surface temperature reconstructions showed that a sustained cooling occurred synchronously in both hemispheres, culminating with ocean surface temperatures dipping to near-modern values and a steepening of the pole-to-equator gradient between about 7 and 5.4 Ma (Herbert et al., 2016). The period of maximum cooling coincides with evidence for transient glaciations in southern Greenland (Wolf and Thiede, 1991; Jansen and Sjøholm, 1991; Larsen et al., 1994; Wolf-Welling et al., 1995; Bierman et al., 2016; St. John and Krissek, 2002), the Arctic (St. John, 2008), and southern Alaska (Krissek, 1995). The Early Pliocene period is instead characterized by an increase in atmospheric CO_2 (>400 ppm; Seki et al., 2010), a global mean temperature 2°–3°C higher relative to present with a culmi-

nating warmth at around 4.4 Ma (Fedorov et al., 2013), and a weaker meridional temperature gradient compared to present (Ford et al., 2015). Episodic seasonal Arctic sea ice was found through the Late Miocene (Stein et al., 2016) and was also recorded during the Early Pliocene on the Yermak Plateau at ~4.5 Ma with a substantial expansion observed from ~4 Ma (Clotten et al., 2019). A hypothesis relates this ice expansion to an increased northward transport of heat and moisture to the North Atlantic, likely leading to a fresher Arctic Ocean favoring sea ice formation (Clotten et al., 2019). The paucity of field information on this transition hampered the constraint of the possible forcing mechanisms.

2.4.2. Mid-Pliocene warm period

Many scientists look at the mid-Pliocene warm period (mPWP) (3.3–3.0 Ma) as the best analog to modern climatic conditions, and studying it can give important information to predict future scenarios. The Pliocene was characterized by a progressive rise of atmospheric CO_2 (>450 ppm) and temperatures, with values compatible with modern ones at about 4 Ma. This trend was suddenly interrupted at the beginning of the mPWP by a short cold period: the M2 glaciation (3.312–3.264 Ma) (Lisiecki and Raymo, 2005), which is of particular interest because of its short duration (50 ky only) compared to the Pleistocene glaciations, its global character (20–60 m of global sea level drop), and its sharp termination (De Schepper et al., 2014) with a particularly intense interglacial (Warm Isotopic Stage KM5c) reaching temperature comparable to present day in a similar-to-present orbital context (Haywood et al., 2016). It is not yet understood what triggered the M2 glaciation (e.g., Tan et al., 2017) and what caused the following KM5c warm conditions; however, such climatic events appear approximately coeval with transitory tectonic shallowing and deepening of the Central American Seaway preceding its final close (Schmidt, 2007).

The final closure of the Central American Seaway with the formation of the Panama Isthmus at ~2.8 Ma (Coates and Obando, 1996; Burton et al., 1997; O'Dea et al., 2016) is postulated for the onset of the modern NAW configuration, and intensification of NHG occurred since ~2.7 Ma. This also marks the first large-scale glaciation of western Svalbard (~2.7 Ma) prograding onto the southernmost Yermak Plateau (Mattingsdal et al., 2014). Uncertainties remain about the timing of the Central American Seaway closure (Montes et al., 2015; Bacon et al., 2015), and numerical studies estimated that the heat provided by the strengthening of the NAW hindered hemispheric glaciations (e.g., Haug et al., 2005; Schmidt, 2007; Lunt et al., 2008; Tan et al., 2017), leaving the identification of possible forcing mechanisms still unsolved.

2.4.3. Onset of shelf edge glaciations, mid-Pleistocene transition, mid-Brunhes event, and millennial-scale oscillations

Although based on poor age control, the paleo-SBSIS is interpreted to have reached the shelf break at different ages along the western Barents Sea/Svalbard margin. According to Alexandropoulou et al. (2021), an early, transient phase of shelf edge glaciation occurred soon after 2.58 Ma and a second phase occurred between 1.95 and 1.78 Ma. Widespread shelf edge glaciation started at only ~1.5 Ma, reaching the shelf edge at the mouth of Bjørnøyrenna (Andreassen et al., 2007) and subsequently (~1.2 Ma) on the Storfjorden/southern Spitsbergen margin (Rebesco et al., 2014b). The reasons for such diachronic onset, prograding from south to north under similar forcing mechanisms (Forsberg et al., 1999; Butt et al., 2000; Knies et al., 2009; Rebesco et al., 2014b), is still unclear.

There is a general lack of consensus on the forcing mechanisms to explain the mid-Pleistocene transition (MPT) (1.2–0.7 Ma; Pisias and Moore, 1981), also known in the literature as the "100,000-year problem" (Shackleton, 2000; Raymo and Nisancioglu, 2003; Clark et al., 2006; Rial et al., 2013; Nyman and Ditlevsen, 2019). Recent studies indicated the interplay between atmospheric CO_2 concentration, orbital forcing, ocean circulation, and ice sheet dynamics to explain the shifts in glacial cyclicity from ~41 to 100 ka during the Middle Pleistocene (Holbourn et al., 2013; Levy et al., 2019), but robust constraints and definition of the main forcing mechanism are still missing.

The causes of the mid-Brunhes event (MBE) (~400 ka), which marked the transition from cooler to warmer interglacials (Tzedakis et al., 2009; Cronin et al., 2017) characterized by larger amplitude stable oxygen isotope and CO_2 cycles, with CO_2 overshooting 300 ppm (Tzedakis et al., 2009),

and marked sea level highstands sometimes above present-day global mean sea level (e.g., Dutton et al., 2015), remain largely unclear.

The millennial-scale isotopic oscillations that occurred during the last 100 ky are the most similar past events to forecast future rapid climatic transition due to ice sheets melting. Those events were observed in ice core and sediment records, and they are referred to as Dansgaard-Oeschger (D-O) oscillations (warming abrupt event; Dansgaard et al., 1993) and Heinrich events (cooling events during cold stadials). In particular, 25 D-O oscillations (each from around 2000 y to a few centuries in duration) have been identified in the North Greenland Ice Core Project (NGRIP) ice core record over the last 125 ky (NGRIP Members, 2004), and at least six Heinrich events (marked IRD layers) have been found in the North Atlantic sediment records (Bond et al., 1992), likely caused by massive iceberg discharge due to Laurentide ice sheet instabilities (Broecker et al., 1992). D-O and Heinrich events are not unrelated, and their alternance could be caused by the bipolar seesaw (Stocker and Johnsen, 2003); in other words, oceanic heat and salt transfer from one hemisphere to another to balance freshwater incomes. This concept is also supported by the numerical simulations conducted by Golledge et al. (2019) and Turney et al. (2020), which clearly indicate the close tie existing between the antipode polar areas.

3. Scientific objectives

3.1. Scientific goal, objectives, and hypotheses

Expedition 403 was primarily a paleoceanographic and paleoclimatic expedition. The overarching scientific goal was to recover a sedimentary record that could be used to reconstruct the WSC (i.e., NAW influx) variability; its influence on climate changes, particularly during key climate transitions (Late Miocene–Pliocene transition, Late Pliocene–Pleistocene transition, MPT, mid-Brunhes transition, and suborbital Heinrich-like events); and its impact on the Arctic glaciations, ice shelves development and stability, and sea ice distribution.

The primary objectives to meet the overarching paleoceanographic/paleoclimatic goal included:

1. The development of a high-resolution, Late Miocene–Quaternary chronostratigraphic record based on a suite of independent chronostratigraphic methods to temporally constrain paleoceanographic and paleoclimatic events and the paleo-SBSIS dynamics.
2. The generation of multiproxy data sets to better constrain the potential concurrent forcing mechanisms responsible for Late Miocene to Quaternary climatic transitions.
3. The identification of orbital, suborbital, millennial-scale climate variations such as Heinrich events and possible associated prominent meltwater events (i.e., pulses of water discharge from ice sheet margins).
4. The evaluation of the impact of past prominent sediment-laden meltwater events on the paleoceanography, paleoenvironment, and paleoclimate.
5. The reconstruction of the paleo-SBSIS dynamic history in relation to changes in the WSC pathways and characteristics as mechanisms inducing ice sheet instability and fast retreat.

In meeting these primary objectives with good sediment recovery, the following hypotheses are testable.

3.1.1. Hypothesis 1: the onset of the WSC, transporting NAW, was the main forcing mechanism for the intensification of NHG and was a main forcing mechanism for climatic variability in the Northern Hemisphere through the supply of heat and salt modulating the growth and decay of the Arctic ice sheets and sea ice.

The establishment of the modern NAW has been indicated as one of the main forcing mechanisms for the intensification of NHG (e.g., Haug et al., 2005; Schmidt, 2007; Lunt et al., 2008). North Atlantic water flux and properties (salinity and temperature) control the extent and dynamics of circum-Arctic and circum-North Atlantic ice sheets, sea ice formation and distribution modulating brine production, deepwater mass characteristics, and hence climate. How the ocean system worked during past warmer intervals of high insulation and/or high atmospheric CO_2 content is

still unknown and debated. Another critical issue is the timing and evolution of the transitions into such warm intervals as gradual transition or punctuated by tipping points (e.g., Lenton et al., 2019).

3.1.2. Hypothesis 2: Quaternary variations in sea ice cover in the central Arctic Ocean were influenced by changes in the properties of the WSC, which in turn were affected by hemispheric or global climate shifts.

Only a few studies exist that directly target the role of sea ice during Pleistocene glacial–interglacial cycles. Gildor and Tziperman (2001) used a simple box model of the ocean–atmosphere–sea ice–land ice climate system to propose the so-called sea ice climate switch to explain Pleistocene transitions from ice sheet advance into ice sheet retreat phases. The mechanism is based on the impact of sea ice on both the evaporation from high-latitude ocean areas and atmospheric moisture transport, which are pivotal for the continental ice sheet dynamics.

Massive discharge of Arctic sea ice through the Fram Strait during the Younger Dryas is increasingly suggested to have caused the weakening of the AMOC, resulting in a significant cooling at the end of the last deglaciation, and highlights the importance of nonterrestrial freshwater sources (as opposed to glacial meltwater) for abrupt climate shifts (e.g., Bradley and England, 2008; Condron et al., 2020; Müller and Stein, 2014; Not and Hillaire-Marcel, 2012). Extended sea ice cover in the subpolar North Atlantic since 1 Ma has further been linked to lower primary productivity and elevated input of IRD during glacials (Stein and Fahl, 2013), but highly resolved records have been missing to better constrain the role of sea ice during climate transitions.

3.1.3. Hypothesis 3: during the Quaternary, the variations of WSC pathway and characteristics triggered past SBSIS instabilities.

Reconstructions of the Barents Sea paleobathymetry suggest an evolution similar to that of West Antarctica. The Barents Sea was much shallower and partly emerged until the Late Pliocene (Butt et al., 2002; Laberg et al., 2012; Zieba et al., 2017; Patton et al., 2024) and gradually deepened due to substrate erosion during past glaciations until most of the paleo-SBSIS became marine based with alternation of glaciations (Laberg et al., 2010). In analogy with West Antarctica during the Miocene (Colleoni et al., 2018), the paleo-SBSIS could have become more vulnerable to WSC intrusion on the continental shallow shelf.

We hypothesized that at some point in the Pleistocene, the paleo-SBSIS became subject to more frequent instabilities of its grounding line, with rapid inland retreat and large IRD delivery and freshwater discharges along the Svalbard margin during warm intervals (e.g., interglacials, D-O events, and meltwater pulses). Those instabilities, combined with those of the Laurentide Ice Sheet, could have paced and shaped the glacial–interglacial cycles and their evolution throughout the Pleistocene (e.g., Clark et al., 1999).

3.1.4. Secondary objectives and hypotheses

In addition to the primary paleoceanographic/paleoclimatic objectives, two secondary objectives have tectonic and microbiological foci:

1. Constraining the spatial location of the Miocene–Pliocene transition (~5.3 Ma) north and south of the MTF, at the Vestnesa Ridge and the Svyatogor Ridge, respectively, thus reducing the existing uncertainties about the spreading rate of the Molloy and north Knipovich Ridges inferred from magnetic anomalies Chron 2A (2.8 Ma) and Chron 5 (9.8 Ma) (e.g., Engen et al., 2008; Johnson et al., 2015). Geomechanical and petrophysical data from these key regions will help constrain spatial variations in the effect of glacial and tectonic stresses on subseabed sediment deformation. In addition, such data can inform our understanding of carbon migration within sediment and carbon transfer between sediment-ocean-atmosphere reservoirs under different paleoclimatic conditions.
2. Investigating the influence of the WSC variability, ice coverage, and climate on the microbial populations through time and to what extent these interactions still affect contemporary geochemical fluxes.

In support of these secondary objectives, the following hypotheses may be testable:

- Hypothesis 4: glacial rebound has imposed significant forcing to the already complex tectonic stress field since the opening of the Fram Strait, enhancing sediment fracturing, fault reactivation, and associated carbon migration and transfer during key glacial–interglacial transitions.
- Hypothesis 5: differences in organic carbon input between glacial versus interglacial periods will affect microbial community abundance, diversity, and activity.
- Hypothesis 6: microbial communities will have changed in response to freshwater input during glacial termination events.

It is anticipated that glacial deposits will be enriched in microbial groups specialized in degrading organic matter of terrestrial origin and reflect in a higher frequency in metabolic pathways facilitating the degradation of more recalcitrant carbon, as observed in the equatorial Atlantic and Baltic Seas (Freitas et al., 2020).

The sedimentary deep biosphere extends thousands of meters below the surface and hosts a vast and ecologically significant microbial population that continues to be active even after millions of years of burial (Røy et al., 2012; Orsi, 2018; Zhao et al., 2019; Morono et al., 2020). Through their activity, they regulate the fluxes of dissolved geochemical species in and out of the seafloor and exert primary control on the long-term fate of sequestered organic carbon (Hoehler and Jørgensen, 2013). To this end, the microbial activity and population size are tightly coupled to the input of organic carbon to the seafloor (Kallmeyer et al., 2012). This in turn is a function of several parameters where key variables, such as primary productivity, are strongly influenced by ocean currents and sea ice coverage. However, our understanding to what extent past ocean circulation patterns and sea ice cover is preserved in the contemporary sedimentary microbial population in the form of abundances, diversity, and activity and if this continues to influence modern geochemical fluxes is still unclear and the investigation is limited by the absence of suitable records especially for the older depositional units (Orsi et al., 2017).

The expedition drill sites are located in an area where profound changes in Earth's climate history are stored in the sedimentary record. Sampling of these relevant sedimentary sequences couple the effect of changing climate, including changes in sea ice cover, to potential variability in microbial populations. The possibility to sample identical climatic periods at different geographical locations along the main path of the WSC provides an exceptional opportunity to study whether specific oceanographic/climatic periods translate into specific microbial communities or regional variables are more important. By extension, such information allows more precise prediction of potential future scenarios caused by changing climate.

3.2. Relationships to the 2013–2023 IODP Science Plan and the 2050 Science Framework

Expedition 403 operated under the guidance of the 2013–2023 IODP Science Plan (Bickle et al., 2011). Specifically, the expedition science addressed challenges (i.e., program-wide guiding questions) posed by three IODP Science Plan research themes:

- Climate and Ocean Change, Challenges 1 and 2: How does Earth's climate system respond to elevated levels of atmospheric CO_2? How do ice sheets and sea level respond to a warming climate?
- Biosphere Frontiers, Challenge 7: How sensitive are ecosystems and biodiversity to environmental change?
- Earth in Motion, Challenge 13: What properties and processes govern the flow and storage of carbon in the subseafloor?

The science objectives of Expedition 403 are also convergent with several areas of scientific inquiry described in the 2050 Science Framework (Koppers and Coggon, 2020). In particular, the Expedition 403 primary objective directly supports 2050 Science Framework Strategic Objective 3 (Earth's Climate System) to examine variations in ice sheets, ocean and atmospheric dynamics, and sea level. Understanding the interconnections among the ocean, atmosphere, cryosphere, and marine biosphere in the eastern Fram Strait is an overarching Expedition 403 goal. In addition, the

Expedition 403 secondary objectives focus on tectonic and deep biosphere scientific inquiries. These foci directly support 2050 Science Framework Strategic Objective 2 (The Oceanic Life Cycle of Tectonic Plates), which aims to investigate the genesis, aging, motion, and destruction of oceanic lithosphere, and 2050 Science Framework Strategic Objective 1 (Habitability and Life on Earth), which aims to define the conditions for and the role of life in the marine realm. Because Expedition 403 strived to obtain high-resolution paleoarchive records of Late Miocene to Pleistocene climate system events and transitions (including rapid warming events and paleo–ice sheet destabilizations), 2050 Science Framework Objective 5 (Tipping Points in Earth's History), which aims to use Earth's geologic past to illuminate future environmental change, is also of direct relevance. Finally, the scientific outcomes of Expedition 403 are expected to contribute data that can enable more robust modeling of direct and indirect cause and effect relationships in the Earth system under a range of CO_2 conditions, both similar to today and at levels projected for the near future. Therefore, the expedition science also contributes to 2050 Science Framework Flagship Initiative 1 (Ground Truthing Future Climate Change).

3.3. Connection to other expeditions

Expedition 403 builds upon the success of ODP Legs 151 and 162 and Integrated Ocean Drilling Program Expedition 302 in the Fram Strait and Arctic Ocean. The primary objectives of ODP Legs 151 and 162 were reconstructing the paleoceanography of the Fram Strait and glacial evolution in the circum-Nordic Seas during the Neogene (Jansen and Raymo, 1996; Thiede and Myhre, 1996). Expedition 302 (Arctic Coring Expedition [ACEX]) focused on the long-term Cenozoic paleoenvironmental history of the central Arctic Ocean (Backman and Moran, 2009). These previous expeditions mainly focused on recovery of condensed sequences, having the aim to reach the older units to reconstruct the dynamic history of the Arctic and Subarctic oceans. In contrast, Expedition 403 specifically focused on recovery of expanded sequences to increase the resolution of paleoclimatic reconstruction and complex feedback among the atmosphere-ocean-cryosphere. The objectives of Expedition 403 are also complementary to IODP Expedition 400 (NW Greenland Glaciated Margin; Knutz et al., 2024) by working to understand pan-Arctic ice sheet/ocean dynamics and to IODP Expedition 401 (Mediterranean–Atlantic Gateway Exchange; Flecker et al., 2024) by providing a wider picture of the evolution of North Atlantic ocean circulation, including heat and salt exchange.

Given that the Arctic is so sensitive to climate and ocean change now and in the geologic past, there is an ongoing need for expanded subseafloor sampling at targeted pan-Arctic locations. The paleoperspectives that only scientific ocean drilling can provide are essential for informing predictive models of future climate and ocean change. Although the landscape of scientific ocean drilling is changing with the conclusion of IODP, the need to obtain high-resolution and long-time series subseafloor samples and data sets remains. Prioritization of pan-Arctic subseafloor sampling is necessary to provide a more complete reconstruction of pan-Arctic paleocirculation, related glacial and sea ice histories, and the characterizations of paleoanalog times of rapid change, as well as periods of globally warm climate states.

4. Site summaries

In this report, unless otherwise stated, subseafloor depths are reported as meters below seafloor (mbsf). The mbsf scale is equivalent to meters core depth below seafloor, Method A (CSF-A). In total, seven sites (U1618–U1624) were drilled during Expedition 403 (Table **T1**; Figure **F5**). Summaries of key shipboard results are described below.

4.1. Site U1618

4.1.1. Background and objectives

Site U1618 is located in the Fram Strait near the western continental margin of Svalbard at 78°56.91′N, 7°28.39′E and a 1196 m water depth (Table **T1**; Figure **F5**) (see **Background and objectives** in the Site U1618 chapter [Lucchi et al., 2026a]). Site U1618 is the first of two sites drilled on the Vestnesa Ridge, a prominent bathymetric feature north of, and nearly parallel to, the

Table T1. Hole summary, Expedition 403. mbsl = meters below sea level, mbsf = meters below seafloor, — = no data. **Download table in CSV format.**

Hole	Latitude	Longitude	Water depth (mbsl)	Total cores (n)	Cored interval (m)	Recovered length (m)	Recovery (%)	Drilled interval (m)	Penetration (mbsf)	Time on hole (days)	Time on site (days)
U1618A	78°56.9070′N	7°28.3866′E	1196.0	37	276.9	252.62	91	—	276.9	2.06	
U1618B	78°56.8855′N	7°28.4818′E	1195.2	54	414.3	375.24	91	—	414.3	3.88	
U1618C	78°56.8960′N	7°28.4368′E	1195.8	61	411.1	450.59	110	2.0	413.1	3.24	
			Site U1618 totals:	152	1102.3	1078.45		2.0			9.18
U1619A	79°09.5894′N	4°29.3227′E	1676.2	85	627.9	728.35	116	—	627.9	5.17	
			Site U1619 totals:	85	627.9	728.35		—	627.9	5.17	5.17
U1620A	78°16.3087′N	5°53.3789′E	1577.7	31	239.9	277.10	116	—	239.9	1.73	
U1620B	78°16.3566′N	5°53.8545′E	1597.1	1	0.4	0.34	85	—	0.4	0.15	
U1620C	78°16.3566′N	5°53.8567′E	1597.1	21	169.9	186.87	110	—	169.9	0.99	
U1620D	78°16.3332′N	5°53.6161′E	1586.0	73	616.0	667.89	108	—	616.0	4.81	
			Site U1620 totals:	126	1026.2	1132.20			1026.2		7.68
U1621A	76°31.2956′N	12°44.3175′E	1638.6	28	215.3	180.40	84	—	215.3	1.42	
U1621B	76°31.3053′N	12°44.3358′E	1636.5	33	216.1	203.39	94	—	216.1	1.60	
U1621C	76°31.3152′N	12°44.3552′E	1635.9	28	207.9	195.18	94	—	207.9	1.25	
			Site U1621 totals:	89	639.3	578.97			639.3		4.27
U1622A	76°27.4495′N	12°33.2859′E	1705.5	7	46.5	46.26	99	—	46.5	0.54	
			Site U1622 totals:	7	46.5	46.26		—	46.5		0.54
U1623A	76°31.8394′N	12°34.3958′E	1707.7	51	369.3	330.72	90	—	369.3	2.26	
U1623B	76°31.8500′N	12°34.4118′E	1707.7	1	0.1	0.05	50	—	0.1	0.12	
U1623C	76°31.8594′N	12°34.4276′E	1706.4	55	369.0	322.38	87	—	369.0	2.85	
U1623D	76°31.8551′N	12°34.4722′E	1715.6	56	370.0	351.06	95	—	370.0	3.24	
U1623E	76°31.8573′N	12°34.4499′E	1707.2	1	9.6	9.63	100	—	9.6	0.10	
U1623F	76°31.8565′N	12°34.4501′E	1706.7	22	162.3	147.04	91	—	162.3	0.75	
U1623G	76°31.8694′N	12°34.4465′E	1704.8	19	142.1	153.50	108	—	142.1	0.98	
			Site U1623 totals:	205	1422.4	1314.38			1422.4		10.30
U1624A	77°35.2627′N	10°05.6277′E	1319.8	1	1.3	1.33	102	—	1.3	0.23	
U1624B	77°35.2625′N	10°05.6399′E	1319.8	45	258.0	223.05	86	—	258.0	1.54	
U1624C	77°35.2543′N	10°05.6072′E	1319.6	43	258.0	240.24	93	—	258.0	1.46	
			Site U1624 totals:	89	517.3	464.62			517.3		3.23
			Expedition 403 totals:	753	5381.9	5343.23		2.0	5383.9		

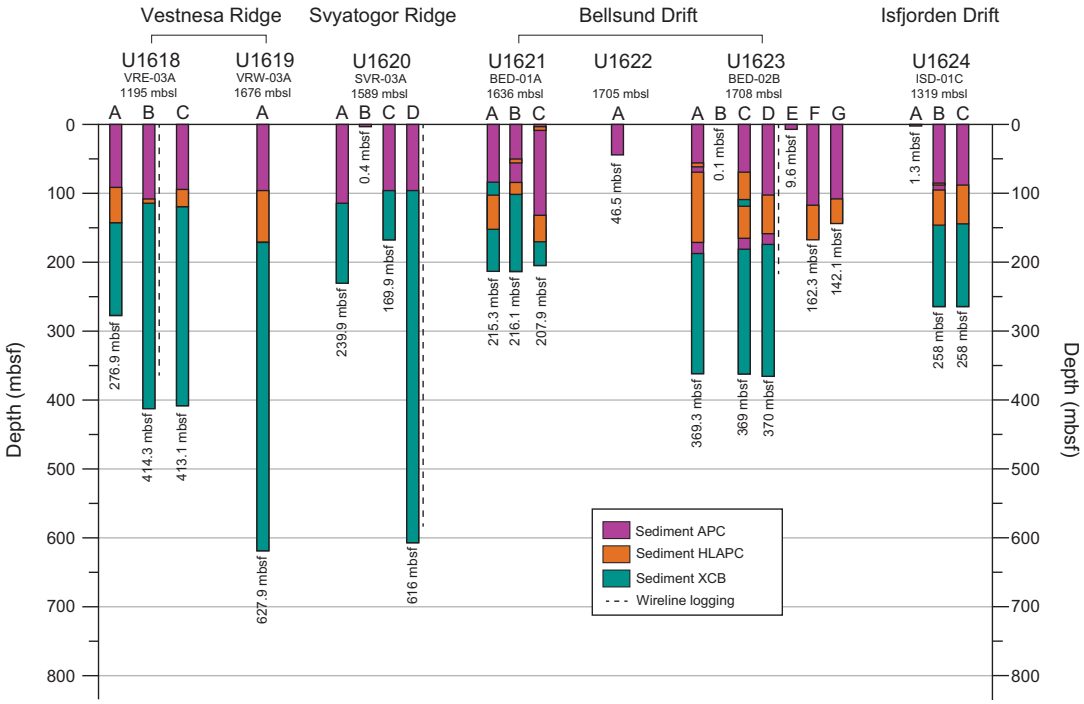

Figure F5. Drilling operations, Expedition 403. Sites and holes are organized (left to right) in order of operation, except for Holes U1623D–U1623G, which were drilled upon return to the site following operations at Site U1624.

MTF. The evolution of the Vestnesa Ridge is linked to the tectonic, sedimentary, and climatic history of the region, making it a focal point for multidisciplinary scientific research. The 100 km long ridge is a sediment drift generated by persistent bottom currents associated with the WSC (Eiken and Hinz, 1993) that developed over oceanic crust since the Fram Strait opening (17–10 Ma; Jakobsson et al., 2007; Engen et al., 2008; Ehlers and Jokat, 2013). It has been hypothesized that the main axis of the Vestnesa Ridge has migrated orientation from north–south to east–west over time due to the eastward motion of the plate north of the MTF (Johnson et al., 2015), forcing a lateral displacement of the main path of the WSC to follow the bathymetric contour around the Vestnesa Ridge.

Although the chronology of the Vestnesa Ridge sediment record deposited since the last glacial is well established (e.g., Rasmussen and Nielsen, 2024, and references therein) and regionally correlatable (Lucchi et al., 2023), the chronology prior to Marine Isotope Stage (MIS) 5 has been limited to extrapolations made through seismic correlations to previously drilled sites on the Yermak Plateau (ODP Site 912) and the Molloy Basin (south of the MTF; ODP Site 909) (Eiken and Hinz, 1993; Knies et al., 2014; Mattingsdal et al., 2014; Alexandropoulou et al., 2021).

During the Pliocene–Pleistocene, marine sedimentation in this region was heavily influenced by the intensification of NHG, ice sheet growth and decay over Svalbard and the Barents Sea, and variations in Arctic sea ice extent (Jakobsson et al., 2014). Shallow sediment records from piston and gravity cores along the western Svalbard continental margin document depositional facies representing a range of glaciogenic processes since MIS 3. These include ice rafting events, downslope sediment mass transport, and subglacial meltwater plumes, which alternated with bioturbated, bottom current–driven sediments that settled during warmer periods (e.g., Rasmussen et al., 2007; Jessen et al., 2010; Lucchi et al., 2013, 2015; Caricchi et al., 2019). Concurrent stratigraphic intervals from the Vestnesa Ridge are consistent with these depositional patterns (Schneider et al., 2018; Sztybor and Rasmussen, 2017b; Plaza-Faverola et al., 2023; Rasmussen and Nielsen, 2024); therefore, we anticipated that this depositional framework could be applied to a much longer stratigraphic sequence drilled at Site U1618.

The geologic setting of the Vestnesa Ridge is additionally influenced by the presence of gas hydrates and associated fluid migration, which both complicates the paleoclimatic sedimentary record and creates additional research opportunities. The east Vestnesa Ridge is characterized by large pockmarks connected to chimneys with ongoing seepage of methane and other hydrocarbons along its narrow crest (~3 km wide) (Plaza-Faverola et al., 2015; Sztybor and Rasmussen, 2017a; Schneider et al., 2018). Seismic surveys also reveal a regional gas hydrate–related bottom simulating reflector (BSR) and thus the presence of gas hydrate and free gas at depth. Previous studies indicate that the hydrate stability zone is several hundred meters thick and can extend to the seafloor (Himmler et al., 2019; Pape et al., 2020; Plaza-Faverola et al., 2023; Rasmussen and Nielsen, 2024).

The drilling location for Site U1618 (Lucchi et al., 2023) was chosen for its proximity to the continental margin and outer reaches of the northwestern area of the paleo-SBSIS, making this site well suited to reconstruct the ice sheet dynamics. Seismic Reflectors R1–R8 were drilling targets, with a total depth target of 738 mbsf. For safety, and to maximize recovery toward the primary paleoclimatic science objectives, Site U1618 was positioned away from the regional BSR.

At Site U1618, the main initial objective was to recover a complete stratigraphy from Seismic Reflector R8 (~5.8 Ma) to present. Such recovery would support the following research goals:

- Reconstruction of a high-resolution sediment stratigraphy since the Late Miocene–Early Pliocene transition;
- Study of ocean-cryosphere interactions and forcing mechanisms on the paleo-SBSIS dynamics;
- Definition of the effect of glacial and tectonic stresses on subseafloor sediment deformation and carbon migration/transfer; and
- Investigation of the influence of the WSC variability, ice coverage, and climate on the microbial populations through time and to what extent this is still affecting contemporary geochemical fluxes.

Additionally, this location offers the opportunity to explore possible relationships (including feedbacks and tipping points) among paleo–ice sheets, gas hydrate stability, and tectonic stress.

4.1.2. Operations

We arrived at Site U1618 on 14 June 2024 after transiting from Amsterdam (The Netherlands). In total, we spent 9 days on site, drilled three holes along Seismic Line CAGE20-5-HH-02-2D (Figure **F6**), and logged one hole (Figure **F5**; Table **T1**). Hole U1618A was located 3.8 km from a gas chimney and 1.1 km from a fault, which may be a conduit for fluid migration (Figure **F6**). Holes U1618B and U1618C were located farther from these features, 50 and 25 m northeast of Hole U1618A, respectively. All three holes had intervals in which the sediments significantly expanded due to the presence of gas, resulting in recoveries often exceeding 100%. Additional borehole temperature measurements were made at Site U1618 to determine the geothermal gradient, which was necessary data for hydrocarbon safety monitoring. Each hole had to be terminated prematurely for anomalous methane/ethane (C_1/C_2) ratios (Figure **F7**) and/or for increased presence of higher (e.g., C_5, C_6) hydrocarbons. Coring reached a maximum depth of 414.3 mbsf, several hundred meters shy of the target depth (738 mbsf). Nevertheless, a combined cored interval of 1102.3 m resulted in a recovered length of 1078.45 m. Because formation characteristics (e.g., gas content and sediment stiffness) changed at each hole, deployment of the advanced piston corer (APC) system shifted to the half-length APC (HLAPC) system and then to the extended core barrel (XCB) drilling system, at different downhole depths. At Site U1618, there were 152 cores in total: 40 APC (26.3%), 17 HLAPC (11.2%), and 95 XCB (62.5%). To minimize magnetic overprinting on the cored sediment, the nonmagnetic collars and core barrels were used for all APC and HLAPC coring. Shattered core liners posed a challenge at each hole. To mitigate the impact of sediment expansion and potential core disturbance and to release the overpressure, holes were drilled into the liners both by the drill crew on the rig floor and the technical staff on the core receiving platform.

Hole U1618A was started on 14 June. Cores 1H–37X penetrated from the seafloor to 276.9 mbsf with 252.62 m recovered (91.23%). In situ temperature measurements were taken on Cores 4H, 7H, 10H, and 13F using the advanced piston corer temperature (APCT-3) tool. A fifth temperature measurement was taken using the Sediment Temperature 2 (SET2) probe after Core 34X (249.0 mbsf). In total, we spent 2.1 days on Hole U1618A (Table **T1**).

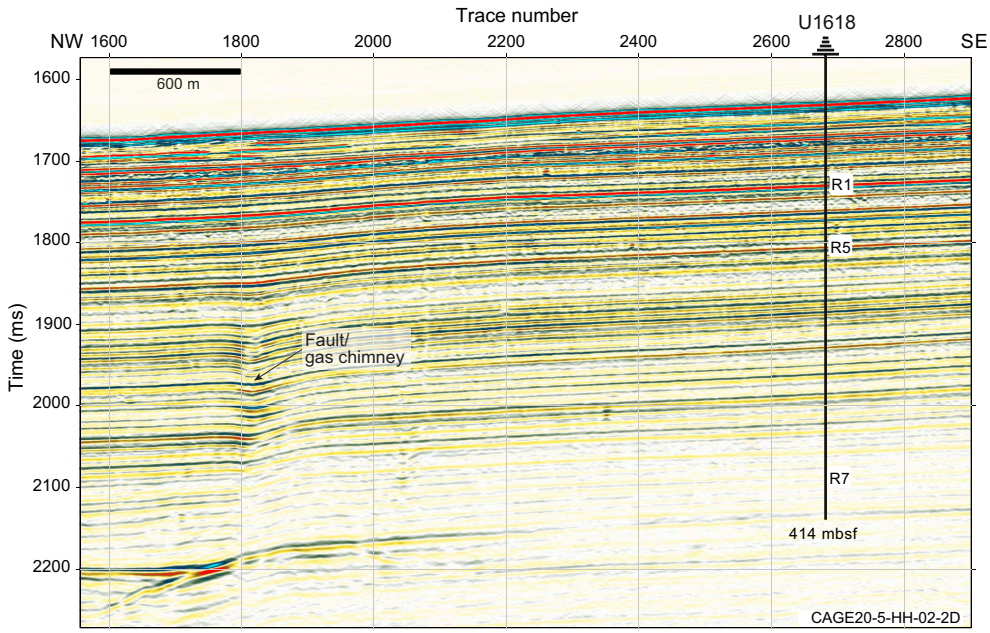

Figure F6. Seismic profile along northwest–southeast Seismic Line CAGE20-5-HH-02-2D showing the location of Site U1618 annotated with interpreted Reflectors R1, R5, and R7 and the maximum penetration depth of 414 mbsf. Interpreted locations of a fault and possible gas chimney are indicated.

Hole U1618B was spudded on 16 June. Its location was offset 50 m from Hole U1618A at a bearing of 139°. A total of 54 cores (Cores 1H–54X) were taken in Hole U1618B over a 414.3 m interval with 375.24 m recovered (90.57%). The SET2 probe was used to get the two deepest in situ temperature measurements after coring Cores 403-U1618B-42X and 52X at 324.8 and 401.5 mbsf, respectively. Coring was terminated on 19 June. Because Hole U1618B was deeper than Hole U1618A, and possible coring success in Hole U1618C was uncertain, Hole U1618B was selected for wireline logging. The triple combination (triple combo) logging tool string and Formation MicroScanner (FMS)-sonic logging tool were successfully deployed and collected geophysical borehole data; however, the Versatile Seismic Imager (VSI) tool was inoperable after a power surge caused a failure in the electronics. Logging operations ended on 20 June. In total, we spent 93.0 h (3.9 days) on Hole U1618B (Table **T1**).

Hole U1618C was offset 25 m northwest at a bearing of 319° from Hole U1618B, halfway toward Hole U1618A. Coring commenced on 20 June. A total of 61 cores were taken in Hole U1618C, and a 2 m interval (Core 161) was drilled without recovery to address a correlation offset. Cores 1H–62X penetrated from the seafloor to 413.1 mbsf; the cored interval was 411.1 m long, and the recovery was 450.59 m (109.61%) (Table **T1**). After 3.24 days on this hole, preparations were made to get underway to Site U1619.

4.1.3. Principal results

4.1.3.1. Lithostratigraphy

The Quaternary sediment record recovered at Site U1618 is primarily siliciclastic, mainly composed of dark gray to greenish black silty clay, with interbedded coarser intervals ranging from clayey silt to diamicton. Detrital clasts are present throughout most of the record in varying abun-

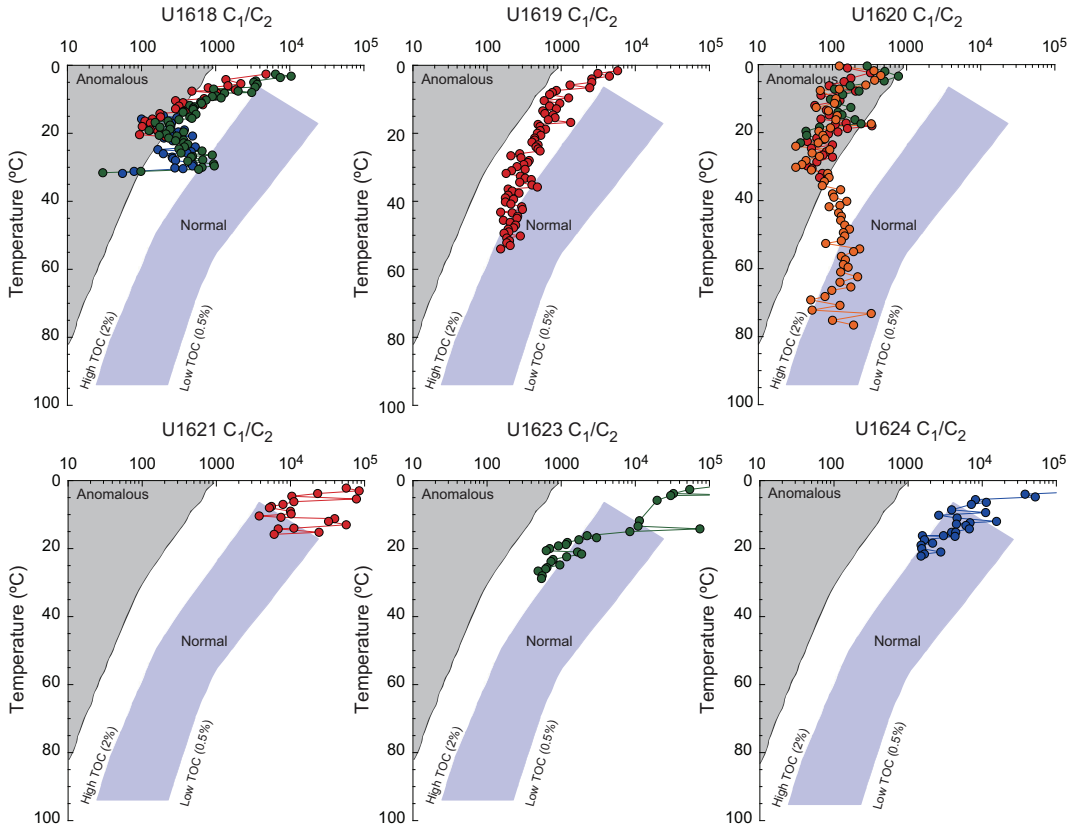

Figure F7. Headspace hydrocarbon C_1/C_2 ratios versus downhole temperatures for each site, Expedition 403. Diagram includes shaded anomalous versus normal zones. The relationship between C_1/C_2 ratios and downhole (i.e., sediment) temperature is one criterion to evaluate the nature of hydrocarbon occurrence. Anomalously low C_1/C_2 ratios suggest the presence of migrated thermogenic hydrocarbons (Pimmel and Claypool, 2001; JOIDES Pollution Prevention and Safety Panel, 1992).

dances. Although sedimentary structures were often not visible on the split core surfaces (i.e., described as structureless), laminated and bioturbated intervals were distinguishable on the X-radiographs (Figure **F8A**). Preliminary comparisons between patterns of sedimentary facies observed on the Site U1618 X-radiographs and well-established lithofacies from shallow piston cores of the western margin of Svalbard (i.e., Lucchi et al., 2013, 2023) suggest that the sedimentary record at Site U1618 can be used to identify evidence of past shelf edge glaciation, ice-calving, and paleomeltwater events.

Diagenetic overprinting of the primary depositional record becomes increasingly common downcore, especially below ~150 mbsf, which corresponds to Seismic Reflector R5. The postdepositional alteration is evident by the presence of authigenic carbonate minerals and iron sulfide (pyrite and/or greigite) minerals, sometimes occurring as concretions or burrow infillings (Figure **F8B**). Gas escape features, including voids and fractures, are common, especially between ~150 and 190 mbsf.

The base of the Site U1618 record is Pliocene in age (Figure **F9**). It is marked by the presence of prominent laminations in dark gray to black silty clay, an increase in the relative abundance of smectite, and the absence of diamictons.

4.1.3.2. Biostratigraphy

No microfossil group is consistently present in the Site U1618 sediment record, and several intervals are barren. This was not unexpected given the high-latitude setting. During ODP Leg 151, similar challenges were experienced in the Fram Strait, with limited diversity and abundance in the Quaternary to Early Pliocene sediments (Myhre et al., 1995; Thiede and Myhre, 1996). Addition-

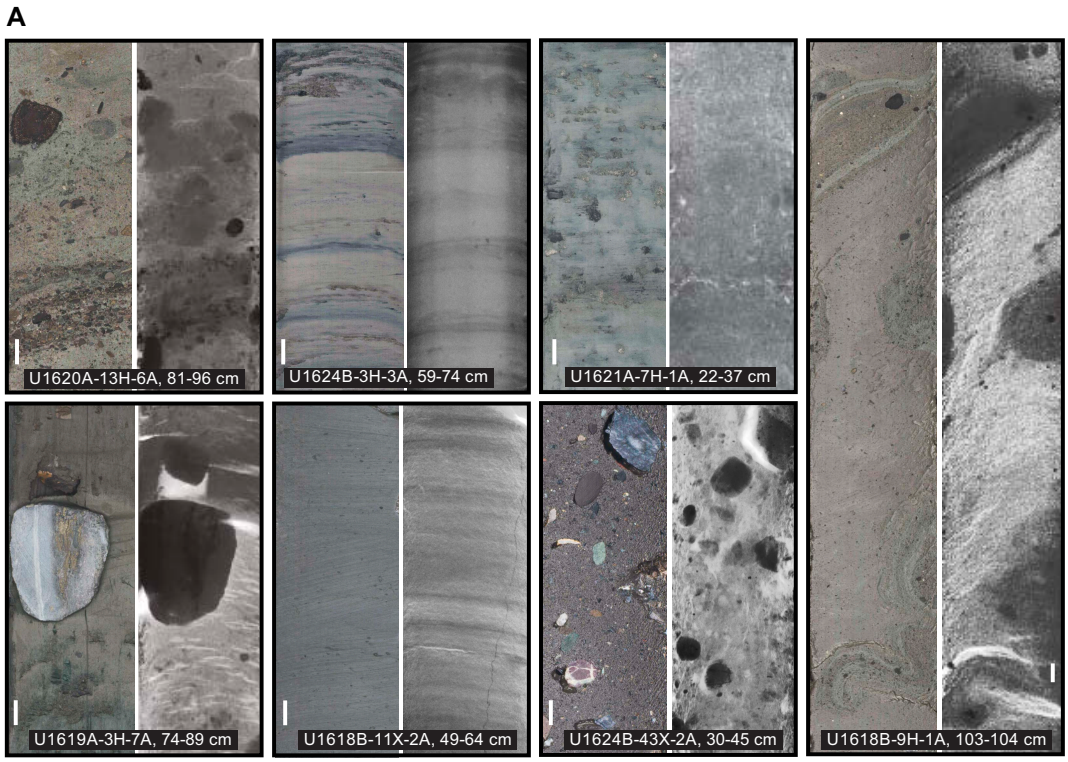

Figure F8. Paired linescan core images and X-radiographs of representative features, Expedition 403. X-radiographs: black = high density. Scale bar = 1 cm. A. Lithologies and sedimentary structures. Top left: sand with layered and dispersed clasts. Top center: interbedded silty clay and silt layers. Top right: silty clay containing abundant sand patches interpreted as iceberg-rafted sediment pellets. Right: debrite with contorted muddy clasts in a muddy matrix. Bottom left: dropstone. Bottom center: laminated silty clay. Bottom right: diamicton. B. Sedimentary authigenic minerals. Top left: yellowish orange sand-sized authigenic carbonate grains. Top right: authigenic iron sulfide nodules (greigite). Bottom left: authigenic carbonate nodules (light brown). Bottom right: black-yellow-brown laminations and selective enrichment (black laminae) and authigenic carbonates (yellow laminae) in an overall quartz and clay mineral–rich bulk sedimentation (brown sediments). (Continued on next page.)

ally, postdepositional interstitial water (IW) reactions in the Vestnesa Ridge gas hydrate–bearing sedimentary system may have influenced the preservation of biogenic carbonate and biogenic silica. At Site U1618, diatoms are present at the very top (Holocene), with limited occurrences of mostly fragments downcore. Foraminifers are present in the upper part but disappear downcore. Calcareous nannofossils are generally present with a moderate abundance; however, the lower part of the record is mainly barren. Dinocysts are present throughout the sediment column but are absent occasionally.

An initial paleoenvironmental assessment based on the four microfossil groups generally indicates Arctic to polar surface waters and seasonal sea ice conditions throughout most of the Quaternary. Polar surface waters are colder and slightly less saline than Arctic water masses that are defined as a mixture of Polar and Atlantic water masses following definitions of water masses in the Fram Strait today (e.g., Hopkins, 1991). Exceptions are the cold–temperate conditions and Atlantic water incursion during the Middle Pleistocene and occasional incursions of temperate waters in the Early Pleistocene. Some reworking of pre-Neogene deposits is evident in all microfossil groups. Input of reworked microfossils is consistent with processes of glacial erosion of sedimentary outcrops on Svalbard, remobilization of deposits in fjords and on the shelf, and delivery to the ocean through glaciomarine depositional processes (Figure **F4**).

Barren intervals notwithstanding, age-diagnostic microfossils are present from the seafloor to the base of Site U1618, with calcareous nannofossils and dinoflagellate cysts (dinocysts) providing most of the initial microfossil-based age-depth markers (Figure **F10**). Late Pleistocene intervals constraining MISs 1, 5–8, and 11–13 and older are defined by age-diagnostic markers. Dinocyst biostratigraphy indicates hints of Pliocene flora (older than ~2.7 Ma) near the base of the record (>390 m). This finding is supported by intermittent intervals of diatom fragments, which indicate ages of at least 2.58 Ma.

4.1.3.3. Paleomagnetism

Site U1618 sediments have a wide range of magnetic properties that likely reflect contribution from detrital and authigenic sources. Stratigraphically below the first reversed direction (at ~90 mbsf), many intervals appear to have been remagnetized. These data are consistent with the for-

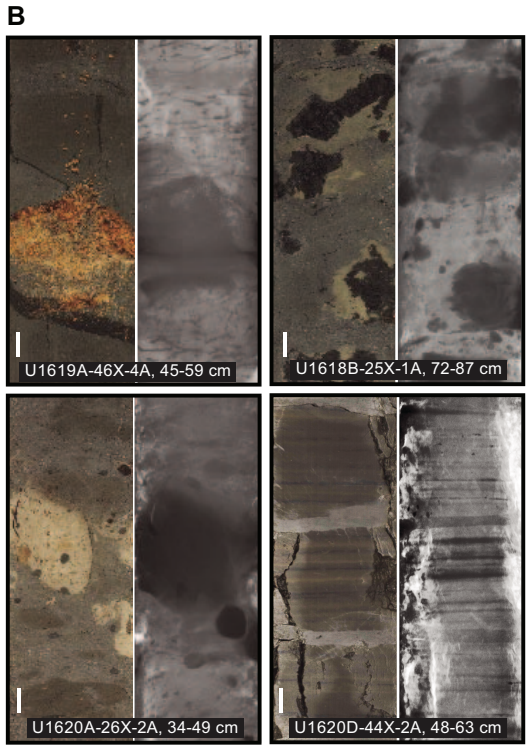

Figure F8 (continued).

mation of authigenic greigite (Figure **F8B**), which would acquire a chemical remanent magnetization that is younger than the detrital remanent magnetization of the surrounding sediment. Nevertheless, intervals dominated by detrital sources provided suitable paleomagnetic constraints to determine an initial magnetic stratigraphy. There is great potential to refine the magnetic stratigraphy at Site U1618 with higher resolution paleomagnetic investigation to characterize the natural remanent magnetization (NRM) in the context of detailed rock magnetic investigations to characterize magnetic mineral assemblages (Figure **F11**).

4.1.3.4. Age model

Although determination of magnetic polarity zones was complicated by the potential for chemical remanent magnetizations hosted by the authigenic mineral greigite, three major polarity zones were interpreted to reflect Chrons C1n (Brunhes; 0–0.773 Ma), C1r–C2r (Matuyama; 0.773–2.595 Ma), and C2An (Gauss; 2.595–3.596 Ma). These interpretations are in good agreement with the shipboard biostratigraphy. No hiatuses are identified at this early stage. The preliminary age model indicates an average sedimentation rate of 147 m/My between ~2.6 and ~1 Ma (Figure **F11**). A high sedimentation rate is expected given the proximity of Site U1618 to the paleo-SBSIS, which was documented to have first reached the shelf edge concurrent with the expansion of NHG at 2.7 Ma (Alexandropoulou et al., 2021). A decrease in sedimentation rate to 104 m/My since ~1.0 Ma is consistent in timing with decreased sedimentation at ODP Site 908 (Hovgaard Ridge), ODP Site 909 (Molloy Basin), and ODP Site 911 (Yermak Plateau) (Myhre et al., 1995; Thiede and Myhre, 1996). Such a regional change in sedimentation rate may reflect changes in the depositional environment, perhaps related to the position or strength of the WSC, which is a bathymetrically con-

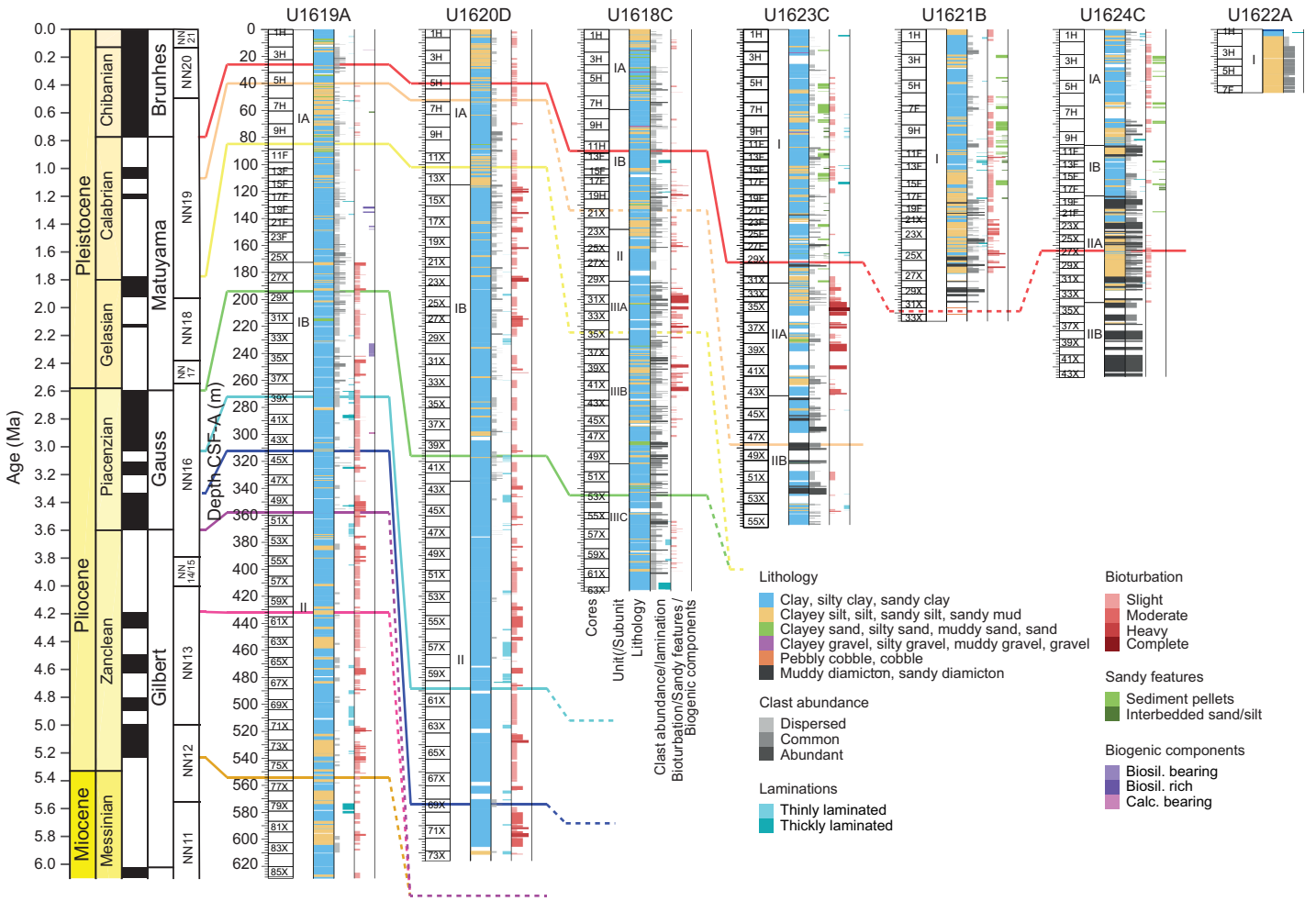

Figure F9. Lithostratigraphic summary, Expedition 403. The longest record from each site is included. The biozone scheme follows Martini (1971) and the revision by Razmjooei et al. (2023) for the boundaries of the upper nannofossil biozones NN20 and NN21.

trolled current and therefore may also be related to climate-induced relative sea level changes. Alternatively, or additionally, these sedimentation rate changes may be related to change in ice sheet dynamics as glacial cyclicity shifted from 41 to 100 ky cycles during the MPT (~0.9–1.0 Ma).

4.1.3.5. Physical properties

Results from physical property measurements for Site U1618 show relationships to both lithologic and paleomagnetic findings and appear to be influenced by glaciogenic deposition and postdepositional processes. Below 25 mbsf, fractures and voids in the recovered sediment cores caused

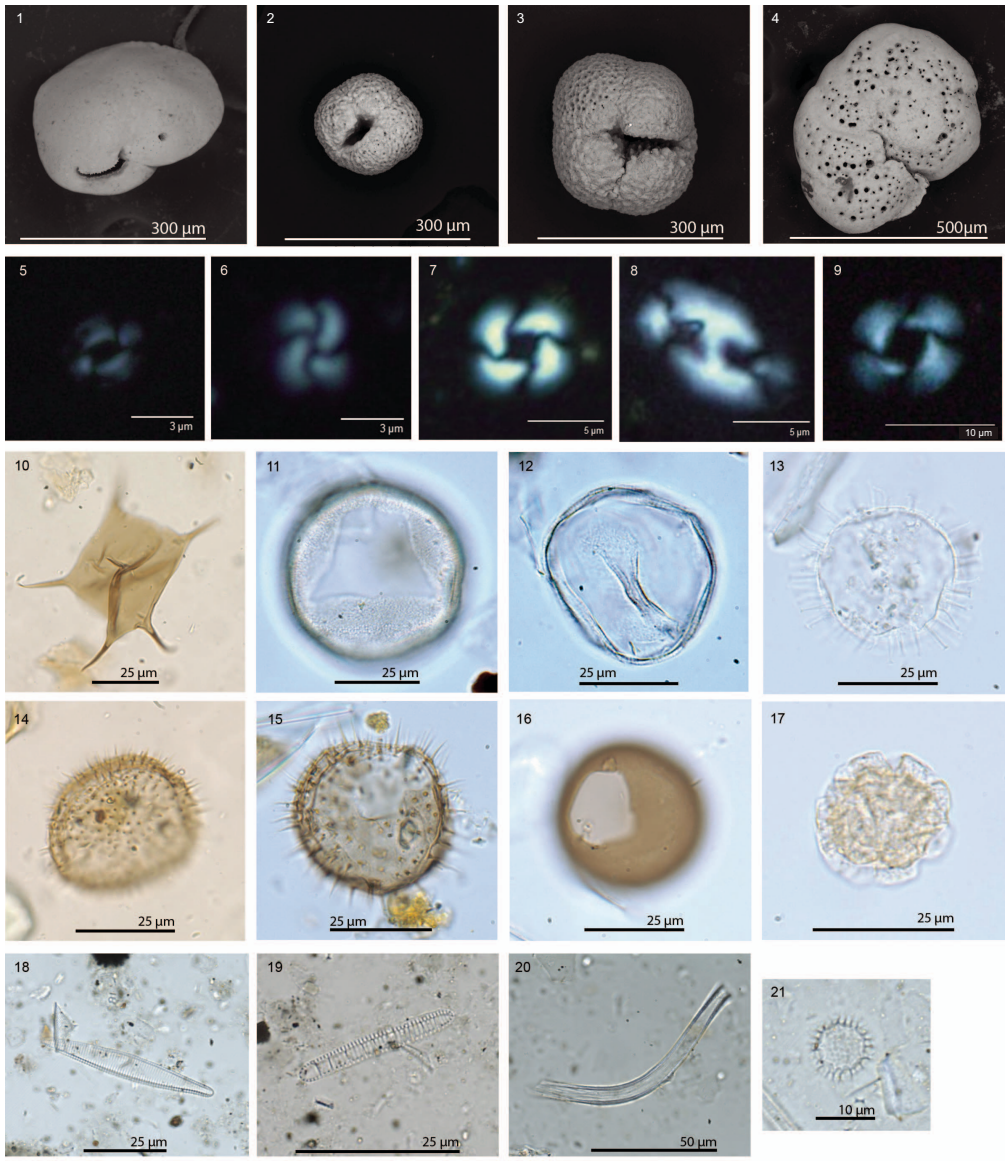

Figure F10. Important biostratigraphic microfossils encountered during analyses of sediments, Expedition 403. Foraminifers: 1. *Cassidulina teretis* (403-U1619A-25X-CC). 2. *Neogloboquadrina atlantica* (umbilical view) (403-U1619A-45X-CC). 3. *Neogloboquadrina pachyderma* (umbilical view) (403-U1621A-1H-CC). 4. *Cibicides grossa* (umbilical view) (403-U1619A-45X-CC). Calcareous nannoplankton: 5. *Emiliania huxleyi* (403-U1621C-1H-2W, 60 cm). 6. *Gephyrocapsa caribbeanica* (403-U1618A-7H-1W, 50 cm). 7. *Reticulofenestra asanoi* (403-U1623A-41X-3, 63 cm). 8. *Helicosphaera sellii* (403-U1620B-24X-CC). 9. *Reticulofenestra pseudoumbilicus* (403-U1619A-55X-CC). Dinocysts: 10. Cyst of *Protoperidinium stellatum* (403-U1618A-14F-CC). 11. *Filisphaera filifera* (403-U1618A-10H-CC). 12. *Habibacysta tectata* (403-U1619A-14F-CC). 13. Cyst of *Protoceratium reticulatum* (403-U1624B-4H-4A, 69–81 cm). 14. *Islandinium brevispinosum* (403-U1618A-14F-CC). 15. *Islandinium minutum* (403-U1624B-5H-CC). 16. *Brigantedinium* sp. (403-U1621C-4H-4A, 82–92 cm). Acritarchs: 17. *Lavradosphaera canalis* (403-U1620D-45X-CC). Diatoms: 18. *Fragilariopsis fossilis* (403-U1623A-41X-3, 107 cm). 19. *Neodenticula seminae* (403-U1623A-33X-5, 38 cm). 20. *Proboscia curvirostris* (403-U1621A-9H-1, 72 cm). 21. *Thalassiosira jouseae* (403-U1619A-19F-1, 79 cm).

strong attenuation of the acoustic signal and resulted in erratic shipboard *P*-wave measurement. This *P*-wave behavior was observed at all Expedition 403 sites and will not be reported further. Magnetic susceptibility (MS) co-varies with natural gamma radiation (NGR) and gamma ray attenuation (GRA) bulk density above ~150 mbsf, and NGR and GRA density show a positive linear correlation over this interval. Based on initial comparison to shallow sediment records from piston cores on the Svalbard margin, these physical property data show potential for identifying different glaciogenic lithofacies, such as meltwater events and mass transport deposition related to shelf edge glaciation, which are important for reconstructing paleo–ice sheet dynamics. Below ~150 mbsf, irregularly spaced, large peaks in MS become prevalent and appear to correlate with the occurrence of authigenic iron sulfide minerals.

In addition to the standard suite of physical property measurements, anelastic strain recovery (ASR) experiments were conducted on three whole-round samples using strain gauges connected to the sample. Preliminary results show that after temperature equilibrium, strain released loga-

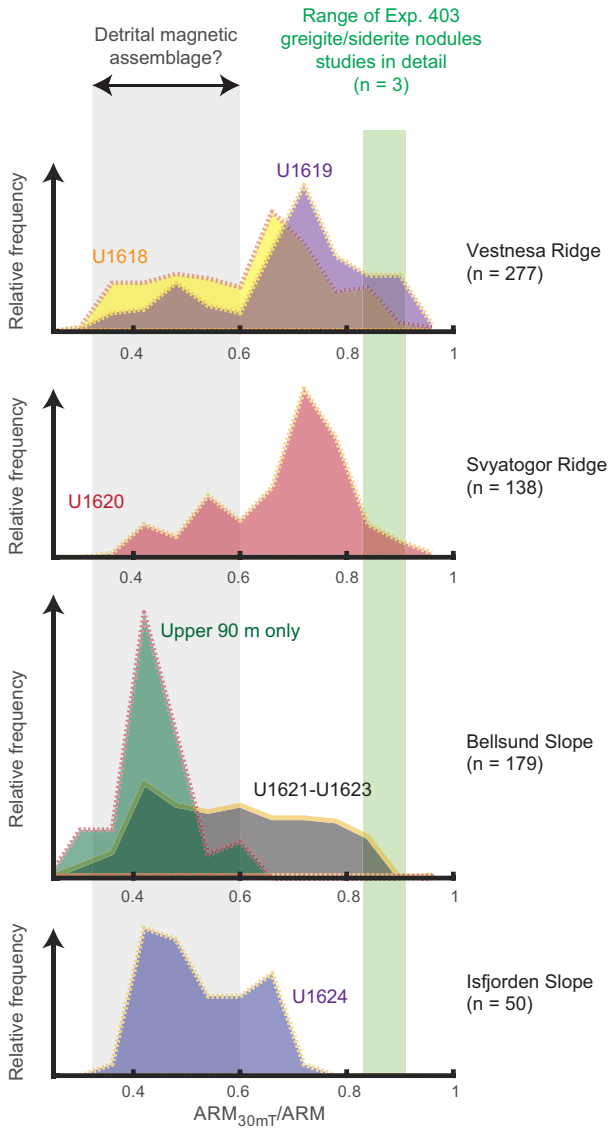

Figure F11. Histograms illustrating variability of ARM coercivity, Expedition 403. Values are tracked by the ratio of the ARM after 30 mT peak alternating field demagnetization to the initial ARM. Higher values indicate greater resistance to demagnetization. Green vertical shading = range of values observed in authigenic greigite and siderite nodules. Gray vertical shading = range commonly observed in near-surface samples that we interpret to be consistent with the properties of the primary detrital magnetic mineral assemblage. Further rock magnetic, mineralogical, and microscopic investigation will help improve our understanding of what drives the distributions of ARM coercivity in these regions.

rithmically, but some gauges showed shrinking of the sediments. Additional processing postexpedition will aim to determine the principal stress azimuths; such information contributes to the tectonics objectives of the expedition.

4.1.3.6. Stratigraphic correlation

Stratigraphic correlation between holes was primarily accomplished using MS in the uppermost 150 m and red-green-blue color space (RGB)-red and NGR for constructing the deeper splice because the MS signal was influenced by postdepositional alteration. The best recovered stratigraphic interval of Hole U1618C was used as the backbone of the splice. Because of gas expansion, a growth factor of 1.1 was applied to cores below 294.2 m core composite depth below seafloor (CCSF). Calculation of mass accumulation rates based on the CCSF scale should account for the expansion by dividing apparent depth intervals by the appropriate growth factor.

4.1.3.7. Geochemistry

Headspace gas measurement and IW analyses suggest anaerobic conditions below ~20 mbsf. The sulfate–methane transition zone (SMTZ), characterized by sulfate depletion and methane increase, occurs between ~12 and 20 mbsf. These and other (e.g., calcium [Ca] and iron [Fe]) IW chemistry findings document fluid migration in the sediments. The effects of fluid migration may explain the diachronous formation of iron sulfide minerals. Documented methane seeps at the surface of the east Vestnesa Ridge (Bünz et al., 2012; Smith et al., 2014; Plaza-Faverola et al., 2015; Panieri et al., 2023) are also likely related to fluid migration. Additionally, highly alkaline IW likely contributed to the poor preservation of diatoms in the sediment record.

A co-related linear decrease of chloride (Cl), sodium (Na), and salinity downcore indicates freshening of the IWs, suggesting a diffusion of fluids deeper than 406.26 m and possibly indicating that gas hydrate dissociation occurred deeper than core recovery.

Total organic carbon (TOC) at Site U1618 ranges between 0% and 2% and generally increases with depth. TOC/total nitrogen (TN) (i.e., C/N) ratios, which are commonly used to identify sources of sedimentary organic matter, indicate contributions from both continental (e.g., ice sheet derived) and marine sources of organic matter. Low-resolution shipboard sampling also suggests that increased C/N ratios generally correlate to coarse-grained lithologies, consistent with a terrestrial origin of the organic carbon at those horizons.

4.1.3.8. Microbiology

In addition to standard shipboard geochemistry measurements, samples for sedimentary ancient DNA (sedaDNA) were taken in contamination-controlled conditions. Although analyses of the sedaDNA samples will occur postexpedition, the analysis of control samples indicated that coring with the APC systems (i.e., APC and HLAPC) resulted in lower drill fluid contamination of the sedaDNA control samples (15%) than occurred when coring with the XCB system (57%). The contamination difference is likely due to the increased core disturbance (e.g., fracturing or biscuiting) produced by the XCB system. Nevertheless, these findings also indicate that it is possible to obtain uncontaminated sedaDNA samples with both types of coring approaches, extending the potential for sedaDNA studies in a wider range of drilling conditions than previously documented in marine sediments.

4.1.3.9. Downhole logging

Downhole logging measurements of natural gamma ray, GRA density, and MS showed similar trends as shipboard scanning data, including apparent cyclic changes in amplitude of natural gamma ray and GRA density. FMS imaging of the borehole was limited because the FMS calipers were not able to maintain contact with the borehole walls. Although the absolute values of the porosity data are anomalously high due to poor borehole conditions, the relative changes in porosity show correlation with density and electrical resistivity across several intervals. At ~190–200 wireline log matched depth below seafloor (WMSF), low electrical resistivity values were observed, which correspond to a logged interval of low density and high porosity material, pointing to the possibility of higher water content. These conditions are tentatively hypothesized to mark the base of the gas hydrate stability zone. In marine sedimentary sequences, the gas hydrate stability zone can be estimated from pressure (i.e., depth) and downhole temperature data (Kvenvolden and Barnard, 1983). Linear regression of the in situ formation temperature measurements

made during coring indicates a typical geothermal gradient at Site U1618. Based on this geothermal gradient, the base of the gas hydrate stability zone at Site U1618 is estimated to be at ~200 mbsf, coinciding with the anomalous zone of higher water content.

At Site U1618, downhole logging Dipole Sonic Imager (DSI) measurements of acoustics waves are muted, similar to failed *P*-wave measurements in the core laboratory on the ship. These observations appear consistent with the presence of gas hydrate or free gas in the sediment. However, postprocessing of the DSI data provided meaningful *P*-wave velocities at depth, with the most prominent variability below ~230 WMSF. These data seem to support the hypothesis that the gas hydrate stability zone is above this depth.

4.2. Site U1619

4.2.1. Background and objectives

Like Site U1618, Site U1619 is located on the Vestnesa Ridge but was sited at the west termination (Figure **F1**) (see **Background and objectives** in the Site U1619 chapter [St. John et al., 2026a]), representing a distal glaciogenic depositional reach and a potentially better location to record the WSC variability. The Vestnesa Ridge is a roughly east–west-oriented prominent bathymetric feature situated in the southeastern side of the Fram Strait next to the western continental margin of Svalbard. Its evolution is linked to the tectonic, sedimentary, and climatic history of the region, making it a focal point for multidisciplinary scientific research. The 100 km long ridge is a sediment drift generated by persistent bottom currents associated with the WSC (Eiken and Hinz, 1993) that developed over oceanic crust since the Fram Strait opening (17–10 Ma; Jakobsson et al., 2007; Engen et al., 2008; Ehlers and Jokat, 2013). Although the chronology of the Vestnesa Ridge sediment record deposited since the last glacial is well established and regionally correlatable (Lucchi et al., 2023), the chronology prior to MISs 4 and 5 is limited to extrapolation made through seismic from previously drilled sites on the Yermak Plateau (ODP Site 912) and south of the MTF (ODP Site 909) (Eiken and Hinz, 1993; Knies et al., 2014; Mattingsdal et al., 2014).

The sedimentation and geologic development in this area has been heavily influenced by the Pliocene–Pleistocene glaciations, especially the ice sheet extent over Svalbard and the Barents Sea, as well as the Arctic Ocean sea ice extent (Jakobsson et al., 2014). Depositional facies representing a range of glaciogenic and bottom current depositional processes are well documented in the recent sedimentary record along the western Svalbard continental margin (e.g., Jessen et al., 2010; Lucchi et al., 2013, 2015; Caricchi et al., 2019) and the Vestnesa Ridge (Schneider et al., 2018; Sztybor and Rasmussen, 2017b; Plaza-Faverola et al., 2023). The presence of gas hydrates and associated fluid migration are additional controls on the sedimentary record of the Vestnesa Ridge, although they have more effect in the central and eastern areas of the ridge than in the western extension.

The west termination of the Vestnesa Ridge is characterized by a larger (>10 km wide) crest than exists in the east; it contains small, apparently inactive pockmarks, although multidisciplinary investigations point to the presence of methane in the subseafloor (e.g., Bünz et al., 2012; Consolaro et al., 2015; Plaza-Faverola et al., 2015; Sultan et al., 2020).

Site U1619 (Lucchi et al., 2023) on the Vestnesa Ridge west termination was chosen as the northernmost site of Expedition 403. The site is well situated to provide a record of both high-resolution variability and long-term changes in the northward penetration of North Atlantic waters transported by the WSC across the gateway to the Arctic (Fram Strait). The more distal setting of Site U1619 compared to Site U1618 also provides the opportunity to laterally trace glaciogenic deposits originating from the paleo-SBSIS, as well as examine the history of Arctic sea ice extent into the Fram Strait. For these reasons, sediment drift Site U1619 is ideal for paleoceanographic and paleoclimatic studies that can complement the research from prior scientific ocean drilling sites farther north (e.g., ODP Sites 910 and 912 [Yermak Plateau]) and to the south (e.g., ODP Sites 908 [Hovgaard Ridge] and 909 [Molloy Basin]) (Myhre et al., 1995; Thiede and Myhre, 1996). Seismic Reflectors R1–R8 were drilling targets for Site U1619, with a total depth target of 696 mbsf (Figure **F12**). No gas hydrate–related BSR was detected close to Site U1619.

At Site U1619, the main initial objective was to recover a complete stratigraphy from Seismic Reflector R8 (~5.8 Ma) to present. Such recovery would support the following research goals:

- Definition of a high-resolution sediment stratigraphy since the Late Miocene–Early Pliocene transition;
- Reconstruction of the variability of the WSC transporting warm Atlantic Water to the Arctic;
- Definition of the effect of glacial and tectonic stresses on subseafloor sediment deformation and carbon migration/transfer; and
- Investigation of the influence of the WSC variability, ice coverage, and climate on the microbial populations through time and to what extent this is still affecting contemporary geochemical fluxes.

4.2.2. Operations

Site U1619 comprises a single hole (U1619A) drilled at a 1676 m water depth and reaching a subseafloor penetration of 628 mbsf (Figure **F5**; Table **T1**). Hole U1619A is positioned at the cross point of two seismic lines: CAGE20-5-HH-10-2D and CAGE20-5-HH-11-2D (Figure **F12**). The hole was spudded on 23 June 2024. Because the Vestnesa Ridge is known to contain gas hydrates and free gas, methane and other hydrocarbon gases were monitored with headspace gas measurements on each core and select void gas sample (VAC) sampling. Although gas expansion affected core recovery and handling, the C_1/C_2 ratios remained inside the safety zone for drilling operations (Figure **F7**). To relieve gas overpressure, holes were drilled into liners both by the drill crew on the rig floor and the technical staff on the core receiving platform. Shattered liners were an occasional challenge. As formation characteristics changed, deployment of the APC system shifted to the HLAPC system and later to the XCB drilling system at depth. Most XCB cores were advanced by 6–8 m to allow for gas expansion of the sediments in the liners. Gas expansion resulted in core recoveries typically between 104% and 120%. To minimize magnetic overprinting on the cored sediment, the nonmagnetic collars and core barrels were used for all APC and HLAPC coring. A total of 85 cores were drilled: 11 APC (13%), 11 HLAPC (13%), and 63 XPC (74%). The cored interval of 627.9 m resulted in a recovered length of 728.35 m. Formation temperature measurements were taken with the APCT-3 and SET2 tools.

Ice navigation was essential for this site. When the marginal sea ice zone had moved to within 3 nmi of the vessel, the bridge determined that it was necessary to move off location. Hole U1619A was terminated on 28 June before sea ice began to move into the immediate area. At that point, a

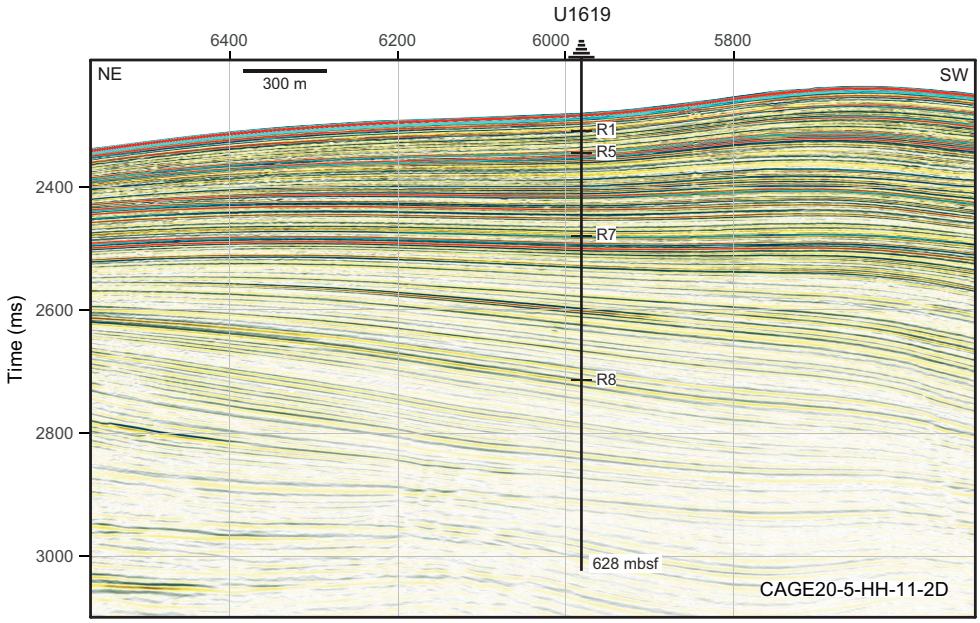

Figure F12. Seismic profile along northwest–southeast Seismic Line CAGE20-5-HH-11-2D showing the location of Site U1619 with interpreted Reflectors R1, R5, R7, and R8 and the maximum penetration depth of 627.9 mbsf.

drilling depth of 629.9 m had been reached. A free-fall funnel was deployed in hopes that the ship could reoccupy the hole to reach the target depth (696 mbsf); however, ongoing unfavorable sea ice conditions prevented a return to this location. A total of 5.2 days were spent on Hole U1619A, which provided the longest cored sequence of the expedition.

4.2.3. Principal results

4.2.3.1. Lithostratigraphy

The Site U1619 sediments are primarily siliciclastic, composed of gray to dark greenish-gray silty clay, clayey silt, clay, and sandy mud. Sediments are commonly bioturbated from the base of the record to ~175 mbsf, with occasionally laminated intervals occurring from the base of the record to ~268 mbsf (Figure **F9**). These depositional characteristics suggest the older sequence at Site U1619 contains a long duration contouritic deposition settled under variable-strength and well-oxygenated bottom currents. Detrital clasts are present throughout the stratigraphic record (Figures **F8A**, **F9**), with a stepwise, uphole increase in clast abundances at ~268 mbsf. The timing closely matches the initial, regular appearance of dark patches on the split core surface and likely marks the expansion of NHG. High clast abundance continues to ~170 mbsf; above this depth the clast abundance becomes more variable, possibly in response to global climate cycles, sea ice variability, and the dynamics of the paleo-SBSIS.

Similar to Site U1618, diagenetic overprinting of the primary depositional record at Site U1619 is documented by the presence of authigenic carbonate minerals in the form of layers, laminations, granular crystals, and iron sulfide (pyrite and/or greigite) minerals, which typically occur as burrow infillings and concretions (Figure **F8B**). Authigenic mineral occurrences are most common below ~150 mbsf. The iron sulfide intervals typically corresponded to very high MS values and were often associated with high-density materials in X-ray images (Figure **F8B**).

4.2.3.2. Biostratigraphy

No microfossil group (Figure **F10**) is consistently present in the Site U1619 sediment record, and several intervals were barren. Calcareous nannofossil concentrations range from rare to common, and assemblages with moderate to good preservation appear intermittently across the entire cored sequence. Some intervals of reworked nannofossils were also intermittently noted. Diatom assemblages are primarily present at the core top, although some intervals at depth contain traces of poor assemblages formed by highly silicified diatoms. Dinocysts are present throughout the sediment record, with the number of taxa decreasing downhole. Small acritarchs were also recorded, especially at depth. Moderately preserved foraminifers are present with rare to frequent occurrences in the upper part of Site U1619 and are present intermittently downcore. Below ~400 mbsf, samples are barren of foraminifers.

Paleoenvironmental information based on the latest Pleistocene microfossil assemblages indicates Arctic-polar water with seasonal sea ice, with occasional influence of warm Atlantic waters. Given the many barren intervals and limited assemblage counts, any environmental conclusions for the older Site U1619 sediments are premature.

The combined information yields of all microfossil groups contributed to an initial biostratigraphy for Site U1619, with calcareous nannofossil zones and dinocyst/acritarch age markers providing the backbone of the record (Figure **F10**). An acritarch with a Late Miocene–Pliocene age range is present near the base of the sampled record. Collectively, the suite of age-diagnostic microfossils indicates a highly expanded Late Miocene to Early Pleistocene record at Site U1619. A Late Pleistocene record, containing interglacial MISs, including 5 and 7–13, are confirmed by multiple biostratigraphic age markers.

4.2.3.3. Paleomagnetism

Site U1619 had similar magnetic properties to Site U1618. Anhysteretic remanent magnetization (ARM) coercivity, tracked by the ARM_{30mT}/ARM ratio, shows a wide range of values and has a bimodal distribution (Figure **F11**), which is likely indicative of the sediments containing a mix of detrital and authigenic (e.g., greigite) mineral sources. Further work using temperature-dependent, in-field, mineralogical, and scanning electron microscope (SEM)/energy dispersive

spectrometry (EDS) methods will be needed to gain a more complete understanding of the magnetic minerals present at both Vestnesa Ridge sites.

Based on shipboard rock magnetic investigations, low MS intervals were identified as having a greater potential to record high-fidelity remanent magnetization. Therefore, discrete cube samples from undisturbed low MS intervals were used to refine the magnetic stratigraphy derived from the archive section half NRM and alternating field demagnetization data. A number of polarity reversals were identified using this process, with depth uncertainties ranging <1–40 m. Postexpedition analyses of cube samples will aim to reduce these and other difficult to quantify uncertainties. The Site U1619 magnetic stratigraphy indicates that the recovered sequence captures the entire Pliocene and Pleistocene record, which is particularly expanded during the Pliocene and Early Pleistocene in agreement with biostratigraphic interpretations. The base of recovery contains sediments deposited in the latest Miocene during Chron C3r (lower Gilbert), younger than 6 Ma.

4.2.3.4. Age model

The preliminary age model based on the combined magnetic stratigraphy and biostratigraphy indicates linear sedimentation rates of approximately 110 m/My from the base of the record until ~3.8 Ma (Figure **F13**). Between 3.8 and 2.0 Ma, sedimentation rates were approximately 160 m/My, indicating continuous high rates of deposition during both the warm mid-Pliocene and the transition to widespread NHG. After 2 Ma, sedimentation rates decrease drastically: first decreasing to ~70 m/My between about 2 and 1 Ma and then decreasing to approximately 30 m/My since 1 Ma. This later change in sedimentation rates coincides with the MPT, and it is also observed at the eastern Vestnesa Ridge (Site U1618). Site U1619 is well suited to examine if more extensive sea ice cover (e.g., Stein and Fahl, 2013) may have a role in changing depositional patterns and thus sedimentation rates in the Fram Strait region.

4.2.3.5. Physical properties

Like Site U1618, the measured physical property data for Site U1619 show relationships to both lithologic and paleomagnetic findings. MS peaks orders of magnitude higher than the background appear below ~150 mbsf and become more prominent downcore. These MS maxima are likely associated with the formation of authigenic iron sulfide minerals including greigite. There is a positive linear correlation between NGR and GRA bulk density; both generally show high-amplitude variability in the uppermost ~270 m, and the mean values of both parameters increase downhole. Both parameters have modes that differ between the clast-rich silty clays present in the upper part of the record and the bioturbated, clast-poor silty clays present in the lower part of the record. Two different MS modes are observed within the lower lithostratigraphic unit (below ~268 m): broad stratigraphic intervals of low MS (<50 IU) alternating with shorter stratigraphic intervals of large MS peaks. Higher NGR and GRA bulk density combined with both low and high MS modes may suggest that clay-rich (high NGR), compacted sediments (high GRA bulk density) are less likely to accommodate fluid movement, leading to greater retention of a primary magnetization (low MS) flanked by horizons associated with the formation of authigenic iron sulfide minerals (high MS). This hypothesis can be explored further with postexpedition analyses.

In addition to standard shipboard physical property data collection, Site U1619 included one whole-round sample that relates to the tectonic objectives of the expedition. Initial results show that after temperature equilibrium, strain released logarithmically. Initial results also show some shrinking, which is hypothesized to be related to pore pressure changes from degassing.

4.2.3.6. Stratigraphic correlation

Because only a single hole was drilled at Site U1619, there was no need for stratigraphic correlation. Very good recovery with minimal coring gaps provides a good record for long-term reconstructions. The CCSF scale takes into account core expansion and has a growth factor of ~1.18. Calculation of mass accumulation rates based on the CCSF scale should account for the expansion by dividing apparent depth intervals by the appropriate growth factor.

4.2.3.7. Geochemistry

Shipboard sulfate measurements of the Site U1619 IW and headspace gas measurements indicate that the SMTZ is likely between ~7 and 18 mbsf. The geochemical profiles above and within the

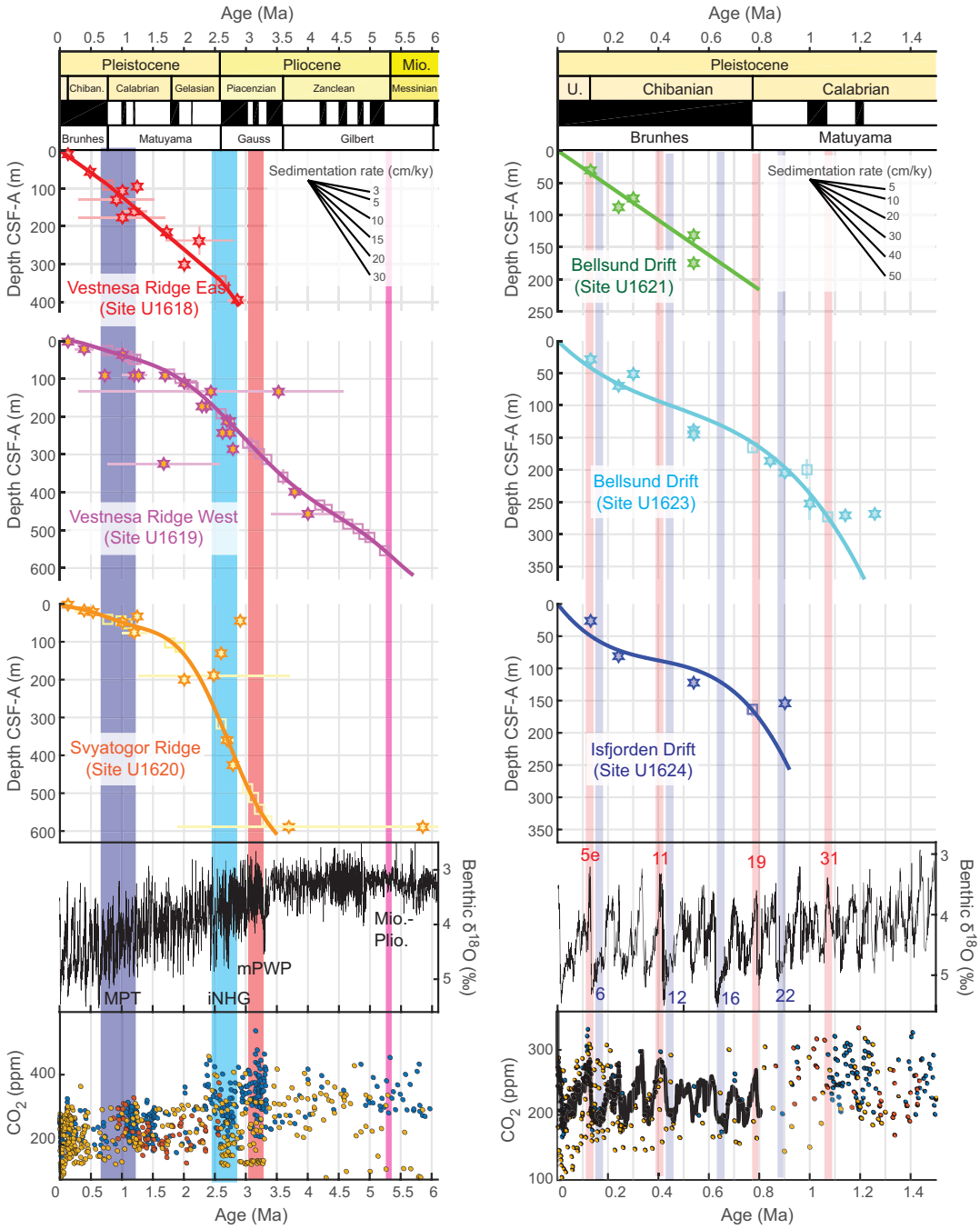

Figure F13. Approximate age-depth relationship, Expedition 403. Biostratigraphic constraints from calcareous nannofossils, planktonic foraminifers, diatoms, and dinocysts (stars); magnetic reversals (squares); and a polynomial fit to select age constraints (dark solid line) are shown. Depth and age ranges for the stratigraphic constraints are indicated with light horizontal and vertical lines, respectively. Top: 2020 Geologic Timescale (Gradstein et al., 2020). Bottom: benthic $\delta^{18}O$ compilation of Westerhold et al. (2020), which uses data from a Ceara Rise stack (Bickert et al., 1997; Wilkens et al., 2017), ODP Site 1264 (Westerhold et al., 2020), and IODP Site U1337 (Drury et al., 2017; Tian et al., 2018) in this interval. Estimates of atmospheric CO_2 concentration from the compilation of The Cenozoic CO_2 Proxy Integration Project (CenCO2PIP) Consortium (2023) from boron proxies (blue), phytoplankton proxies (yellow), and paleosols (red) are shown (Andersen et al., 1999; Badger et al., 2013, 2019; Bolton et al., 2016; Brown et al., 2022; Da et al., 2019; de la Vega et al., 2020; Dyez et al., 2018; González-Lanchas et al., 2021; Henehan et al., 2013; Jasper and Hayes, 1990; Martínez-Botí et al., 2015; Rae et al., 2021; Seki et al., 2010; Sosdian et al., 2018; Tanner et al., 2020; Zhang et al., 2017, 2019, 2020). Black line = Bereiter et al. (2015) compilation of atmospheric CO_2 reconstructed from Antarctic ice cores (Ahn and Brook, 2014; Bereiter et al., 2012, 2015; MacFarling Meure et al., 2006; Marcott et al., 2014; Monnin et al., 2001, 2004; Petit et al., 1999; Rubino et al., 2013; Schneider et al., 2013; Siegenthaler et al., 2005). Key climate transitions and isotopic stages that these new records capture are indicated. iNHG = inception of Northern Hemisphere glaciation, Mio-Plio = Miocene–Pliocene transition.

SMTZ show decreases in salinity, Ca, magnesium (Mg), strontium (Sr), Fe, manganese (Mn), and sulfate (SO_4^{2-}) and increases in barium (Ba), phosphate (PO_4^{3-}), alkalinity, and ammonium (NH_4^+). Below the SMTZ, Mg concentrations and alkalinity continue to decrease, whereas Ca, Sr, Ba, lithium (Li), and PO_4^{3-} concentrations increase. Reducing conditions and diagenetic processes associated with free gas and possible gas hydrate are likely important controlling processes on several of the IW profiles, as well as on methane and other hydrocarbon abundances at Site U1619. In addition, sediment geochemistry results showing highly variable calcium carbonate ($CaCO_3$) abundances that peak at ~480 mbsf likely point to authigenic mineral formation during diagenesis (Figure **F8B**).

Other geochemical results appear to be driven by paleoceanographic and/or paleoclimatic processes. Dissolved silica (Si) shows considerable stratigraphic variability. The maximum Si in IW appears at ~280 mbsf, which, given the initial age model, may correspond to mPWP. The C/N ratio shows stratigraphic variations as well. After an increase in mean C/N ratios from the base of the record to ~380 mbsf, the C/N ratio decreases to its lowest level at ~280 mbsf, indicating a strong marine organic carbon signal at that time. A second stepwise increase in the C/N ratio immediately follows and peaks at ~150 mbsf. This timing suggests increased organic matter from continental sources during the intensification of NHG.

4.2.3.8. Microbiology

In addition, microbiological sampling of the sediment at ~400 mbsf was done to test (postexpedition) for the oldest recoverable sedaDNA.

4.2.3.9. Downhole measurements

Borehole measurements made while coring Hole U1619A show that formation temperature at the western Vestnesa Ridge increases almost linearly with depth and has a geothermal gradient typical for oceanic sediments when compared with the statistical data set (Kolawole and Evenick, 2023).

4.3. Site U1620

4.3.1. Background and objectives

The Svyatogor Ridge is a northwest–southeast elongated contouritic sediment drift lying on a young (<10 Ma) oceanic crust. This sediment drift has a length of 46 km and a width of 5 km (Johnson et al., 2015; Waghorn et al., 2018) and is located ~130 km from the western margin of Svalbard on the northwestern flank of the ultraslow-spreading Knipovich Ridge, south of the MTF (Figure **F1**) (see **Background and objectives** in the Site U1620 chapter [St. John et al., 2026b]). The sediment record at Svyatogor has been influenced by multiple factors, including the locally complex tectonic history, the evolution of the WSC, the development of regional ice sheets, and the presence and migration of methane gas with likely biotic and abiotic sources (Waghorn et al., 2020).

According to Eiken and Hinz (1993), three main stratigraphic units provide the chronological constraints on the northwestern margin of Svalbard. Unit YP-1 is the oldest, and it is composed of syn- and postrift sediments lying directly on the oceanic crust after the opening of the Fram Strait during the Early Miocene (~17 Ma; Jakobsson et al., 2007; Ehlers and Jokat, 2013), creating an environment favorable for the onset of contour currents (Eiken and Hinz, 1993; Gebhardt et al., 2014). Seismic Stratigraphic Unit YP-2 contains the sedimentation associated with contour current deposition having a basal age between ~7 and 10 Ma (Eiken and Hinz, 1993; Gebhardt et al., 2014), whereas Unit YP-3 comprises the deposition associated with the onset of glacially transported sediments like glaciomarine deposits and glacial debris flows. Correlation with the cores drilled during ODP Leg 151 indicates a boundary age between Units YP-2 and YP-3 of ~2.7 Ma, corresponding to the intensification of the NHG (Geissler et al., 2011; Mattingsdal et al., 2014). Based on the supposition that the Svyatogor Ridge experienced its initial growth as a southern extension of the Vestnesa Ridge across the MTF at ~2.7 Ma (Johnson et al., 2015), Unit YP-3 and potentially the upper portion of Unit YP-2 should also be present on the Svyatogor Ridge.

Besides this general stratigraphic information for the area, the chronostratigraphy at the Svyatogor site is largely unknown because exploration has mostly been limited to geophysical surveys focused on characterizing the unique fluid flow system of this ridge. Because of the underlying young crust and the proximity to the ultraslow-spreading Knipovich Ridge, the Svyatogor sediment drift likely contains a unique combination of biogenic-derived methane and abiotically derived gas generated from the serpentinization of exhumed mantle rocks; this complex system contributes to an extensive occurrence of free gas, gas hydrate, and fluid flow systems in the region, with gas chimney and faults acting as a major pathway for fluid migration (Johnson et al., 2015; Waghorn et al., 2020).

Site U1620 (Lucchi et al., 2023) on the Svyatogor Ridge was chosen for its distal location from the western margin of Svalbard; therefore, it has a reduced (yet discernible) continental influence on the sedimentation and an enhanced paleoceanographic signal that is mainly driven by the oceanic current. The relationships between sediment drift development, bathymetry, and tectonic motion are additional factors unique to this location that can be examined. Furthermore, because this is an almost unexplored area, the documented presence of a young oceanic crust and active seepage system can drive unexpected new findings in relation to fluid flow, diagenesis, and the subsurface microbial community.

At Site U1620, the main initial objective was to recover a complete stratigraphy from Seismic Reflector R7 (2.7 Ma) to present. Such a recovery would support the following research goals:

- Definition of a high-resolution sediment stratigraphy since the Late Pliocene intensification of the NHG;
- Reconstruction of the variability of the WSC transporting warm Atlantic water to the Arctic;
- Definition of the effect of glacial and tectonic stresses on subseafloor sediment deformation and carbon migration/transfer; and
- Investigation of the influence of the WSC variability, ice coverage, climate, and the active seepage system on the microbial populations through time and to what extent this is still affecting contemporary geochemical fluxes.

Additionally, because the drilled stratigraphic sequence at Site U1620 is the first recovered record of the Svyatogor Ridge that extends hundreds of meters deeper than any previous coring work in this area, there is a unique opportunity to groundtruth hypotheses concerning gas-charged sediment drifts that overlie young (i.e., warm) oceanic crust.

4.3.2. Operations

We arrived at Site U1620 (Lucchi et al., 2023) on 29 June 2024 after transiting from Site U1619. During the approximately 8 days on site, four holes were drilled along Seismic Line Svyatogor2014_3D-XL222 (Figure **F14**) and one hole was logged (Table **T1**; Figure **F5**). The holes are between 1589 and 1609 meters below sea level (mbsl). Careful attention was given to the location of holes because of the tectonic setting and subseafloor gas hydrate system. Hole U1620A is located ~0.75 km northeast of a fault, which on seismic profile (Figure **F14**) appeared to be a conduit leading to a gas chimney. Holes U1620B–U1620D are located within 200 m northeast of Hole U1620A, away from these subsurface features. The mudline was poorly recovered in Hole U1620B, and therefore Hole U1620C was spudded immediately adjacent to it. Hole U1620D is located approximately halfway between Holes U1620A and U1620B/U1620C and is the deepest hole, meeting the target depth of 616 mbsf; therefore, it was selected for logging. The combined cored interval from all four holes was 1026.2 m.

The presence of subsurface gas was a challenge at each hole. Methane and other hydrocarbon gases were monitored with headspace gas measurements on each core and select VAC sampling. Although C_1/C_2 ratios consistently plotted in or near the anomalous zone for the uppermost 255 m in all holes (Figure **F7**), the methane was deemed biogenically sourced and coring was approved to continue. When C_1/C_2 ratios remained low in several consecutive cores and higher hydrocarbons (e.g., C_5 and C_6) were also present, the holes were terminated. For gas safety when handling the cores and to minimize core expansion, holes were drilled into the liner on the rig floor and on the core receiving platform and Kevlar blankets were used as shields during the initial core handling.

Shattered or broken liners were common. Core expansion resulted in core recovery often exceeding 100%, with a total recovered length of 1132.2 m (110%). Knowing that the Site U1620 sediment sequence overlies young (i.e., warm) oceanic crust and that the geothermal gradient factors into the gas safety evaluation, additional borehole temperature measurements were made. These measurements ceased when the borehole SET2 tool approached the instrumental limit (50°C). As formation characteristics changed at each hole, deployment of the APC system shifted to the XCB drilling system at different depths with advances by 6–8 m to allow for gas expansion of the sediments in the core liner. At Site U1620, a total of 126 cores were retrieved: 38 APC (30%) and 88 XCB (70%). To minimize magnetic overprinting on the cored sediment, the nonmagnetic collars and core barrels were used for all APC coring.

Hole U1620A was started on 29 June. Cores 1H–31X penetrated from the seafloor to 239.9 mbsf with a recovery of 116%. Formation temperature measurements were taken on core runs for Cores 4H, 7H, 10H, and 13H using the APCT-3 tool. Two additional temperature measurements were taken using the SET2 probe after Cores 18X (48 mbsf) and 31X (239.9 mbsf). In total, we spent 1.7 days on Hole U1620A.

Hole U1620B was offset 200 m from Hole U1620A at a bearing of 63.9°. It was spudded on 30 June, but after two attempts at a mudline core and a recovery of only 0.34 m, the hole was terminated. Hole U1620C was promptly spudded at the same location and retrieved a good mudline core. A total of 21 cores (1H–21X) were taken in Hole U1620C over a 169.9 m interval with 186.9 m recovered (109.99%). The APCT-3 tool was deployed on Cores 4H, 7H, 10H, and 13H for in situ temperature measurement. Coring was terminated on 1 July.

Hole U1620D was offset 100 m southeast of Hole U1620C at a bearing of 244°, halfway toward Hole U1620A. The first core was spudded on 2 July. A total of 73 cores were taken in Hole U1620D. The cored interval spanning Cores 1H–73X was 616 m long, and the recovery was 667.89 m (108.42%). The SET2 tool was used to take the two deepest borehole temperature measurements for the site: one after Core 38X (298 mbsf) and one after Core 44X (346.8 mbsf). Because Hole U1620D was the deepest hole, it was selected for wireline logging. The triple combo logging tool string was successfully deployed and collected geophysical borehole data; however, due to poor hole stability, the planned logging run of the FMS-sonic tool was canceled and operations were terminated on 6 July. In total, we spent 4.8 days on Hole U1620D and 7.7 days at Site U1620.

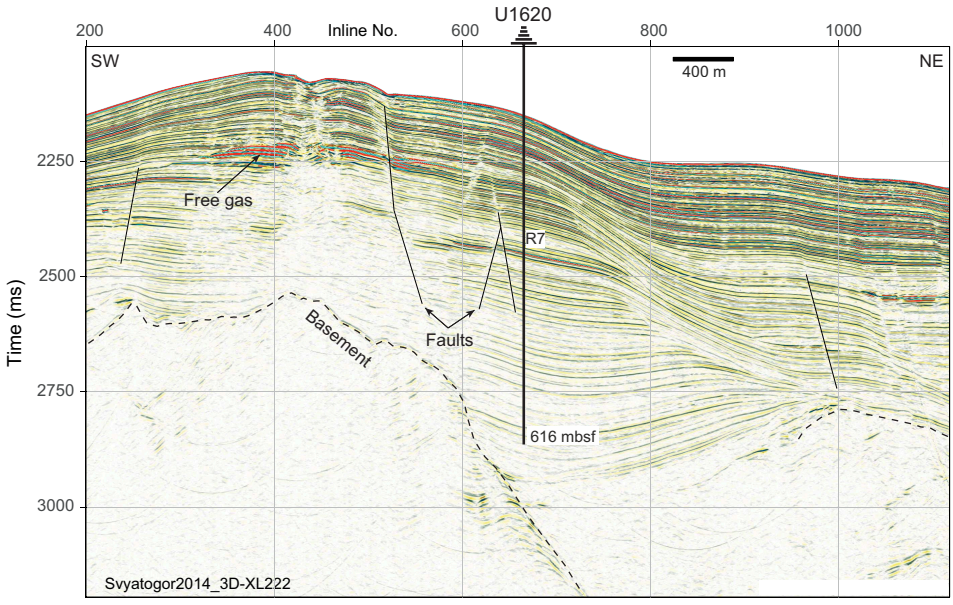

Figure F14. Seismic profile along southwest–northeast Seismic Line Svyatogor2014_3D-XL222 showing the location of Site U1620 with interpreted Reflector R7 and the maximum penetration depth of 616 mbsf. Interpreted location of the underlying basement, multiple faults, and free gas are also shown.

4.3.3. Principal results

4.3.3.1. Lithostratigraphy

The entire record at Site U1620 is siliciclastic dominated, composed primarily of gray/dark gray to greenish gray silty clay, with coarser intervals of clayey silt, sandy clay, sandy mud, and uncommonly diamicton (Figure **F8A**). The stratigraphically deepest part of the record tends to be more clay rich overall; coarser intervals become more common above ~321 mbsf. Dispersed to abundant detrital clasts are present throughout, with stepwise increases in abundance above ~334 mbsf, likely corresponding to the expansion of NHG, and above ~220 mbsf, possibly corresponding to a second-phase expansion of the paleo-SBSIS. Toward the top of the sequence, above ~30–50 mbsf, silty lithologies dominate, whereas clast abundance is more variable by hole. This lithologic transition appears to occur during the MPT (~0.9–1.0 Ma). Throughout the record, heavily bioturbated intervals tend to contain fewer large clasts. Laminated intervals are infrequent and contain varying amounts (none to abundant) of clasts.

Secondary minerals, including authigenic carbonate (e.g., calcite and siderite) and iron sulfides (e.g., pyrite and/or greigite) are evidence of postdepositional alteration likely caused by elemental exchanges between the sediment and IW as fluids migrate in this gas- and gas hydrate–enriched sediment drift. Authigenic carbonate minerals occur in many forms, including as selective laminations (Figure **F8B**), granules, and nodules, as well as intergranular cement, lithifying sand-rich layers over 10 cm thick. These minerals appear below ~118 mbsf and are most abundant below ~550 mbsf. Authigenic iron sulfide minerals often appear as granular layers and as burrow infillings; they begin to appear at ~110 mbsf and are most prevalent below ~155 mbsf.

4.3.3.2. Biostratigraphy

Preliminary shipboard analyses indicate that the presence of microfossil groups (Figure **F10**) at Site U1620 ranges from abundant to barren. Calcareous nannofossils appear intermittently; when present, the diversity is low but the concentration of specimens ranges between common and abundant with moderate to good preservation. Planktonic foraminifers are low in diversity and appear more preservationally challenged than the calcareous nannofossils, showing deterioration at 39 mbsf, and are generally absent below 40 mbsf. Rare encrusted and/or partially dissolved planktonic foraminifers reappear near the base of the record. Samples are also almost barren of diatoms, except at the top of the record (Holocene), which shows well-preserved, high-diversity assemblages, and in some intermittent intervals downhole in Holes U1620A–U1620D. Dinocyst assemblages are also low in diversity but present throughout the Site U1620 record with few exceptions. The dinocysts show good to excellent preservation in the upper part of the record and medium to good preservation in the lower part of the record. Reworking of all microfossils is frequently observed, likely related to transport and redeposition of glacially eroded old stratigraphic units from the Svalbard margin. Reworked palynomorphs include large amounts of terrestrial plant material.

Initial paleoenvironmental assessment based on the microfossil assemblage suggests a Pleistocene paleoenvironment dominated by Arctic to polar surface waters with (seasonal) sea ice, as well as times with cool-temperate conditions, increased presence of Atlantic water, and seasonal sea ice. During the Late Pliocene, sea ice was reduced and surface waters were temperate.

Shipboard biostratigraphic data show that the Site U1620 stratigraphy ranges in age from at least the Late Pliocene to Pleistocene, with Holocene at the very top of the record. Age-diagnostic markers for intervals containing MISs 1–5 and 7–13 and older warm interglacial periods (e.g., MIS 31) are present, as well as taxa that place the deeper samples firmly in narrow age brackets within the Middle and Early Pleistocene, and the Late Pliocene.

4.3.3.3. Paleomagnetism

The sediment magnetic properties at Site U1620 are similar to those observed at Sites U1618 and U1619, reflecting contributions from both detrital and authigenic sources. Additional shipboard analyses were done to evaluate the magnetic overprinting from authigenic iron sulfide (e.g., greigite; Figure **F11**) formation that produces anomalously high MS peaks and chemical remanent magnetization that is younger than the detrital remanent magnetization of the surrounding sediment. Whereas Pleistocene magnetic reversals could be identified from archive-half measure-

ments, a Late Pliocene magnetic polarity pattern emerged by filtering discrete-sample NRM data for intervals with lower MS and by augmenting routine NRM analyses with additional rock magnetic experiments. Magnetic chrons from the top of Chron C2An.1n (Gauss/Matuyama Boundary; 2.6 Ma) through the C2An.2r Subchron (Mammoth; 3.21–3.33 Ma) were identified.

4.3.3.4. Age model

Biostratigraphy and magnetostratigraphy are the basis for the preliminary age-depth model for Site U1620 (Figure **F13**). These data are in good agreement for the uppermost ~115 m and below ~420 mbsf, but some age discrepancies exist between these horizons; additional sampling and postexpedition analyses are needed to better constrain ages. The preliminary age model indicates a very high sedimentation rate of approximately 325 m/My between ~3.33 and ~2 Ma. In contrast, between 2 and 1 Ma, average sedimentation rates were probably closer to 75 m/My, and since 1 Ma they have been approximately 50 m/My.

4.3.3.5. Physical properties

Physical property measurements of NGR and GRA bulk density display robust and correlative patterns suggestive of cyclicities throughout the Site U1620 sediment record. MS also correlates with these data from the seafloor to ~125 mbsf, below which iron sulfide minerals cause authigenic magnetic overprinting. Color reflectance (L*) of the split core surfaces shows patterns suggestive of orbital cyclicity throughout the record and additionally displays prominent long-term (30–90 m thick) packages of lighter versus darker sediment that occur below ~125 mbsf (Hole U1620D); this depth coincides with the four-fold change in sedimentation rates at ~2 Ma. The physical property measurements included three ASR experiments to study tectonic stress. Similar to Sites U1618 and U1619, initial findings show strain released logarithmically, but some strain gauges showed shrinking. Information on principal stress azimuths will be determined after postexpedition data processing.

4.3.3.6. Stratigraphic correlation

Stratigraphic correlation for holes at Site U1620 was primarily accomplished using MS. The best recovered stratigraphy of Hole U1620D was used as the backbone of the splice. Because core recovery was generally good, most coring gaps could be covered using data from Holes U1620A, U1620C, and U1620D down to ~190 m CCSF, and from Holes U1620A and U1620D between ~191 and 271 m CCSF. Only Hole U1620D extends below 271 m CCSF. Gas expansion below ~134 mbsf resulted in growth factors of 15%–30%, which was consistent among all three holes. Calculation of mass accumulation rates based on the CCSF scale should therefore account for the expansion by dividing apparent depth intervals by the appropriate growth factor.

4.3.3.7. Geochemistry

The IW geochemistry, bulk sediment geochemistry, and headspace gas primarily reflect the influence of deep fluid flow migration at Site U1620. The IW profiles of salinity, Cl, and Na are reflective of (bio)geochemical impacts of a gas hydrate system on IW chemistry at the Svyatogor Ridge. Elemental analysis of bulk sediment samples revealed overall high concentrations of carbon and nitrogen across most intervals, with variations being related to the lithologic changes. The C/N ratios, an indicator of the relative contribution of marine and terrestrial sources of carbon, show inflection points and trends that appear to coincide with some global-scale changes in climate and ocean conditions. Peaks in $CaCO_3$ abundance correlate to high total carbon (TC) and are likely indicators of authigenic carbonate minerals in the sediment. TOC ranges between 0.5 and 1.5 wt% and generally shows an inverse relationship to the alkalinity of the IW, suggesting that the changes in TOC may be closely related to methanogenesis accompanied by the decomposition of organic matter. The SMTZ at Site U1620 is near the sediment/water interface, which is expected given the high methane supply in the sediment (generally above 5000 ppmv). Immediately below the SMTZ, the methane profile increases (~20 mbsf) and then decreases (~80 mbsf) and remains relatively stable before increasing again from 516 mbsf to the bottom of the record. The extrapolated temperatures of the sediment toward the base of the hole imply that the elevated methane levels at depth are not from an active biological process of methanogenesis, given the thermal limitations of methanogenic microbes (Katayama et al., 2022). The additional presence of heavier C_2–C_6 hydrocarbons at depth suggests either a thermogenic source (i.e., heating of buried organic mat-

ter) or an abiotic source, with the most likely candidate being the serpentinization of ultramafic basement rocks (Johnson et al., 2015).

4.3.3.8. Microbiology

At Site U1620, microbiological sampling for sedaDNA followed the procedures used at Site U1618. Low-resolution sampling spanned the Holocene to Early Pleistocene. High-resolution sampling focused on two intervals tentatively identified by biostratigraphy, magnetostratigraphy, and physical property patterns as interglacials MISs 5e through 11 and 31. In addition, an exploratory sample to test for preservation of the oldest sedaDNA was taken deeper in the core record.

4.3.3.9. Downhole logging

Borehole logging data suffered from noises caused by alternately swelling and washed-out formations, especially in the uppermost 260 m. The logging natural gamma ray values are lower than those from shipboard scanning but show almost the same trends, and core and log depth scales can be readily correlated. Downhole logging (Hostile Environment Litho-Density Sonde [HLDS]) density measurements are very similar to densities derived from shipboard GRA core scans and discrete moisture and density measurements within the intervals with good borehole condition. Accelerator Porosity Sonde (APS) porosity data are extremely limited and show unclear and unstable trends in the available data. No significant downcore trend was observed in electrical resistivity measurements. Borehole temperature measurements made in Holes U1620A, U1620C, and U1620D show formation temperature at the Svyatogor Ridge increased almost linearly with depth, and the slope of linear regression provides a higher geothermal gradient than typical oceanic sediments compared to the statistical data set (Kolawole and Evenick, 2023).

4.4. Sites U1621–U1623

4.4.1. Background and objectives

The Bellsund drift drilling sites (Figure **F1**) (see **Background and objectives** in the Sites U1621–U1623 chapter [Lucchi et al., 2026c]) are located on a plastered sediment drift that developed along the lower continental slope (1700–1800 m water depth) of the western margin of Svalbard under the influence of the northward-flowing WSC (Rebesco et al., 2013). The Bellsund drift has built up over millions of years since the opening of the Fram Strait (17–10 Ma; Jakobsson et al., 2007; Engen et al., 2008; Ehlers and Jokat, 2013) that determined the onset of the contour current circulation system in the area (Eiken and Hinz, 1993; Gebhardt et al., 2014), with development of sediment drifts covering large areas of the European North Atlantic margin including the Norwegian Sea, Barents Sea, western margin of Svalbard, and eastern side of the Fram Strait (Laberg et al., 2005). The Bellsund drift recorded the continental input associated with the expansion and retreat of the paleo-SBSIS during the past glacial and interglacial cycles (glacial debris flows and sediment-laden meltwater plumes) and the variability of the warm WSC through its effect on the marine biological productivity in the water column (Lucchi et al., 2018; Caricchi et al., 2019; Torricella et al., 2022, 2025; Gamboa Sojo et al., 2024). Its location between the Storfjorden TMF to the south and the Bellsund TMF to the north provided some protection from direct glaciogenic input from the paleo-SBSIS during the past glaciations while still capturing a record of the ice sheet dynamics.

Piston core work in this area demonstrates that the Bellsund drift is an excellent setting to recover continuous, expanded, and datable sedimentary sequences for detailed paleoclimatic and paleoceanographic analyses. The 2014 Eurofleets2 PREPARED project (Lucchi et al., 2014) recovered a long Calypso piston core from the Bellsund drift that contains a continuous, very expanded paleoclimatic record spanning the last 40 ky with up to subcentennial resolution. A robust age model was defined through paleomagnetic and biostratigraphic analyses, the identification of tephras, and radiocarbon dating of the abundant biogenic carbonate fraction (Caricchi et al., 2019, 2020). The sedimentologic analyses indicated the consistent presence of contouritic deposition and the existence of short-lived, abrupt depositional events associated with prominent meltwater events, including the MWP-1A (Lucchi et al., 2013, 2015), the MWP-19ka (Caricchi et al., 2019), and Heinrich-like events indicating a highly dynamic paleo-SBSIS during the last 60 ky (Lucchi et al., 2018; Caricchi et al., 2019).

The drill sites on the Bellsund drift are designed to recover an expanded sedimentary sequence to specifically examine suborbital oscillations of the last 100 ky, the MBE (~400 ka), the MPT (~1.2–0.7 Ma), and the primary establishment of shelf edge glaciation in this area at about 1.3 Ma corresponding to Seismic Reflector R4A (Rebesco et al., 2014b). Site U1621 (Lucchi et al., 2023) was chosen because seismic profiles indicate a highly expanded sediment record down to Seismic Reflector R3 (~0.75 Ma; Figure **F15A**), with sedimentation rates potentially exceeding 300 m/My. Three holes were drilled at Site U1621 down to Seismic Reflector R3 (~216 mbsf). Due to a discrepancy in coordinate transcription, Site U1622 was drilled into the Storfjorden TMF (Figure **F15B**) ~8 km from the intended location, down to 46.5 mbsf. Site U1623 (Lucchi et al., 2023) was located ~4.4 km downslope from Site U1621 to drill a longer record down to Seismic Reflector R4A (~1.3 Ma; ~347 mbsf; Figure **F15A**). Seven holes (U1623A–U1623G) were drilled at Site U1623 (Figure **F5**) with a maximum drill depth of 370 mbsf. Water depths at all three sites were between 1647 and 1708 m.

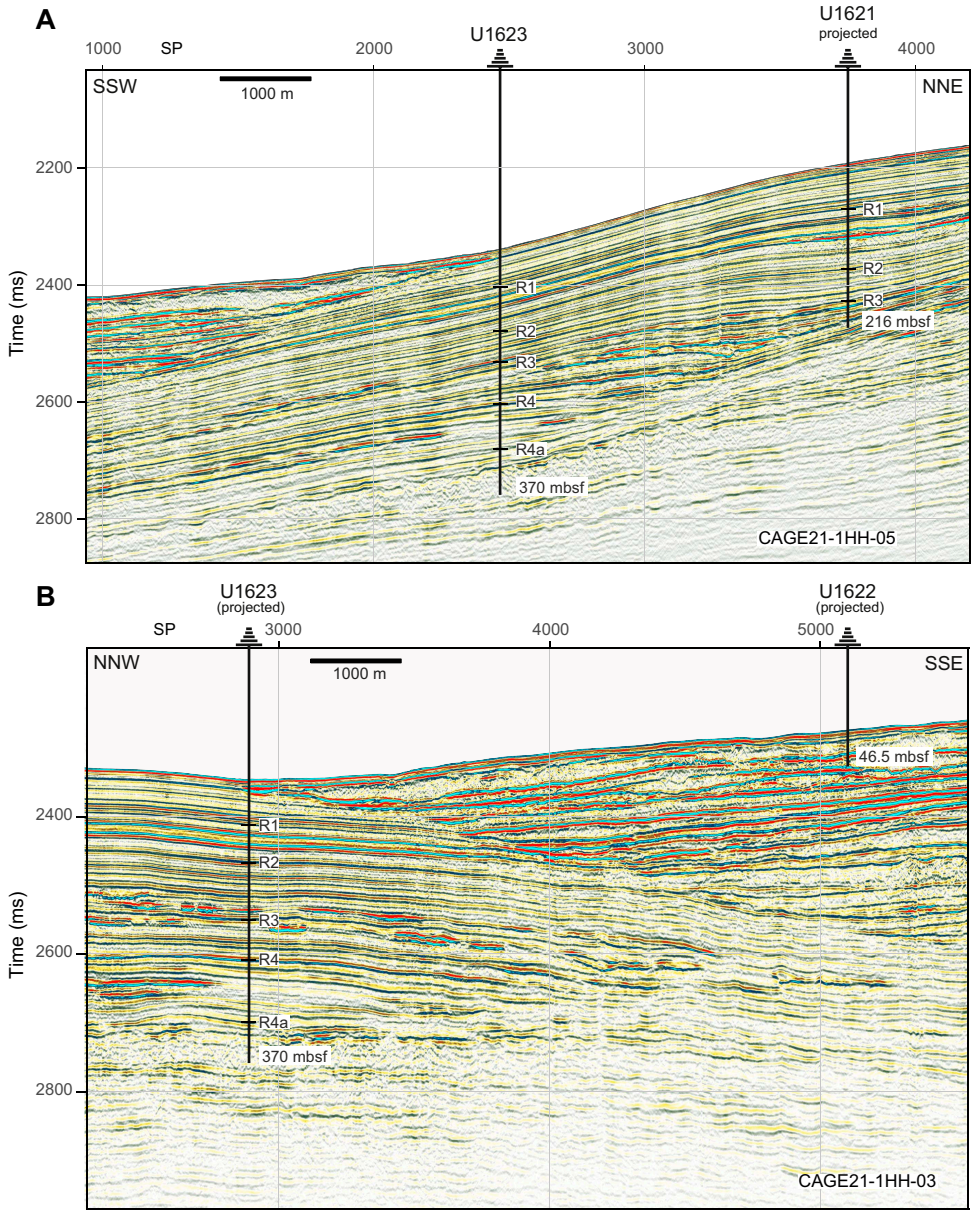

Figure F15. A. Seismic profile along northwest–southeast Seismic Line CAGE21-1-HH-05 showing the projected location of Site U1621 and the location of Site U1623 with interpreted Reflectors R1–R4a and the maximum penetration depth of 216 mbsf (Site U1621) and 370 mbsf (Site U1623). B. Seismic profile along northwest–southeast Seismic Line CAGE21-1HH-03 showing the projected locations of Sites U1623 and U1622 (penetration = 46.5 mbsf).

At Sites U1621 and U1623, the main initial objectives were to recover complete and overlapping stratigraphic sequences extending from the present down to Seismic Reflectors R3 (~0.75 Ma) and R4A (~1.3 Ma), respectively. Such a recovery would support the following research goals:

- Reconstruction of a high-resolution sediment stratigraphy since the onset of Pleistocene shelf edge glaciation;
- Study of ocean–cryosphere interactions and forcing mechanisms on the paleo–ice sheet dynamics; and
- Investigation of the influence of the WSC variability through time on the ice coverage, climate, and microbial populations and to what extent this is still affecting contemporary geochemical fluxes.

In addition, Site U1622 offers a unique opportunity for research on a sedimentary package recovered directly from the nearby TMF.

4.4.2. Operations

Operations for coring the Bellsund drift sites occurred over two time windows. Sites U1621 and U1622 and Holes U1623A–U1623C were drilled between 12 and 17 July 2024 (Table **T1**; Figure **F5**). Later, after completion of coring at Isfjorden drift (Site U1624), we returned to Site U1623 and drilled Holes U1623D–U1623G. This second period of Bellsund drift coring operations took place between 21 and 25 July. Fortunately, C_1/C_2 ratios consistently plotted in (or near) the normal range at all three sites (Figure **F7**). Gas expansion still occurred while coring some intervals, and it was standard practice to relieve gas pressure by drilling holes in the core liner when voids were observed. As formation characteristics changed at Sites U1621 and U1623, deployment of the APC and HLAPC systems shifted to the XCB drilling system, with advances by 6–8 m to allow for gas expansion of the sediments in the core liner. To minimize magnetic overprinting on the cored sediment, the nonmagnetic collars and core barrels were used for all APC/HLAPC operations at all three sites.

Three holes (U1621A–U1621C) were drilled at Site U1621 over 4 days; these are ~20 m apart along Seismic Line SV15-04. Although approved to drill to 397 mbsf, the highest priority was to recover an expanded Late Pleistocene sequence, which would be accomplished by reaching Seismic Reflector R3, a suspected gravelly formation. This goal was met at all three holes, penetrating to a maximum depth of 216.1 mbsf and providing a combined cored interval of 517.3 m. At Site U1621, a total of 89 cores were retrieved: 40 APC (45%), 21 HLAPC (24%), and 28 XCB (31%). In Hole U1621A, Cores 1H–28X penetrated from the seafloor to 215.3 mbsf with a recovery of 84%. Formation temperatures were measured using the APCT-3 tool on Cores 4H, 7H, and 10H. In Hole U1621B, Cores 1H–33X penetrated from the seafloor to 216.1 mbsf with a recovery of 94%. In Hole U1621C, Cores 1H–28X penetrated from the seafloor to 207.9 mbsf with a recovery of 94%.

Site U1622 is a single hole (U1622A) that was drilled in half a day. During coring operations, it was discovered that the coordinates provided in the Scientific Prospectus (Lucchi et al., 2023) were not the location of the approved shotpoint for proposed Site BED-02B. Upon discovery of the mismatch of shotpoint and coordinates, coring was terminated, with a maximum penetration of 46.5 mbsf (99% recovery). The correct shotpoint coordinates were calculated, and we moved to that location, which was sufficiently distant from Site U1622 to deem it a new site (U1623). At Site U1622, a total of seven cores were retrieved: six APC (86%) and one HLAPC (14%).

Seven holes (U1623A–U1623G) were drilled at Site U1623 over 10 nonconsecutive days. Hole U1623A is located on Seismic Line CAGE21-1-HH-05 (Figure **F15**), and all other holes are located within a 30 m × 60 m area to the northeast. The target depth of ~370 mbsf (below Seismic Reflector R4A) was met in Holes U1623A, U1623C, and U1623D. Holes U1623B and U1623E were poor mudlines and were abandoned after one core each. Hole U1623F reached a maximum penetration of 162.2 mbsf; however, the deepest ~71 m (Cores 11H–22F) are suspect because evidence from coring operations (no weight on bit), observations from physical properties (extremely low GRA density), visual observation of the sediments through the plastic liner (mousselike sediments in absence of gas pressure), and gas analyses (normal gas composition) strongly suggested that the

drilling bit sidetracked into a nearby hole. When the cores from this interval were later split, they displayed mousselike core disturbance, which supports this conclusion. Hole U1623G was drilled during the remaining time available. Overall, at Site U1623 a total of 205 cores were retrieved: 58 APC (29%), 62 HLAPC (30%), and 85 XCB (41%). The combined cored interval of all Site U1623 holes (U1623A–U1623G) was 1422.4 m. Summaries of Holes U1623A, U1623C, U1623D, and U1623G, which were the most complete and undisturbed, are provided below.

Hole U1623A (Cores 1H–51X) penetrated from the seafloor to 269.3 mbsf with a recovery of 90%. Formation temperatures were taken on Cores 4H, 7H, and 10H using the APCT-3 tool. Hole U1623C (Cores 1H–55X) penetrated from the seafloor to 369 mbsf with a recovery of 87%. Following coring, logging was attempted in Hole U1623C; however, the tool string encountered obstructions in the pipe and later the bit, and logging was terminated. Hole U1623D (Cores 1H–56X) penetrated from the seafloor to 370 mbsf with a recovery of 95%. Logging in Hole U1623D was successful, with complete runs of the triple combo tool string and partial runs with the FMS-sonic tool. Because of a technical issue, the APS was not deployed. Hole U1623G (Cores 1H–19F) penetrated from the seafloor to 142.1 mbsf with a recovery of 108%. With much gratitude to the R/V *JOIDES Resolution* crew, and under the applause of all *JOIDES Resolution* Science Operator staff and scientists, the final core of *JOIDES Resolution* under IODP was on deck at 1220 h on 25 July 2024.

4.4.3. Principal results

Sites U1621 and U1623 are companion records from the Bellsund drift. Although the distance (~4.4 km) between these two site locations is sufficiently far to require designation as separate IODP sites, their sedimentologic, paleontological, paleomagnetic, and geochemical characteristics are similar in their overlapping stratigraphic sequences, justifying their designation as a set of sites. For this reason, their principal results are summarized together. Site U1622 is from a different depositional setting because it was drilled into the nearby Storfjorden TMF and not into a sediment drift, but its proximity (~8 km) to the two Bellsund drift sites, as well as its comparable lithology and time period, justifies its inclusion in this grouped summary.

4.4.3.1. Lithostratigraphy

Sediments at the two Bellsund drift sites are mainly siliciclastic and primarily composed of dark gray to greenish gray silty clay, with coarser intervals containing reddish gray to dark reddish gray sandy mud and diamictons (Figure **F9**). Clast abundance is variable but generally displays an increase downhole, with diamictons more common below ~170–190 mbsf at upslope Site U1621 and below ~300 mbsf at downslope Site U1623. In comparison to the northern sites (U1618–U1620), the Bellsund drift and TMF sites are characterized by the frequent occurrences of small patches of fine sand recovered along the entire sequence cored at Site U1621 and in the correlative upper unit of Site U1623 (above ~190 mbsf) (Figure **F8A**). These sand patches are mostly lighter in color and coarser-grained than the surrounding sediment and are likely to be iceberg-rafted sediment pellets (Goldschmidt et al., 1992), although further investigation is warranted. Intervals containing light-colored silty or sandy laminations sometimes also occur within this stratigraphic unit of both Bellsund drift sites, whereas heavily bioturbated sediment distinctly characterizes the deeper stratigraphic sequence at Site U1623 between ~190 and ~270 mbsf. Below 270 mbsf, the bioturbation is not apparent to slight and there is a greater occurrence of very large clasts (i.e., dropstones), consistent with the increased presence of diamictons at depth.

Given that Site U1622 is located on the TMF, the lithology is somewhat different than the two Bellsund drift sites (U1621 and U1623). The uppermost 5 m of Site U1622 are primarily soft silty clay and include a small interval of nannofossil ooze. Firm sandy mud with common clasts characterize the Site U1622 sediments from 5 mbsf to the base of the drilled sequence (46 mbsf).

4.4.3.2. Biostratigraphy

The most continuous and abundant representation of all microfossil groups (Figure **F10**) for the Expedition 403 sites was at Bellsund drift Sites U1621 and U1623. Shipboard sample analysis mainly focused on core catchers, supposed warm water intervals based on lithologic and physical properties. One or more microfossil groups were present at levels that enabled documentation of glacial–interglacial variability for most of the records. Calcareous nannofossils are generally pres-

ent with good to moderate preservation; they are low in diversity but have frequent to common abundances along the studied sequences and alternate with barren intervals. A generally well preserved low-diversity assemblage of planktonic foraminifers is found continuously in the upper part of both sites; foraminifers become more poorly preserved downhole to a point where samples are barren. Diverse and well-preserved diatoms assemblages are present in high abundance in the uppermost part of the record and in some intervals of the lower record but are otherwise nearly barren at these sites too. Most samples, especially those from targeted interglacials, contain abundant dinocysts of low-diversity assemblages, although barren intervals exist. Reworked microfossils from older stratigraphic levels are intermittently present in the sequences.

Initial paleoenvironmental assessment based on the microfossil assemblages suggests a Pleistocene paleoenvironment dominated by nutrient-rich, cool Arctic to polar surface water conditions with seasonal sea ice cover, alternating with cool-temperate Atlantic surface water conditions with seasonal sea ice.

Age-diagnostic markers allow the determination of Late Pleistocene intervals containing MISs 1, 5, and 7–13 and older warm interglacial periods. Shipboard biostratigraphic data indicate that the Site U1621 stratigraphy ranges in age from at least ~0.5 Ma to the Holocene and that the Site U1623 stratigraphy above the basal diamicton ranges in age from Middle–Late Pleistocene to the Holocene. Calcareous nannofossil content in the bioturbated silty clay sediments at the bottom of the section could indicate Pleistocene age moderately older than 1.14 Ma. The clast-rich sandy mud lithology at Site U1622 does not favor biostratigraphic investigation; however, calcareous nannofossils marking an interval younger than MIS 8 were present in the uppermost part of the record, and reworked planktonic foraminifers (ages <1.7 Ma) are also present in the record.

4.4.3.3. Paleomagnetism

The paleomagnetic records of sediments at Sites U1621 and U1623 are not as complicated by authigenic mineral magnetic overprints as those at Sites U1618–U1620. The uppermost 90–100 m at the Bellsund drift sites have a magnetic mineral assemblage consistent with detrital magnetic mineral (Figure **F11**). Below this depth, iron sulfide precipitants were sometimes present, causing higher ARM coercivities and/or higher MS intervals. This complication was managed by using the same methods from earlier drilled sites to filter the discrete sample NRM data for intervals with lower MS and by augmenting routine NRM analyses with rock magnetic experiments. The paleomagnetic data for Site U1621 indicates that the sediments were entirely or almost entirely deposited during Chron C1n (Brunhes), with a maximum age limit of 0.773 Ma determined near the base of recovery. At Site U1623, the base of Chron C1n and the top and base of Subchron C1r.1n (Jaramillo; 0.99–1.07 Ma) were identified. The base of recovery at Site U1623 is likely between 1070 and 1775 ka, younger than Subchron C2n (Olduvai). The well-resolved magnetizations, magnetic mineral assemblages, and success in coring multiple holes with limited coring disturbance indicate great potential for generating a longer high-resolution paleomagnetic reconstruction at both Bellsund drift sites for at least the uppermost 90–100 m. No paleomagnetic reversals were identified in the 46 m Site U1622 record, and it is likely to be deposited during Chron C1n (Brunhes).

4.4.3.4. Age model

Because the Brunhes/Matuyama boundary is not identified at Site U1621 and the shipboard biostratigraphic age control markers are poorly constrained at depth, it is premature to report sedimentation rate estimates for the interval below ~74 mbsf at Site U1621. However, sedimentation rates in the uppermost ~74 m (~0.3 Ma) of Site U1621 are approximately 245 m/My (Figure **F13**). A more complete preliminary age model based on both biostratigraphy and magnetostratigraphy is available for Site U1623. Here, sedimentation rates are approximately 193 m/My over the same time interval, confirming the preexpedition interpretation based on seismic data that Site U1621 contained a more expanded Late Pleistocene record than Site U1623. Taking a longer view, sedimentation rates over the last ~1 My average approximately 201 m/My at Site U1623.

Between the base of the record and ~1 Ma, there are discrepancies in the different age control datums but the datums suggest sedimentation rates were high (somewhere between 183 and 924 m/My). Though widely ranging, these data point to decreased sedimentation rates after ~1 Ma, an

observation also made at Sites U1618–U1620 and regionally at several ODP sites (908, 909, and 911; Myhre et al., 1995; Thiede and Myhre, 1996). As noted earlier, this timing is concurrent with the climate reorganization of the MPT.

No age model was developed for Site U1622.

4.4.3.5. Physical properties

The physical property measurements at the two Bellsund drift sites display clear cyclic variabilities over the lengths of their records. Generally, NGR tracks GRA bulk density trends downcore, with some exceptions in the deeper portions of Hole U1621B, likely related to an increased occurrence of diamictons near the base of this hole, interpreted as Seismic Reflector R3. Higher overall NGR values at Site U1623 compared to Site U1621 may be associated with higher clay content farther from the shelf edge. Some high MS values are present in the Bellsund drift sediment records but are less pervasive than those observed at Sites U1618–U1620; this is consistent with fewer iron sulfide minerals observed at depth on the split core surfaces or in X-radiographs at the Bellsund drift sites. Because the Bellsund drift sites are less affected by secondary alteration, there are more apparent similarities between MS and other physical properties (e.g., NGR), recording the detrital input signals.

Unlike the two Bellsund drift sites, GRA bulk density at Site U1622 displays a sharp increase at 5 mbsf that remains high to the base of the record. This observation is consistent with the clast-rich sandy mud–dominated lithology. Higher NGR at Site U1622 compared to Sites U1621 and U1623 likely results from the lithology of this glaciogenic sequence and its low porosity. Together, the geographic setting, lithology, and physical property data suggest that Site U1622 is a sedimentary package of debris flows and/or other glacial mass transport deposits (MTDs). Motivated by the recovery of this MTD, ASR experiments were set up using cores from nearby Site U1623 to study the stress that MTD emplaced at Site U1622 may have had on preexisting slope deposits at Site U1623. In addition, a new component to the ASR experiments was incorporated at Site U1623: headspace gas measurements of the ASR samples became part of the experimental protocol to evaluate if sediment degassing is a plausible explanation for the shrinkage noted in the strain gauge finding from experiments already underway for Sites U1618 and U1620.

4.4.3.6. Stratigraphic correlation

Stratigraphic correlation for Sites U1621 and U1623 was primarily accomplished using MS. Cores from all three Site U1621 holes were used to construct the splice, with Hole U1621B serving as the backbone. Most coring gaps were covered with this approach, producing a splice from 0 to ~188 m CCSF. The offset between CSF and CCSF depth scales is nearly linear; below 60 mbsf, the growth factor is a little higher because of gas expansion. For Site U1623, both a primary and an alternative splice were generated. The primary splice for Site U1623 based on cores from Holes U1623A, U1623C, U1623D, and U1623F is complete for the entire 404 m record, with only one small gap. The alternative splice is from 0 to 174 m CCSF. In construction of the alternative splice, cores from Hole U1623G were used as the backbone; gaps in the uppermost 90 m were filled in with cores from Hole U1623F, and most gaps below this depth could be filled in with cores from Holes U1623A, U1623D, and U1623G. The Site U1623 cores have similar, nearly linear growth rates, although differences exist between the holes and increase below ~150 mbsf. For all three splices (one for Site U1621 and the primary and alternative splices for Site U1623), calculations of mass accumulation rates based on their CCSF scales should account for the expansion by dividing apparent depth intervals by the appropriate growth factor. No correlation or splice was required for Site U1622, as it was a single hole to only 46 mbsf.

4.4.3.7. Geochemistry

Sediment organic geochemistry at the two Bellsund drift sites display cyclic variations in $CaCO_3$, TOC, and TN over the uppermost ~190–200 m. Given the preliminary sedimentation rates and the prevalence of microfossil groups in the Site U1621 and U1623 records, these results suggest possible orbital pacing of marine productivity and/or their dilution by terrestrial input over the last 1 My. Intervals of increased C/N ratios generally correlate to low $CaCO_3$ abundances; these results tentatively point to C/N ratios marking times of intense glaciogenic erosion and transport to the marine environment. Below ~200 mbsf, the overall $CaCO_3$ abundances decrease and Ca in

the IW increases; both are consistent with increases in barren intervals of calcareous microfossils with depth. Site U1622 is low in $CaCO_3$ but higher in TOC (compared to Sites U1621 and U1623) and has the highest C/N ratios of all Expedition 403 sites; these results all support the interpretation that Site U1622 is a record of MTDs in the form of clast-rich glaciogenic debris flows, which delivered very large amounts of terrigenous sediment, building up glacial TMF in the marine environment on the continental margin.

The headspace gas measurements at the Bellsund drift sites remained in the normal zone (a change welcomed after drilling the Vestnesa and Svyatogor Ridge locations) (Figure **F7**). Although methane concentrations increased moving below the seawater interface through a shallow SMTZ at Sites U1621 and U1623, they remained steady at ~10,000 ppmv to the base of the records. Ethane (C_2 hydrocarbon gas) concentrations at Site U1623 showed some relationship to lithology, becoming more concentrated with depth, suggesting some lithologic influence on gas formation and/or migration. Some elements in the Site U1623 IW, including Fe and PO_4^{3-} as well as IW alkalinity, also display downcore changes in concentrations that show some relationship to lithology.

4.4.3.8. Microbiology

At Sites U1621 and U1623, microbiological sampling for sedaDNA followed the procedures described previously. These sites provided the best chronological control for high-resolution sampling during the expedition. Sampling focused on collecting sedaDNA records of targeted, expanded intervals at Site U1621, including the period of paleo-SBSIS advance and retreat from ~30 ka to present day and interglacial stage MIS 5e. Interglacials MIS 11 and MIS 31 were targeted for sampling in the deeper record from Site U1623. Postexpedition sedaDNA analyses will primarily investigate the polar marine ecosystem responses to past warming.

4.4.3.9. Downhole logging

Downhole logging was performed in Hole U1623D using the triple combo and FMS-sonic tool strings to obtain multiple in situ property measurements. The natural gamma ray and HLDS measurements show trends similar to shipboard scanning data with an average density of 1.84 g/cm^3 in the interval 105.1–239.0 m WMSF (below the pipeline).

Borehole diameter variations affect some of the logging results for Hole U1623D. Nevertheless, natural gamma ray and density show almost the same trends observed in the shipboard scanning data between ~105 and 239 mbsf, with some cyclic variability. Lower amplitude fluctuations of both parameters were observed between 105 and ~160 mbsf, likely related to poor borehole conditions and potential gas presence. Electricity resistivity logs indicate some intervals that may have large pore spaces and high water content. *P*-wave acoustic velocity data show cyclic changes mimicking that observed in other logging data. This was one of only two sites (U1618 and U1623) for which borehole resistivity images were acquired. Borehole temperature measurements were made in Holes U1621A and U1623A; these data show formation temperature in the Bellsund drift increasing almost linearly with depth. The slope of the linear regression provides geothermal gradients typical for oceanic sediments (Kolawole and Evenick, 2023).

4.5. Site U1624

4.5.1. Background and objectives

The Isfjorden drift drill site is located on the slope proximal area (~1320 m water depth; Figures **F1**, **F3**) (see **Background and objectives** in the Site U1624 chapter [Lucchi et al., 2026b]) of a plastered sediment drift that developed along the western continental margin of Svalbard under the influence of the northward-flowing WSC (Rebesco et al., 2013). The Isfjorden drift has built up over millions of years since the opening of the Fram Strait (17–10 Ma) (Jakobsson et al., 2007; Engen et al., 2008; Ehlers and Jokat, 2013). The opening determined the onset of the contour current circulation system in the area (Eiken and Hinz, 1993; Gebhardt et al., 2014), with development of sediment drifts covering large areas of the European North Atlantic margin, including the Norwegian and Barents Seas, western margin of Svalbard, and eastern side of the Fram Strait (Laberg et al., 2005). Sediment drifts are depocenters developing under persistent bottom currents that substantially rework the sediments delivered to the marine environment through terrestrial and marine processes (Stow et al., 2002; Rebesco, 2014a). In addition to sediments, the bottom

currents transport oxygen and nutrients, generating ideal environmental conditions for the biological productivity with sediments rich in carbonate biogenic fraction if postmortem diagenetic conditions allow for their preservation.

A previous ODP Leg 162 drill site (986; Jansen and Raymo, 1996) was located in the deeper, distal slope facing the Isfjorden drift to examine the onset of glaciation in the European Arctic and establish the history of the paleo-SBSIS. Site 986 recovered a sequence of ~2.4 My primarily consisting of fine- to coarse-grained siliciclastic sediments with varying amounts of gravel interpreted as IRD and considered to represent the depositional record after the onset of NHG. The sequence contains a main shift in the glacial style with an increased volume of debris flow sedimentation that was related with the onset of shelf edge glaciations in the western margin of Svalbard (Raymo et al., 1999) considered to correspond to Seismic Reflector R4A, dating ~1.3 My (Rebesco et al., 2014b).

The Isfjorden drift drill Site U1624 (Lucchi et al., 2023) was specifically designed to recover an expanded sedimentary sequence in a slope proximal area to reconstruct the dynamic of the paleo-SBSIS under past oceanographic and climatic forcing after the onset of shelf edge glaciations. Because of its close location to the continental shelf break and former ice sheet terminus during glacial maximum, the Isfjorden drift contains most of the meltwater events associated with the paleo–ice sheet decay deriving from ocean and climate forcing. Located between the Bellsund TMF to the south and the Isfjorden TMF to the north, the Isfjorden drift was partially shielded from the massive glaciogenic input building TMFs, allowing also for a partial preservation of the interglacial contouritic sedimentation that can provide biostratigraphic and paleoceanographic constraints.

Piston cores collected in this area demonstrate that in addition to its proximal location to the paleo-SBSIS, the Isfjorden drift is a good setting to recover continuous, relatively expanded, and datable sedimentary sequences. The 2014 Eurofleets2 PREPARED project (Lucchi et al., 2014) recovered a long Calypso piston core containing a continuous, submillennial paleoclimatic record spanning the last 60 ky. A robust age model was defined through paleomagnetic and biostratigraphic analyses together with radiocarbon dating of the biogenic carbonate fraction collected from the interglacial intervals of contouritic sedimentation (Caricchi et al., 2019, 2020). The sedimentologic analyses indicated the presence of glacial debris flows, recording shelf edge glaciations and an extensive record of plumites, indicating ice sheet melting that appears well developed at the site (Caricchi et al., 2019).

Located close to the Bellsund drift, drilling at Isfjorden drift Site U1624 aimed to provide complementary information on the WSC characteristics and variability allowing discrimination between climate-driven events related to local or regional effects. Site U1624 was drilled to a maximum depth of 258 mbsf at a 1320 m water depth. Drilling targeted a stratigraphic sequence extending from the present down to Seismic Reflector R4A (~1.3 Ma). Such a recovery would support the following research goals:

- Stratigraphic reconstruction of the paleo-SBSIS dynamics since the onset of Pleistocene shelf edge glaciation;
- Study of ocean–cryosphere interactions and forcing mechanisms on the paleo–ice sheet dynamics; and
- Identification of tipping points between the late stages of glaciations and the onset of glacial terminations.

4.5.2. Operations

Operations commenced at Site U1624 on 18 July 2024. During the 3.23 days on site, three holes were drilled (U1624A–U1624C), two of which had substantial core recovery (Figure **F5**; Table **T1**). Hole U1624A is located on Seismic Line CAGE20-5HH-13, and all three holes are located just southeast of Seismic Line EG-01A (Figure **F16**). The mudline was poorly recovered in Hole U1624A; therefore, it was abandoned. Holes U1624B and U1624C both reached the target depth. The combined cored interval from all three holes was 517.3 m. As the most proximal site of the expedition to the Svalbard shelf edge, drilling encountered more coarse sediment deposits than at other sites, hampering core recovery in some intervals. Thus, although some cores had >100%

recovery due to gas expansion in mud-rich intervals, recovery was low for a few cores with coarser sediments. Because formation characteristics changed at each hole, deployment of the APC system shifted to the HLAPC system and ultimately to the XCB drilling system at different depths. At Site U1624, a total of 89 cores were recovered: 22 APC (25%), 24 HLAPC (27%), and 43 XCB (48%). To minimize magnetic overprinting on the cored sediment, the nonmagnetic collars and core barrels were used for all APC and HLAPC coring. To mitigate for gas pressure and expansion, holes were drilled into the liners and most XCB cores were advanced by 6–8 m.

One 1.3 m long core was recovered from Hole U1624A; however, because it was extruded from the liner by water pressure onto the rig floor, the mudline was uncertain and the hole was terminated. Hole U1624B was drilled 5 m east at a 1320 m water depth. Cores 1H–45X penetrated from the seafloor to 258 mbsf with a recovery of 86%. Formation temperature measurements were taken on Cores 4H, 7H, 10H, and 14F using the APCT-3 tool. In total, we spent 1.5 days on Hole U1624B. Hole U1624C was located 20 m southwest of Hole U1624B. It was spudded on 20 July at a water depth of 1320 m. Cores 1H–43X penetrated from the seafloor to 258 mbsf with a recovery of 93%. In total, we spent 1.5 days on Hole U1624C. Given the short drill depth, downhole logging was not performed at Site U1624.

4.5.3. Principal results

4.5.3.1. Lithostratigraphy

The Isfjorden sediment drift record at Site U1624 is siliciclastic and coarsens with depth. In Holes U1624B and U1624C, the lithology in the uppermost ~86 m is primarily dark gray silty clays with occasional reddish gray sandy mud (Figures **F8A**, **F9**). Clast abundance is variable but generally increases downcore, and below ~202 mbsf the sediment is almost entirely diamicton, with a few interbedded intervals of sandy mud. In general, laminated intervals are occasionally present in the uppermost ~120–150 m of Site U1624. Dark patches are most prevalent over this same depth range, as are the occurrence of thin layers of sand and/or silt interbedded within the silty clay as well as small light patches of fine quartz sand, which are hypothesized to be iceberg-rafted sediment pellets (Goldschmidt et al., 1992). In the uppermost ~202 m, long intervals with slight to moderate bioturbation alternate with intervals showing no apparent bioturbation.

4.5.3.2. Biostratigraphy

Calcareous nannofossils, diatoms, dinocysts, and planktonic foraminifers are present in limited amounts at Site U1624 (Figure **F10**); the highest abundances were generally observed in samples from silty clay intervals in the upper portion of the cored sediment record. The representation of calcareous nannofossils is scarce overall and barren toward the base of the record. When present, diversity is low and the concentration of calcareous nannofossil specimens ranges between rare and common. With the exception of a few fragments observed in deeper samples, diatoms are only found at the very top of the record (Core 1H from both holes), where abundance is rare and pres-

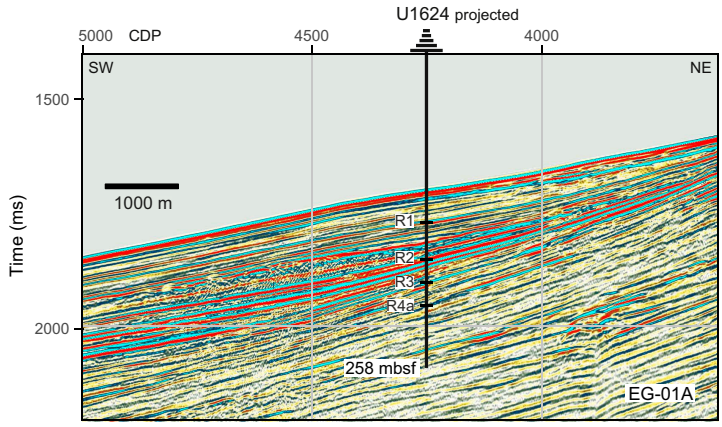

Figure F16. Seismic Line EG-01A showing projected location of Site U1624, evident mass gravity deposits associated with past shelf edge glaciations, interpreted reflectors (R1–R4a), and maximum penetration depth to 258 mbsf. CDP = common depth point.

ervation is moderate. Intervals with rare to abundant concentrations of dinocysts are present to the base of the record but alternate with barren intervals. Often the dinocyst diversity is low, although some samples contain rich warm-water assemblages. Planktonic foraminifers are present in the upper part of the record, ranging from rare to abundant; their diversity is generally low. Preservation decreases with depth, and samples are barren of foraminifers below ~178 mbsf. Reworked dinocysts and terrestrial palynomorphs are sometimes present in the Site U1624 record. Interestingly, notwithstanding the proximal location of Site U1624 to the continental shelf, the presence of reworked nannofossils from older deposits is very limited in the sedimentary sequence.

Calcareous nannofossils and foraminifers provide five age-diagnostic Pleistocene biostratigraphic markers for Site U1624. Additional age-diagnostic microfossils of Late Pleistocene interval containing MISs 5 and 7–13 and older interglacials were also identified. Initial paleoenvironmental assessment based on the microfossil assemblage suggests Pleistocene Arctic to polar surface water conditions with seasonal sea ice cover and intermittent intervals with a relatively warm Atlantic water influence.

4.5.3.3. Paleomagnetism

The magnetic mineral assemblage at Site U1624 is similar to that at the Bellsund drift sites (U1621 and U1623). There were no high MS peaks, and the ARM coercivity was low (but still bimodal), suggesting the Site U1624 magnetic minerals contain a strong detrital signature (Figure **F11**). As a result, demagnetization of the archive-half sections and vertically oriented discrete cube samples was fairly straightforward. The bimodal distribution of the ARM_{30mT}/ARM ratio warrants further investigation. The Site U1624 diamictons and other clast-rich intervals presented a different challenge for reconstructing the magnetic stratigraphy because these XCB-cored intervals likely do not preserve their original sedimentary fabric and rarely recovered intact biscuits. Targeting discrete cube sampling of intact biscuits from fine-grained sediments interbedded with the diamictons shows some promise for refining the magnetic stratigraphy. X-ray image analysis is useful for identifying suitably intact biscuits. Based on the Site U1624 shipboard paleomagnetic work, the onset of Chron C1n (the Matuyama/Brunhes boundary; 0.773 Ma) must have occurred between ~154 and 174 mbsf, and the base of the sediments must be older than 0.773 Ma.

4.5.3.4. Age model

The preliminary age model for Site U1624 is based on biostratigraphy and magnetostratigraphy (Figure **F13**). Linear sedimentation rates over the entire cored sequence are estimated to be approximately 212 m/My, which falls within the range of those estimated for the Bellsund drift sites. Postexpedition research will refine the Site U1624 age model.

4.5.3.5. Physical properties

At Site U1624, NGR and GRA bulk density generally show a positive linear correlation, and the mean values of both properties increase with depth. The MS values at Site U1624 are lower than at previous sites, and the MS signal at Site U1624 appears largely driven by variations in detrital input. The greatest amplitude variability of MS occurs in the uppermost ~90 m, which is rich in silty clay. In contrast, below ~200 mbsf, MS values are much lower and occur in association with high GRA bulk density; at these depths, diamictons are the dominant lithologies.

4.5.3.6. Stratigraphic correlation

Stratigraphic correlation for holes at Site U1624 was primarily accomplished using MS. The best recovered stratigraphy of Hole U1624C was used as the backbone of the splice. Hole U1624B was used to fill most coring gaps down to ~200 m CCSF. Below this depth, more coring gaps exist, including several that occur in both holes, so the cores were appended based on a consistent growth factor of 1.065. Gas expansion was greatest between ~150 and 190 mbsf, resulting in larger cumulative offsets between the CSF-A and CCSF scales for this interval and variable growth factors. Calculation of mass accumulation rates based on the CCSF scale should account for the expansion by dividing apparent depth intervals by the appropriate growth factor.

4.5.3.7. Geochemistry

Shipboard geochemistry results from the Site U1624 IW and headspace gas measurements indicate that the SMTZ is likely between ~4 and 18 mbsf. A maximum alkalinity value of ~22 mM is

likely an indication of bicarbonate production within the SMTZ, and decreased alkalinity with depth likely relates to ongoing microbial methanogenesis. A downhole increase of IW Ca and Sr suggest that carbonate dissolution is occurring with depth; the increase of Ca in the IW is likely at the expense of biogenic carbonate microfossils, which are generally barren below ~200 mbsf. In general, the IW Ca results show an opposite pattern to the sediment geochemistry results of $CaCO_3$, suggesting that biogenic carbonate variability is primarily controlling the downcore $CaCO_3$ pattern. However, below ~200 mbsf, both Ca and $CaCO_3$ increase, suggesting that some authigenic carbonate is precipitating in the sediment at depth, consistent with sedimentologic observations. Fe, Mn, and Si also all vary with depth, and Fe is completely consumed by ~93 mbsf. Overall, Si decreases downhole but shows fluctuations that appear to relate to changes in lithology, with higher concentrations in silty clay and very low concentrations in the diamictons. The C/N ratio indicates there were organic matter contributions from marine and terrestrial sources. The stratigraphic variations in the C/N ratio warrant further investigation once a more robust age model is available. Both ethane and propane showed notable increases below ~200 mbsf, which is below the interval from which retrieved cores had the greatest gas expansion.

4.5.3.8. Downhole measurements

Borehole measurements made while coring Hole U1624B show formation temperature at the Isfjorden drift increased almost linearly with depth, and the calculated geothermal gradient is typical for oceanic sediments when compared with the statistical data set (Kolawole and Evenick, 2023).

5. Preliminary scientific assessment

5.1. Operational considerations related to the science objectives

The operational plan for Expedition 403 laid out in the Scientific Prospectus (Lucchi et al., 2023) was designed to optimize recovery of expanded depositional sequences from sediment drifts along the western margin of Svalbard; as such, we anticipated this would be a high recovery expedition. With 5343 m of total core and an average recovery of 95%, this goal was met (Table **T1**). The APC coring system was used as much as possible, producing cores with minimal drilling disturbance. Use of the HLAPC system and coring by advancement with the XCB system were also both helpful as a means of recovering the best-quality cores for the formation conditions, including sometimes getting through challenging glaciogenic gravel-rich layers.

The operational goal of drilling each of the six primary sites identified in the Scientific Prospectus was also accomplished. As a result, the recovered core records span the intended geographic extent, including a south–north transect within the modern flow direction of the WSC and east–west transects that span proximal to distal settings relative to the Svalbard continental margin (Figure **F1**). Planning also recognized the need for multiple, correlatable records, especially of the younger time intervals, to meet expected high-resolution sampling demands. Except for one location (Site U1619), this goal was met by drilling at least two holes at each site (Figure **F5**). At the two Bellsund drift sites, this operational success was amplified by drilling three good recovery holes of a highly expanded sequence at Site U1621 and five good recovery (and deeper) holes at nearby Site U1623. Additionally, planning aimed to drill at least one very deep hole at several sites to provide long-time series records. This goal was largely met by obtaining >600 m records from both the western Vestnesa Ridge (Site U1619) and Svyatogor Ridge (Site U1620) drill sites.

The operational challenges of the expedition primarily related to sea ice conditions and to the presence of gas hydrates that were not detectable through the geophysical survey. Ice navigation proved essential for decision making on when to drill the most ice-vulnerable northernmost location, Site U1619. Rather than following the initial operational plan to drill sites from south to north (under the assumption that sea ice conditions would improve later in the summer season), we took advantage of open water conditions in the north at the start of the expedition. Had we not made this adjustment, it is unlikely coring would have been possible at Site U1619. As it was, we were only able to stay on site for 5.2 days before the sea ice margin approached within 5 nmi, terminating Hole U1619A. Although a free fall funnel was deployed in hopes of returning to continue cor-

ing to the target depth (696 mbsf) and drilling additional holes for coring and logging, the sea ice conditions never improved; the site remained either at the sea ice margin or within the consolidated sea ice zone for the remaining time of the expedition.

The presence of gas hydrates and related free gas was more of a challenge than expected at several sediment drift locations, especially Vestnesa Ridge East (Site U1618) and Svyatogor Ridge (Site U1620). Although Site U1618 was located in an attempt to avoid gas chimneys and faults that can serve as conduits for fluid migration and was at least 2 km away from a regional gas hydrate–related BSR, chemical and physical evidence of gas (including apparent dissociated gas hydrates) was present. Similar conditions also existed at Site U1620. As a consequence, coring operations were often slower than planned and several holes did not reach their target depth. Vigilant safety monitoring and mitigation were needed. Additional borehole temperatures were taken to determine the geothermal gradient, and hydrocarbon gas levels were continuously monitored. Operations frequently paused between each core run as we waited for results from the headspace gas samples taken from the previous core, which informed decisions on whether coring could continue. Results indicated that coring operations were commonly occurring near or in the hydrocarbon anomalous zone at these two sites (Figure **F7**), and each hole had to be terminated prematurely for anomalous C_1/C_2 ratios and/or for increased presence of higher (e.g., C_5 and C_6) hydrocarbons. The gas hazards also posed risks to those handling core on the rig floor and on the core receiving platform because gas pressure caused liners to shatter (and sometimes explode), necessitating that several mitigation steps were taken, including drilling holes in the core liners and using Kevlar blankets when handling core. The scientific team is grateful to the drilling platform crew and technicians for working under these challenging conditions.

Logging operations were affected by some technical challenges, in addition to the unpredictable nature of the borehole conditions. The primary challenges that affected logging-related progress toward the scientific objectives was the inoperability of the VSI tool for the entire expedition and the inability to use the FMS-sonic tool string at Site U1620. Data collection from the VSI tool was intended to provide groundtruthing data for regional seismic interpretations. Data from the FMS-sonic tool was intended to support tectonic stress regime research. In addition, the logging plan was originally designed to collect data at both Sites U1619 and U1620 to understand alternative stress regimes on either side of the MTF. However, because no logging operations took place at Site U1619, logging data from Site U1618 will substitute and be used in comparison with those from Site U1620. Nevertheless, an important operational accomplishment was acquiring some logging data for these sites, along with Site U1623; collectively, these provide a set of north–south and proximal–distal logs to complement the spatial coverage of the expedition core records.

One unintended operational event occurred during the expedition, as well. Because of a discrepancy between the approved seismic shotpoint and the coordinates provided in the Scientific Prospectus (Lucchi et al., 2023), Site U1622 was the only expedition site that was not drilled into a sediment drift. Although this was not part of the original plan, it provides a unique opportunity to examine recent MTDs forming TMFs, which complements the nearby sediment drift records and will allow collection of important information on TMF formation.

5.2. Preliminary assessment of primary scientific objectives

Expedition 403 was principally conceived as a paleoceanographic and paleoclimatic investigation. The overarching scientific goal was the reconstruction of WSC (North Atlantic Current) variability; its influence on climate changes, particularly during established key climate transitions occurring since the cold Late Miocene/warm Early Pliocene (~5.3 Ma); and its impact on the Arctic glaciations, ice shelf development and stability, and sea ice distribution through heat transfer from low to north high latitudes and the Arctic Ocean. To meet the main research goal, five primary paleoceanographic/paleoclimatic objectives were identified (Lucchi et al., 2023):

- Development of a high-resolution, Late Miocene–Quaternary chronostratigraphic record;
- Generation of multiproxy data sets to better constrain the potential concurrent forcing mechanisms responsible for Late Miocene–Quaternary climatic transitions;

- Identification of orbital, suborbital, millennial-scale climate variations and prominent meltwater events accompanying the ice sheet demise;
- Evaluation of the impact of past prominent meltwater events on the paleoceanography, paleoenvironment, and paleoclimate; and
- Reconstruction of the paleo-SBSIS dynamic history in relation to changes in the WSC pathways and characteristics as mechanisms inducing ice sheet instability and fast retreat.

The accomplishment of such objectives required the identification of expanded, continuous, and temporally extended depositional sequences. Five primary drill sites were initially identified on sedimentary depocenters (sediment drifts) that built since the Miocene along the western margin of Svalbard (Bellsund and Isfjorden drifts) and the eastern side of the Fram Strait (Vestnesa and Svyatogor Ridges) under the direct influence of the WSC receiving at times a considerable sediment input during the growth and decay of the paleo-SBSIS. Three sites located in the close vicinity of the continental margin along a south–north transect (namely, the sites on the Bellsund and Isfjorden drifts and the site on the east termination of the Vestnesa Ridge) will work as sentinels to depict the evolution and dynamic of the paleo-SBSIS, whereas the two sites located far from the continental reaches (on the Svyatogor Ridge and the west termination of the Vestnesa Ridge) contain a better (and longer) record of the WSC variability and can give a better idea of the regional glacial history, skimmed of possible local factors (Figure **F1**). The Bellsund drift, in the southernmost area, was considered particularly suitable for Pleistocene biostratigraphic, paleoenvironmental, and paleoclimatic reconstructions because it contains the most expanded depositional record of very warm Pleistocene interglacials (e.g., MISs 5, 7–13, and 31), and previous studies indicated the consistent presence of biogenic fraction useful for environmental constraints through taxa paleoecology, biomarkers, and stable isotopes. Contextually, because of the close location to the paleo-SBSIS terminus, the Bellsund drift was considered an ideal drilling location for time constraints of ocean–ice sheet interactions and mutual feedback. By accounting those aspects, drill sampling at the Bellsund drift was divided into two sites (U1621 and U1623), with the site located on the upper reaches of the drift (Site U1621) containing the most expanded Late Pleistocene sequence recovered during Expedition 403. The two companion Bellsund sites, together with a third unforeseen site located on a nearby TMF depositional system, were treated as a set of sites. The shipboard investigation of the Bellsund drift sites confirmed our expectations of a very high resolution paleo record, and they will be the main targeted sites for several shore-based investigations. On the other hand, the two sites recovered in the distal area (Site U1619 on the west termination of the Vestnesa Ridge and Site U1620 on the Svyatogor Ridge) contain the longest time record and will allow for a better understanding of the warm Pliocene climate, the onset of the NHG, and the Late Miocene–Early Pliocene transition. Furthermore, as the most distal site from the paleo-SBSIS, the lithology and micropaleontology of Site U1620 (Svyatogor Ridge) will complement the more proximal sites (e.g., U1618 and U1621–U1624) by recording the regional ice-rafting history and the evolution of the WSC, including the variability of water mass characteristics.

Although most of the primary objectives of the paleoceanographic research will need extensive shore-based laboratory work to be accomplished (i.e., isotopic analyses, biomarkers, trace elements, etc.), some preliminary results were achieved during the expedition through onboard multidisciplinary investigation.

5.2.1. High-resolution Late Miocene–Quaternary chronostratigraphy

Expedition 403 successfully recovered highly promising sedimentary records, in total over 5300 m long, dating back to the Late Miocene (~5.3–6.0 Ma) (Figure **F9**). Good preliminary age models were established during the expedition by combining the magnetostratigraphy and biostratigraphy on the identification of main paleomagnetic reversals and nannofossils biomarkers and biozones, in places corroborated by the occurrence at depth of typical age diatoms assemblages, foraminifers, and dinocysts biomarkers (Figure **F13**). The preliminary age model confirmed the presence of expanded sequences suitable for high-resolution paleoceanographic reconstructions. In particular, Site U1619 on the west termination of the Vestnesa Ridge contains continuous high rates of deposition since the Early Pliocene–Late Miocene; Site U1620 on the Svyatogor Ridge contains the most expanded depositional record of the expedition (325 m/My) extending through the mPWP and the inception of NHG; and Site U1621 on the upper reaches of the Bellsund drift contains a

very expanded Quaternary sequence, having an overall sedimentation rate of ~245 m/My. Preliminary biostratigraphic analyses on the recovered record allowed for the identification of main Pleistocene warm interglacials (e.g., MISs 5, 11–13, and 31) as well as warm events that occurred during the Pliocene time.

The age model will be refined during shore-based analyses. In particular, the magnetostratigraphic analyses were complicated by the frequent occurrence of the authigenic iron sulfide mineral greigite, contributing to a diagenetic overprint on the primary detrital magnetization of sediments. The mixture of detrital and authigenic (e.g., greigite) mineral sources is illustrated by bimodal distributions of the ARM coercivity (Figure **F11**). Further work using temperature-dependent, in-field, mineralogical, and SEM/EDS methods will be needed to gain a more complete understanding of the magnetic minerals present, particularly at Sites U1618, U1619 (Vestnesa Ridge sites), and U1620 (Svyatogor Ridge site). Magnetic data from Late Quaternary sediments at Sites U1621, U1622 (Bellsund drift sites), and U1624 (Isfjorden drift site) suggest the detrital magnetic mineral assemblage was less altered by diagenesis and indicate potential for higher resolution magnetostratigraphic studies using paleosecular variation and relative paleointensity.

Dinocyst samples were prepared on board with a nonacid technique for safety reasons. Although this preparation worked well for Pleistocene sediments, it was more problematic for Pliocene and Miocene sediments. Palynological analyses on shore will benefit from a traditional acid-based preparation. Selected samples from the Pleistocene, Pliocene, and Miocene will be prepared and analyzed to improve the resolution of the ship-based dinocyst stratigraphy.

5.2.2. Reconstruction of the paleo-SBSIS dynamic history and identification of cyclicity

A preliminary assessment of the Pleistocene dynamics of the paleo-SBSIS was conducted using the identification of the sediment lithologies and the depositional facies depicted in the X-radiographs following Lucchi et al. (2013). The sediment facies evidenced a marked change in the style of ice sheet dynamic, changing from a less dynamic mode with low frequency delivering of large volume of glacigenic sediments during the Early Pleistocene to a highly dynamic ice sheet with frequent, almost continuous input of glacigenic products during the Late Quaternary. This change in glacial dynamics is also evident in most of the core scan analyses and in particular the NGR and the sediment color reflectance measurements (CIELAB) indexes that clearly depict a sharp shift from a low to high cyclicity mode. Interestingly, this shift in the glacial dynamic corresponds to a consistent decrease in the sedimentation rate that was observed in all the studied drilled sites, and it is coherent with the major findings observed in other previously drilled sites in the area, including the Hovgaard Ridge, Molloy Basin, and Yermak Plateau (ODP Leg 151; Thiede and Myhre, 1996), and therefore reflecting a main regional change in the depositional style. Promising information derived also from the shipboard analysis of the clay mineral assemblage to determine the source area of the glacigenic input and from the determination of the C/N ratios to distinguish periods of continental organic matter input (glacial stages and terminations) versus periods of dominant bottom current sedimentation with organic matter of marine origin (interglacials). Shore-based analyses will benefit the very large stratigraphic record collected in strategic areas for a better constraint of the paleo-SBSIS history.

5.3. Preliminary assessment of secondary scientific objectives

The secondary objectives fall into two categories: tectonic and microbiologic. Initial progress was made toward the secondary science objectives by the inclusion of special shipboard sampling and experiment, as well as by standard coring and logging operations.

One of the tectonic objectives of the expedition science was to acquire geomechanical and petrophysical data to better constrain the spatial variations of subseabed sediment deformation caused by regional tectonic and glacial stresses. Very good progress was made shipboard by collecting time-sensitive geomechanical data in a set of ASR experiments that focused on samples from sites north (U1618 and U1619) and south (U1620) of the MTF. Shipboard results were promising, and postexpedition processing will be performed to determine the principal stress azimuths. Integration of headspace gas measurements in the experimental methods has also enabled research that

can examine carbon transport (methane seepage) in relation to the stress regimes. Additionally, similar experiments were run for two samples from Site U1623, in this case to better understand the stress that the likely glacially induced MTD emplaced at Site U1622 may have had on preexisting slope deposits of Site U1623. The petrophysical data collection toward the tectonic objective was partially met by the logging at Sites U1620 and U1618 (including FMS-sonic imaging at Site U1618). Integrating the ASR experimental results, FMS imaging, and existing seismic data and stress modeling will advance research on this objective.

A second tectonic objective aimed at reducing uncertainties in the spreading rates of the Molloy and Knipovich Ridges by identifying the spatial location of Miocene–Pliocene sediments north and south of the MTF, which connects these two spreading axes. Progress on this objective was made by recovery of the long (>600 mbsf), temporally well constrained records at the Vestnesa Ridge, which at Site U1619 extend to the Late Miocene (~6 Ma), and at the Svyatogor Ridge, which in Hole U1620D extend to at least the mid-Pliocene (~3.3 Ma). Core-seismic data will also be important to map the spatial extent of the record observed in cores from these sites.

The microbiologic objectives of the expedition aimed to investigate the influence of the WSC variability, ice coverage, and climate on the microbial populations through time and to what extent this is still affecting contemporary geochemical fluxes. Although much of the progress toward this objective will occur postexpedition, the sampling protocols, the number of samples obtained, and the shipboard control testing lay the foundation for a robust and relevant postexpedition microbiological research. Samples (including controls) for sedaDNA were collected at all sites except Site U1624 (Isfjorden drift). These included samples collected at high resolution (~every 2 ky) at selected intervals identified through biostratigraphy, targeting the Last Glacial Maximum through the Holocene and the warm interglacials MISs 5, 11, and 31. The samples were collected under strict contamination control during both drilling and sampling. The samples were stored on board the vessel in a temperature-controlled environment, and they will be analyzed at home-based laboratories (Norway and Australia). Additional whole-round samples were also collected in the deep sequence of Sites U1619 and U1620 to investigate the oldest sedaDNA. If sedaDNA is detected (deep sediment age = ~4 Ma), it would significantly advance research in this area because currently the oldest sedaDNA are from Greenland with an age of 2 Ma (Kjær et al., 2022).

5.4. Additional opportunities for cross-disciplinary scientific research

Although the expedition science objectives did not directly focus on gas hydrate systems, the cores and shipboard data (e.g., geochemical, sedimentologic, physical properties, and logging) offer promising opportunities for cross-disciplinary research to better characterize gas hydrate systems and fluid flow in sediment drifts. Although much work has been done on these topics using geophysical surveys and short piston cores, especially on the Vestnesa Ridge, the core records obtained during Expedition 403 open doors to much more extensive research. The drilled stratigraphic sequence of Svyatogor Ridge (Site U1620) is particularly special because it extends hundreds of meters deeper than any previous coring work in this unusual setting; thus, there is a unique opportunity to groundtruth hypotheses about gas-charged sediment drifts that overlie young oceanic crust, including the nature of biotic and abiotic gas generation processes. We also see good potential for gas hydrate studies that intersect with the primary objectives of Expedition 403, such as the possible relationships between gas hydrate stability and paleo–ice sheet stability.

References

Aagaard, K., Swift, J.H., and Carmack, E.C., 1985. Thermohaline circulation in the Arctic Mediterranean Seas. Journal of Geophysical Research: Oceans, 90(C3):4833–4846. **https://doi.org/10.1029/JC090iC03p04833**

Agarwal, S., and Worster, M.G., 2021. Sea-ice distribution and mixed-Layer depths in Fram Strait. arXiv, 1712.07599vi. **https://doi.org/10.48550/arXiv.1712.07599**

Ahn, J., and Brook, E.J., 2014. Siple Dome ice reveals two modes of millennial CO_2 change during the last ice age. Nature Communications, 5(1):3723. **https://doi.org/10.1038/ncomms4723**

Alexandropoulou, N., Winsborrow, M., Andreassen, K., Plaza-Faverola, A., Dessandier, P.-A., Mattingsdal, R., Baeten, N., and Knies, J., 2021. A continuous seismostratigraphic framework for the western Svalbard-Barents Sea margin over the last 2.7 Ma: implications for the late Cenozoic glacial history of the Svalbard-Barents Sea ice sheet. Frontiers in Earth Science, 9:656732. **https://doi.org/10.3389/feart.2021.656732**

Andersen, N., Müller, P.J., Kirst, G., and Schneider, R.R., 1999. Alkenone $\delta^{13}C$ as a proxy for Past PCO_2 in surface waters: results from the late Quaternary Angola Current. In Fischer, G., and Wefer, G. (Eds.), Use of Proxies in Paleoceanography: Examples from the South Atlantic. Berlin, Heidelberg (Springer Berlin Heidelberg), 469–488. **https://doi.org/10.1007/978-3-642-58646-0_19**

Andreassen, K., Ødegaard, C.M., and Rafaelsen, B., 2007. Imprints of former ice streams, imaged and interpreted using industry three-dimensional seismic data from the south-western Barents Sea. In Davies, R.J., Posamentier, H.W., Wood, L.J., and Cartwright, J.A. (Eds.), Seismic Geomorphology: Applications to Hydrocarbon Exploration and Production. Special Publication - Geological Society of London, 277: 151–169. **https://doi.org/10.1144/GSL.SP.2007.277.01.09**

Årthun, M., Eldevik, T., Smedsrud, L.H., Skagseth, Ø., and Ingvaldsen, R.B., 2012. Quantifying the influence of Atlantic heat on Barents Sea ice variability and retreat. Journal of Climate, 25(13):4736–4743. **https://doi.org/10.1175/JCLI-D-11-00466.1**

Auriac, A., Whitehouse, P.L., Bentley, M.J., Patton, H., Lloyd, J.M., and Hubbard, A., 2016. Glacial isostatic adjustment associated with the Barents Sea ice sheet: A modelling inter-comparison. Quaternary Science Reviews, 147:122–135. **https://doi.org/10.1016/j.quascirev.2016.02.011**

Backman, J., and Moran, K., 2009. Expanding the Cenozoic paleoceanographic record in the central Arctic Ocean: IODP Expedition 302 synthesis. Central European Journal of Geosciences, 1(2):157–175. **https://doi.org/10.2478/v10085-009-0015-6**

Bacon, C.D., Silvestro, D., Jaramillo, C., Smith, B.T., Chakrabarty, P., and Antonelli, A., 2015. Biological evidence supports an early and complex emergence of the Isthmus of Panama. Proceedings of the National Academy of Sciences of the United States of America, 112(19):6110–6115. **https://doi.org/10.1073/pnas.1423853112**

Badger, M.P.S., Chalk, T.B., Foster, G.L., Bown, P.R., Gibbs, S.J., Sexton, P.F., Schmidt, D.N., Pälike, H., Mackensen, A., and Pancost, R.D., 2019. Insensitivity of alkenone carbon isotopes to atmospheric CO_2 at low to moderate CO_2 levels. Climate of the Past, 15(2):539–554. **https://doi.org/10.5194/cp-15-539-2019**

Badger, M.P.S., Schmidt, D.N., Mackensen, A., and Pancost, R.D., 2013. High-resolution alkenone palaeobarometry indicates relatively stable pCO_2 during the Pliocene (3.3–2.8 Ma). Philosophical Transactions of the Royal Society A: Mathematical, Physical and Engineering Sciences, 371(2001):20130094. **https://doi.org/10.1098/rsta.2013.0094**

Batchelor, C.L., Christie, F.D.W., Ottesen, D., Montelli, A., Evans, J., Dowdeswell, E.K., Bjarnadóttir, L.R., and Dowdeswell, J.A., 2023. Rapid, buoyancy-driven ice-sheet retreat of hundreds of metres per day. Nature, 614:105–110. **https://doi.org/10.1038/s41586-023-05876-1**

Bensi, M., Kovačević, V., Langone, L., Aliani, S., Ursella, L., Goszczko, I., Soltwedel, T., Skogseth, R., Nilsen, F., Deponte, D., Mansutti, P., Laterza, R., Rebesco, M., Rui, L., Lucchi, R.G., Wåhlin, A., Viola, A., Beszczynska-Möller, A., and Rubino, A., 2019. Deep flow variability offshore south-west Svalbard (Fram Strait). Water, 11(4):683. **https://doi.org/10.3390/w11040683**

Bereiter, B., Eggleston, S., Schmitt, J., Nehrbass-Ahles, C., Stocker, T.F., Fischer, H., Kipfstuhl, S., and Chappellaz, J., 2015. Revision of the EPICA Dome C CO_2 record from 800 to 600 kyr before present. Geophysical Research Letters, 42(2):542–549. **https://doi.org/10.1002/2014GL061957**

Bereiter, B., Lüthi, D., Siegrist, M., Schüpbach, S., Stocker, T.F., and Fischer, H., 2012. Mode change of millennial CO_2 variability during the last glacial cycle associated with a bipolar marine carbon seesaw. Proceedings of the National Academy of Sciences of the United States of America, 109(25):9755–9760. **https://doi.org/10.1073/pnas.1204069109**

Beszczynska-Möller, A., Fahrbach, E., Schauer, U., and Hansen, E., 2012. Variability in Atlantic water temperature and transport at the entrance to the Arctic Ocean, 1997–2010. ICES Journal of Marine Science, 69(5):852–863. **https://doi.org/10.1093/icesjms/fss056**

Bickert, T., Curry, W.B., and Wefer, G., 1997. Late Pliocene to Holocene (2.6–0 Ma) western equatorial Atlantic deep-water circulation: inferences from benthic stable isotopes. In Shackleton, N.J., Curry, W.B., Richter, C., and Bralower, T.J. (Eds.), Proceedings of the Ocean Drilling Program, Scientific Results, 154: College Station, TX (Ocean Drilling Program). **https://doi.org/10.2973/odp.proc.sr.154.110.1997**

Bickle, M., Arculus, R., Barrett, P., DeConto, R., Camoin, G., Edwards, K., Fisher, F., Inagaki, F., Kodaira, S., and Ohkouchi, N., 2011. Illuminating Earth's Past, Present and Future The Science Plan for the International Ocean Discovery Program 2013-2023: Washington, DC (Integrated Ocean Drilling Program). **http://www.iodp.org/about-iodp/iodp-science-plan-2013-2023**

Bierman, P.R., Shakun, J.D., Corbett, L.B., Zimmerman, S.R., and Rood, D.H., 2016. A persistent and dynamic East Greenland Ice Sheet over the past 7.5 million years. Nature, 540(7632):256–260. **https://doi.org/10.1038/nature20147**

Bohrmann, G., Henrich, R., and Thiede, J., 1990. Miocene to Quaternary paleoceanography in the northern North Atlantic: variability in carbonate and biogenic opal accumulation. In Bleil, U., and Thiede, J. (Eds.), Geological History of the Polar Oceans: Arctic versus Antarctic. NATO ASI Series, 308: 647–675. **https://doi.org/10.1007/978-94-009-2029-3_34**

Bolton, C.T., Hernández-Sánchez, M.T., Fuertes, M.-Á., González-Lemos, S., Abrevaya, L., Mendez-Vicente, A., Flores, J.-A., Probert, I., Giosan, L., Johnson, J., and Stoll, H.M., 2016. Decrease in coccolithophore calcification and CO_2 since the middle Miocene. Nature Communications, 7(1):10284. **https://doi.org/10.1038/ncomms10284**

Bond, G., Heinrich, H., Broecker, W., Labeyrie, L., McManus, J., Andrews, J., Huon, S., Jantschik, R., Clasen, S., Simet, C., Tedesco, K., Klas, M., Bonani, G., and Ivy, S., 1992. Evidence for massive discharges of icebergs into the North Atlantic ocean during the last glacial period. Nature, 360(6401):245–249. **https://doi.org/10.1038/360245a0**

Bourke, R.H., Weigel, A.M., and Paquette, R.G., 1988. The westward turning branch of the West Spitsbergen Current. Journal of Geophysical Research: Oceans, 93(C11):14065–14077. **https://doi.org/10.1029/JC093iC11p14065**

Bradley, R.S., and England, J.H., 2008. The Younger Dryas and the sea of ancient ice. Quaternary Research, 70(1):1–10. **https://doi.org/10.1016/j.yqres.2008.03.002**

Broecker, W., Bond, G., Klas, M., Clark, E., and McManus, J., 1992. Origin of the northern Atlantic's Heinrich events. Climate Dynamics, 6(3):265–273. **https://doi.org/10.1007/BF00193540**

Brown, R.M., Chalk, T.B., Crocker, A.J., Wilson, P.A., and Foster, G.L., 2022. Late Miocene cooling coupled to carbon dioxide with Pleistocene-like climate sensitivity. Nature Geoscience, 15:664–670. **https://doi.org/10.1038/s41561-022-00982-7**

Bünz, S., Polyanov, S., Vadakkepuliyambatta, S., Consolaro, C., and Mienert, J., 2012. Active gas venting through hydrate-bearing sediments on the Vestnesa Ridge, offshore W-Svalbard. Marine Geology, 332–334:189–197. **https://doi.org/10.1016/j.margeo.2012.09.012**

Burton, K.W., Ling, H.-F., and O'Nions, R.K., 1997. Closure of the Central American Isthmus and its effect on deep-water formation in the North Atlantic. Nature, 386(6623):382–385. **https://doi.org/10.1038/386382a0**

Butt, F.A., Drange, H., Elverhøi, A., Otterå, O.H., and Solheim, A., 2002. Modelling Late Cenozoic isostatic elevation changes in the Barents Sea and their implications for oceanic and climatic regimes: preliminary results. Quaternary Science Reviews, 21(14–15):1643–1660. **https://doi.org/10.1016/S0277-3791(02)00018-5**

Butt, F.A., Elverhøi, A., Solheim, A., and Forsberg, C.F., 2000. Deciphering late Cenozoic development of the western Svalbard Margin from ODP Site 986 results. Marine Geology, 169(3):373–390. **https://doi.org/10.1016/S0025-3227(00)00088-8**

Caricchi, C., Lucchi, R.G., Sagnotti, L., Macrì, P., Di Roberto, A., Del Carlo, P., Husum, K., Laberg, J.S., and Morigi, C., 2019. A high-resolution geomagnetic relative paleointensity record from the Arctic Ocean deep-water gateway deposits during the last 60 kyr. Geochemistry, Geophysics, Geosystems, 20(5):2355–2377. **https://doi.org/10.1029/2018GC007955**

Caricchi, C., Sagnotti, L., Campuzano, S.A., Lucchi, R.G., Macrì, P., Rebesco, M., and Camerlenghi, A., 2020. A refined age calibrated paleosecular variation and relative paleointensity stack for the NW Barents Sea: implication for geomagnetic field behavior during the Holocene. Quaternary Science Reviews, 229:106133. **https://doi.org/10.1016/j.quascirev.2019.106133**

Carmack, E., Polyakov, I., Padman, L., Fer, I., Hunke, E., Hutchings, J., Jackson, J., Kelley, D., Kwok, R., Layton, C., Melling, H., Perovich, D., Persson, O., Ruddick, B., Timmermans, M.-L., Toole, J., Ross, T., Vavrus, S., and Winsor, P., 2015. Toward quantifying the increasing role of oceanic heat in sea ice loss in the new Arctic. Bulletin of the American Meteorological Society, 96(12):2079–2105. **https://doi.org/10.1175/BAMS-D-13-00177.1**

Clark, P.U., Alley, R.B., and Pollard, D., 1999. Northern Hemisphere ice-sheet influences on global climate change. Science, 286(5442):1104–1111. **https://doi.org/10.1126/science.286.5442.1104**

Clark, P.U., Archer, D., Pollard, D., Blum, J.D., Rial, J.A., Brovkin, V., Mix, A.C., Pisias, N.G., and Roy, M., 2006. The Middle Pleistocene transition: characteristics, mechanisms, and implications for long-term changes in atmospheric pCO_2. Quaternary Science Reviews, 25(23–24):3150–3184. **https://doi.org/10.1016/j.quascirev.2006.07.008**

Clotten, C., Stein, R., Fahl, K., Schreck, M., Risebrobakken, B., and De Schepper, S., 2019. On the causes of Arctic sea ice in the warm Early Pliocene. Scientific Reports, 9(1):989. **https://doi.org/10.1038/s41598-018-37047-y**

Coates, A.G., and Obando, J.A., 1996. The geologic evolution of the central American isthmus. In Jackson, J.B.C., Budd, A.F., and Coates, A.G. (Eds.), Evolution and Environment in Tropical America. Chicago (University of Chicago Press), 21–56.

Colleoni, F., De Santis, L., Montoli, E., Olivo, E., Sorlien, C.C., Bart, P.J., Gasson, E.G.W., Bergamasco, A., Sauli, C., Wardell, N., and Prato, S., 2018. Past continental shelf evolution increased Antarctic ice sheet sensitivity to climatic conditions. Scientific Reports, 8(1):11323. **https://doi.org/10.1038/s41598-018-29718-7**

Condron, A., Joyce, A.J., and Bradley, R.S., 2020. Arctic sea ice export as a driver of deglacial climate. Geology, 48(4):395–399. **https://doi.org/10.1130/G47016.1**

Consolaro, C., Rasmussen, T.L., Panieri, G., Mienert, J., Bünz, S., and Sztybor, K., 2015. Carbon isotope ($\delta^{13}C$) excursions suggest times of major methane release during the last 14 kyr in Fram Strait, the deep-water gateway to the Arctic. Climate of the Past, 11(4):669–685. **https://doi.org/10.5194/cp-11-669-2015**

Cronin, T.M., Dwyer, G.S., Caverly, E.K., Farmer, J., DeNinno, L.H., Rodriguez-Lazaro, J., and Gemery, L., 2017. Enhanced Arctic amplification began at the Mid-Brunhes Event ~400,000 years ago. Scientific Reports, 7(1):14475. **https://doi.org/10.1038/s41598-017-13821-2**

Curry, R., 2010. Wikipedia File: OCP07 Fig-6.jpg. **https://editors.eol.org/eoearth/wiki/File:OCP07_Fig-6.jpg**

Da, J., Zhang, Y.G., Li, G., Meng, X., and Ji, J., 2019. Low CO_2 levels of the entire Pleistocene epoch. Nature Communications, 10(1):4342. **https://doi.org/10.1038/s41467-019-12357-5**

Dansgaard, W., Johnsen, S.J., Clausen, H.B., Dahl-Jensen, D., Gundestrup, N.S., Hammer, C.U., Hvidberg, C.S., Steffensen, J.P., Sveinbjörnsdottir, A.E., Jouzel, J., and Bond, G., 1993. Evidence for general instability of past climate from a 250-kyr ice-core record. Nature, 364(6434):218–220. **https://doi.org/10.1038/364218a0**

de la Vega, E., Chalk, T.B., Wilson, P.A., Bysani, R.P., and Foster, G.L., 2020. Atmospheric CO_2 during the Mid-Piacenzian Warm Period and the M2 glaciation. Scientific Reports, 10(1):11002. **https://doi.org/10.1038/s41598-020-67154-8**

De Schepper, S., Gibbard, P.L., Salzmann, U., and Ehlers, J., 2014. A global synthesis of the marine and terrestrial evidence for glaciation during the Pliocene epoch. Earth-Science Reviews, 135:83–102. **https://doi.org/10.1016/j.earscirev.2014.04.003**

Drury, A.J., Westerhold, T., Frederichs, T., Tian, J., Wilkens, R., Channell, J.E.T., Evans, H., John, C.M., Lyle, M., and Röhl, U., 2017. Late Miocene climate and time scale reconciliation; accurate orbital calibration from a deep-sea perspective. Earth and Planetary Science Letters, 475:254–266. **https://doi.org/10.1016/j.epsl.2017.07.038**

Dutton, A., Carlson, A.E., Long, A.J., Milne, G.A., Clark, P.U., DeConto, R., Horton, B.P., Rahmstorf, S., and Raymo, M.E., 2015. Sea-level rise due to polar ice-sheet mass loss during past warm periods. Science, 349(6244):aaa4019. **https://doi.org/10.1126/science.aaa4019**

Dyez, K.A., Hönisch, B., and Schmidt, G.A., 2018. Early Pleistocene obliquity-scale pCO_2 variability at ~1.5 million years ago. Paleoceanography and Paleoclimatology, 33(11):1270–1291. **https://doi.org/10.1029/2018PA003349**

Ehlers, B.-M., and Jokat, W., 2013. Paleo-bathymetry of the northern North Atlantic and consequences for the opening of the Fram Strait. Marine Geophysical Research, 34(1):25–43. **https://doi.org/10.1007/s11001-013-9165-9**

Eiken, O., and Hinz, K., 1993. Contourites in the Fram Strait. Sedimentary Geology, 82(1–4):15–32. **https://doi.org/10.1016/0037-0738(93)90110-Q**

Engen, Ø., Faleide, J.I., and Dyreng, T.K., 2008. Opening of the Fram Strait gateway: a review of plate tectonic constraints. Tectonophysics, 450(1–4):51–69. **https://doi.org/10.1016/j.tecto.2008.01.002**

Fedorov, A.V., Brierley, C.M., Lawrence, K.T., Liu, Z., Dekens, P.S., and Ravelo, A.C., 2013. Patterns and mechanisms of early Pliocene warmth. Nature, 496(7443):43–49. **https://doi.org/10.1038/nature12003**

Fer, I., Skogseth, R., Haugan, P.M., and Jaccard, P., 2003. Observations of the Storfjorden overflow. Deep Sea Research, Part I: Oceanographic Research Papers, 50(10):1283–1303. **https://doi.org/10.1016/S0967-0637(03)00124-9**

Flecker, R., Ducassou, E., Williams, T., and the Expedition 401 Scientists, 2024. Expedition 401 Preliminary Report: Mediterranean–Atlantic Gateway Exchange. International Ocean Discovery Program. **https://doi.org/10.14379/iodp.pr.401.2024**

Fohrmann, H., Backhaus, J.O., Blaume, F., and Rumohr, J., 1998. Sediments in bottom-arrested gravity plumes: numerical case studies. Journal of Physical Oceanography, 28(11):2250–2274. **https://doi.org/10.1175/1520-0485(1998)028%3C2250:SIBAGP%3E2.0.CO;2**

Ford, H.L., Ravelo, A.C., Dekens, P.S., LaRiviere, J.P., and Wara, M.W., 2015. The evolution of the equatorial thermocline and the early Pliocene El Padre mean state. Geophysical Research Letters, 42(12):4878–4887. **https://doi.org/10.1002/2015GL064215**

Forsberg, C.F., Solheim, A., Elverhoi, A., Jansen, E., Channell, J.E.T., and Andersen, E.S., 1999. The depositional environment of the western Svalbard margin during the late Pliocene and the Pleistocene; sedimentary facies changes at Site 986. In Raymo, M.E., Jansen, E., Blum, P., and Herbert, T.D. (Eds.), Proceedings of the Ocean Drilling Program, Scientific Results, 162: College Station, TX (Ocean Drilling Program). **https://doi.org/10.2973/odp.proc.sr.162.032.1999**

Freitas, L., Appolinario, L., Calegario, G., Campeão, M., Tschoeke, D., Garcia, G., Venancio, I.M., Cosenza, C.A.N., Leomil, L., Bernardes, M., Albuquerque, A.L., Thompson, C., and Thompson, F., 2020. Glacial-interglacial transitions in microbiomes recorded in deep-sea sediments from the western equatorial Atlantic. Science of The Total Environment, 746:140904. **https://doi.org/10.1016/j.scitotenv.2020.140904**

Gamboa Sojo, V.M., Morigi, C., Langone, L., and Lucchi, R.G., 2024. Deciphering paleoceanographic shifts inferred from the foraminiferal record of the western Svalbard Slope (Bellsund Drift) over the past century. Journal of Marine Science and Engineering, 12(4):559. **https://doi.org/10.3390/jmse12040559**

Gebhardt, A.C., Geissler, W.H., Matthiessen, J., and Jokat, W., 2014. Changes in current patterns in the Fram Strait at the Pliocene/Pleistocene boundary. Quaternary Science Reviews, 92:179–189. **https://doi.org/10.1016/j.quascirev.2013.07.015**

Geissler, W.H., Jokat, W., and Brekke, H., 2011. The Yermak Plateau in the Arctic Ocean in the light of reflection seismic data-implication for its tectonic and sedimentary evolution. Geophysical Journal International, 187(3):1334–1362. **https://doi.org/10.1111/j.1365-246X.2011.05197.x**

Gildor, H., and Tziperman, E., 2001. A sea ice climate switch mechanism for the 100-kyr glacial cycles. Journal of Geophysical Research: Oceans, 106(C5):9117–9133. **https://doi.org/10.1029/1999JC000120**

Goldschmidt, P.M., Pfirman, S.L., Wollenburg, I., and Henrich, R., 1992. Origin of sediment pellets from the Arctic seafloor: sea ice or icebergs? Deep Sea Research Part A. Oceanographic Research Papers, 39(2, Part 1):S539–S565. **https://doi.org/10.1016/S0198-0149(06)80020-8**

Golledge, N.R., Keller, E.D., Gomez, N., Naughten, K.A., Bernales, J., Trusel, L.D., and Edwards, T.L., 2019. Global environmental consequences of twenty-first-century ice-sheet melt. Nature, 566(7742):65–72. **https://doi.org/10.1038/s41586-019-0889-9**

González-Lanchas, A., Hernández-Almeida, I., Flores, J.-A., Sierro, F.J., Guitian, J., and Stoll, H.M., 2021. Carbon isotopic fractionation of alkenones and Gephyrocapsa coccoliths over the late Quaternary (Marine Isotope Stages 12–9) glacial-interglacial cycles at the western tropical Atlantic. Paleoceanography and Paleoclimatology, 36(8):e2020PA004175. **https://doi.org/10.1029/2020PA004175**

Gradstein, F.M., Ogg, J.G., Schmitz, M.D., and Ogg, G.M. (Eds.), 2020. Geologic Time Scale 2020: Amsterdam (Elsevier BV). **https://doi.org/10.1016/C2020-1-02369-3**

Gruetzner, J., Matthiessen, J., Geissler, W.H., Gebhardt, A.C., and Schreck, M., 2022. A revised core-seismic integration in the Molloy Basin (ODP Site 909): implications for the history of ice rafting and ocean circulation in the Atlantic-Arctic gateway. Global and Planetary Change, 215:103876. **https://doi.org/10.1016/j.gloplacha.2022.103876**

Hattermann, T., Isachsen, P.E., von Appen, W.-J., Albretsen, J., and Sundfjord, A., 2016. Eddy-driven recirculation of Atlantic Water in Fram Strait. Geophysical Research Letters, 43(7):3406–3414. **https://doi.org/10.1002/2016GL068323**

Haug, G.H., Ganopolski, A., Sigman, D.M., Rosell-Mele, A., Swann, G.E.A., Tiedemann, R., Jaccard, S.L., Bollmann, J., Maslin, M.A., Leng, M.J., and Eglinton, G., 2005. North Pacific seasonality and the glaciation of North America 2.7 million years ago. Nature, 433(7028):821–825. **https://doi.org/10.1038/nature03332**

Haywood, A.M., Dowsett, H.J., and Dolan, A.M., 2016. Integrating geological archives and climate models for the mid-Pliocene warm period. Nature Communications, 7(1):10646. **https://doi.org/10.1038/ncomms10646**

Hegewald, A., and Jokat, W., 2013. Tectonic and sedimentary structures in the northern Chukchi region, Arctic Ocean. Journal of Geophysical Research: Solid Earth, 118(7):3285–3296. **https://doi.org/10.1002/jgrb.50282**

Henehan, M.J., Rae, J.W.B., Foster, G.L., Erez, J., Prentice, K.C., Kucera, M., Bostock, H.C., Martínez-Botí, M.A., Milton, J.A., Wilson, P.A., Marshall, B.J., and Elliott, T., 2013. Calibration of the boron isotope proxy in the planktonic foraminifera Globigerinoides ruber for use in palaeo-CO_2 reconstruction. Earth and Planetary Science Letters, 364:111–122. **https://doi.org/10.1016/j.epsl.2012.12.029**

Herbert, T.D., Lawrence, K.T., Tzanova, A., Peterson, L.C., Caballero-Gill, R.P., and Kelly, C.S., 2016. Late Miocene global cooling and the rise of modern ecosystems. Nature Geoscience, 9(11):843–847. **https://doi.org/10.1038/ngeo2813**

Hesse, R., Khodabakhsh, S., Klaucke, I., and Ryan, W.B.F., 1997. Asymmetrical turbid surface-plume deposition near ice-outlets of the Pleistocene Laurentide ice sheet in the Labrador Sea. Geo-Marine Letters, 17(3):179–187. **https://doi.org/10.1007/s003670050024**

Himmler, T., Sahy, D., Martma, T., Bohrmann, G., Plaza-Faverola, A., Bünz, S., Condon, D.J., Knies, J., and Lepland, A., 2019. A 160,000-year-old history of tectonically controlled methane seepage in the Arctic. Science Advances, 5(8):eaaw1450. **https://doi.org/10.1126/sciadv.aaw1450**

Hoehler, T.M., and Jørgensen, B.B., 2013. Microbial life under extreme energy limitation. Nature Reviews Microbiology, 11(2):83. **http://doi.org/10.1038/nrmicro2939**

Holbourn, A., Kuhnt, W., Clemens, S., Prell, W., and Andersen, N., 2013. Middle to Late Miocene stepwise climate cooling: evidence from a high-resolution deep water isotope curve spanning 8 million years. Paleoceanography, 28(4):688–699. **https://doi.org/10.1002/2013PA002538**

Holbourn, A., Kuhnt, W., Clemens, S.C., Kochhann, K.G.D., Jöhnck, J., Lübbers, J., and Andersen, N., 2018. Late Miocene climate cooling and intensification of southeast Asian winter monsoon. Nature Communications, 9(1):1584. **https://doi.org/10.1038/s41467-018-03950-1**

Hopkins, T.S., 1991. The GIN Sea—a synthesis of its physical oceanography and literature review 1972–1985. Earth-Science Reviews, 30(3):175–318. **https://doi.org/10.1016/0012-8252(91)90001-V**

Howe, J.A., Shimmield, T.M., Harland, R., and Eyles, N., 2008. Late Quaternary contourites and glaciomarine sedimentation in the Fram Strait. Sedimentology, 55(1):179–200. **https://doi.org/10.1111/j.1365-3091.2007.00897.x**

Jakobsson, M., Backman, J., Rudels, B., Nycander, J., Frank, M., Mayer, L., Jokat, W., Sangiorgi, F., O'Regan, M., Brinkhuis, H., King, J., and Moran, K., 2007. The Early Miocene onset of ventilated circulation regime in the Arctic Ocean. Nature, 447(7147):986–990. **https://doi.org/10.1038/nature05924**

Jakobsson, M., Ingólfsson, Ó., Long, A.J., and Spielhagen, R.F., 2014. The dynamic Arctic. Quaternary Science Reviews, 92:1–8. **https://doi.org/10.1016/j.quascirev.2014.03.022**

Jakobsson, M., Mayer, L., Coakley, B., Dowdeswell, J.A., Forbes, S., Fridman, B., Hodnesdal, H., Noormets, R., Pedersen, R., Rebesco, M., Schenke, H.W., Zarayskaya, Y., Accettella, D., Armstrong, A., Anderson, R.M., Bienhoff, P., Camerlenghi, A., Church, I., Edwards, M., Gardner, J.V., Hall, J.K., Hell, B., Hestvik, O., Kristofferson, Y., Marcussen, C., Mohammad, R., Mosher, D., Nghiem, S.V., Pedrosa, M.T., Travaglini, P.G., and Weatherall, P., 2012. The International Bathymetric Chart of the Arctic Ocean (IBCAO) Version 3.0. Geophysical Research Letters, 39(12):L12609. **https://doi.org/10.1029/2012GL052219**

Jansen, E., and Raymo, M.E., 1996. Leg 162: new frontiers on past climates. In Jansen, E., Raymo, M.E., Blum, P., et al., Proceedings of the Ocean Drilling Program, Initial Reports, 162: College Station, TX (Ocean Drilling Program), 5–20. **https://doi.org/10.2973/odp.proc.ir.162.101.1996**

Jansen, E., and Sjøholm, J., 1991. Reconstruction of glaciation over the past 6 Myr from ice-borne deposits in the Norwegian Sea. Nature, 349(6310):600–603. **https://doi.org/10.1038/349600a0**

Jasper, J.P., and Hayes, J.M., 1990. A carbon isotope record of CO_2 levels during the late Quaternary. Nature, 347(6292):462–464. **https://doi.org/10.1038/347462a0**

Jessen, S.P., Rasmussen, T.L., Nielsen, T., and Solheim, A., 2010. A new late Weichselian and Holocene marine chronology for the western Svalbard slope 30,000–0 cal years BP. Quaternary Science Reviews, 29(9–10):1301–1312. **https://doi.org/10.1016/j.quascirev.2010.02.020**

Johnson, J.E., Mienert, J., Plaza-Faverola, A., Vadakkepuliyambatta, S., Knies, J., Bünz, S., Andreassen, K., and Ferré, B., 2015. Abiotic methane from ultraslow-spreading ridges can charge Arctic gas hydrates. Geology, 43(5):371–374. **https://doi.org/10.1130/G36440.1**

JOIDES Pollution Prevention and Safety Panel, 1992. Ocean Drilling Program guidelines for pollution prevention and safety. JOIDES Journal, 18(7):24. **http://www.odplegacy.org/PDF/Admin/JOIDES_Journal/JJ_1992_V18_No7.pdf**

Jokat, W., Geissler, W., and Voss, M., 2008. Basement structure of the north-western Yermak Plateau. Geophysical Research Letters, 35(5). **https://doi.org/10.1029/2007GL032892**

Jordan, J.R., Miles, B.W.J., Gudmundsson, G.H., Jamieson, S.S.R., Jenkins, A., and Stokes, C.R., 2023. Increased warm water intrusions could cause mass loss in East Antarctica during the next 200 years. Nature Communications, 14(1):1825. **https://doi.org/10.1038/s41467-023-37553-2**

Joughin, I., and Alley, R.B., 2011. Stability of the West Antarctic Ice Sheet in a warming world. Nature Geoscience, 4(8):506–513. **https://doi.org/10.1038/ngeo1194**

Kallmeyer, J., Pockalny, R., Adhikari, R.R., Smith, D.C., and D'Hondt, S., 2012. Global distribution of microbial abundance and biomass in subseafloor sediment. Proceedings of the National Academy of Sciences of the United States of America, 109(40):16213–16216. **https://doi.org/10.1073/pnas.1203849109**

Katayama, T., Yoshioka, H., Kaneko, M., Amo, M., Fujii, T., Takahashi, H.A., Yoshida, S., and Sakata, S., 2022. Cultivation and biogeochemical analyses reveal insights into methanogenesis in deep subseafloor sediment at a biogenic gas hydrate site. The ISME Journal, 16(5):1464–1472. **https://doi.org/10.1038/s41396-021-01175-7**

Kjær, K.H., Winther Pedersen, M., De Sanctis, B., De Cahsan, B., Korneliussen, T.S., Michelsen, C.S., Sand, K.K., Jelavić, S., Ruter, A.H., Schmidt, A.M.A., Kjeldsen, K.K., Tesakov, A.S., Snowball, I., Gosse, J.C., Alsos, I.G., Wang, Y., Dockter, C., Rasmussen, M., Jørgensen, M.E., Skadhauge, B., Prohaska, A., Kristensen, J.Å., Bjerager, M., Allentoft, M.E., Coissac, E., Alsos, I.G., Coissac, E., Rouillard, A., Simakova, A., Fernandez-Guerra, A., Bowler, C., Macias-Fauria, M., Vinner, L., Welch, J.J., Hidy, A.J., Sikora, M., Collins, M.J., Durbin, R., Larsen, N.K., Willerslev, E., and PhyloNorway, C., 2022. A 2-million-year-old ecosystem in Greenland uncovered by environmental DNA. Nature, 612(7939):283–291. **https://doi.org/10.1038/s41586-022-05453-y**

Knies, J., and Gaina, C., 2008. Middle Miocene ice sheet expansion in the Arctic: views from the Barents Sea. Geochemistry, Geophysics, Geosystems, 9(2):Q02015. **https://doi.org/10.1029/2007GC001824**

Knies, J., Matthiessen, J., Vogt, C., Laberg, J.S., Hjelstuen, B.O., Smelror, M., Larsen, E., Andreassen, K., Eidvin, T., and Vorren, T.O., 2009. The Plio-Pleistocene glaciation of the Barents Sea–Svalbard region: a new model based on revised chronostratigraphy. Quaternary Science Reviews, 28(9):812–829. **https://doi.org/10.1016/j.quascirev.2008.12.002**

Knies, J., Mattingsdal, R., Fabian, K., Grøsfjeld, K., Baranwal, S., Husum, K., De Schepper, S., Vogt, C., Andersen, N., Matthiessen, J., Andreassen, K., Jokat, W., Nam, S.-I., and Gaina, C., 2014. Effect of early Pliocene uplift on Late Pliocene cooling in the Arctic–Atlantic gateway. Earth and Planetary Science Letters, 387:132–144. **https://doi.org/10.1016/j.epsl.2013.11.007**

Knutz, P.C., 2008. Palaeoceanographic significance of contourite drifts. In Rebesco, M., and Camerlenghi, A. (Eds.), Contourites. Developments in Sedimentology, 60: (Elsevier), 511–535. **https://doi.org/10.1016/S0070-4571(08)10024-3**

Knutz, P.C., Jennings, A., Childress, L.B., and the Expedition 400 Scientists, 2024. Expedition 400 Preliminary Report: NW Greenland Glaciated Margin. International Ocean Discovery Program. **https://doi.org/10.14379/iodp.pr.400.2024**

Koenig, Z., Meyer, A., Provost, C., Sennéchael, N., Sundfjord, A., Beguery, L., Athanase, M., and Gascard, J.-C., 2018. Cooling and freshening of the West Spitsbergen Current by shelf-origin cold core lenses. Journal of Geophysical Research: Oceans, 123(11):8299–8312. **https://doi.org/10.1029/2018JC014463**

Kolawole, F., and Evenick, J.C., 2023. Global distribution of geothermal gradients in sedimentary basins. Geoscience Frontiers, 14(6):101685. **https://doi.org/10.1016/j.gsf.2023.101685**

Koppers, A., and Coggon, R. (Eds.), 2020. Exploring Earth by Scientific Ocean Drilling: 2050 Science Framework: San Diego, CA (UC San Diego Library). **https://doi.org/10.6075/J0W66J9H**

Krissek, L.A., 1995. Late Cenozoic ice-rafting records from Leg 145 sites in the North Pacific; Late Miocene onset, Late Pliocene intensification, and Pliocene-Pleistocene events. In Rea, D.K., Basov, I.A., Scholl, D.W., and Allan, J.F. (Eds.), Proceedings of the Ocean Drilling Program, Scientific Results, 145: College Station, TX (Ocean Drilling Program), 179–194. **https://doi.org/10.2973/odp.proc.sr.145.118.1995**

Kvenvolden, K.A., and Barnard, L.A., 1983. Gas hydrates of the Blake Outer Ridge, Site 533, Deep Sea Drilling Project Leg 76. In Sheridan, R.E., Gradstein, F.M., et al., Initial Reports of the Deep Sea Drilling Project, 76: Washington, DC (U.S. Government Printing Office), 353–365. **https://doi.org/10.2973/dsdp.proc.76.106.1983**

Laberg, J.S., Andreassen, K., Knies, J., Vorren, T.O., and Winsborrow, M., 2010. Late Pliocene–Pleistocene development of the Barents Sea Ice Sheet. Geology, 38(2):107–110. **https://doi.org/10.1130/G30193.1**

Laberg, J.S., Andreassen, K., and Vorren, T.O., 2012. Late Cenozoic erosion of the high-latitude southwestern Barents Sea shelf revisited. Geological Society of America Bulletin, 124(1–2):77–88. **https://doi.org/10.1130/B30340.1**

Laberg, J.S., Stoker, M.S., Dahlgren, K.I.T., Haas, H.d., Haflidason, H., Hjelstuen, B.O., Nielsen, T., Shannon, P.M., Vorren, T.O., van Weering, T.C.E., and Ceramicola, S., 2005. Cenozoic alongslope processes and sedimentation on the NW European Atlantic margin. Marine and Petroleum Geology, 22(9–10):1069–1088. **https://doi.org/10.1016/j.marpetgeo.2005.01.008**

Laberg, J.S., and Vorren, T.O., 2004. Weichselian and Holocene growth of the northern high-latitude Lofoten Contourite Drift on the continental slope of Norway. Sedimentary Geology, 164(1):1–17. **https://doi.org/10.1016/j.sedgeo.2003.07.004**

Langehaug, H.R., and Falck, E., 2012. Changes in the properties and distribution of the intermediate and deep waters in the Fram Strait. Progress in Oceanography, 96(1):57–76. **https://doi.org/10.1016/j.pocean.2011.10.002**

Larsen, H.C., Saunders, A.D., Clift, P.D., Beget, J., Wei, W., and Spezzaferri, S., 1994. Seven million years of glaciation in Greenland. Science, 264(5161):952–955. **https://doi.org/10.1126/science.264.5161.952**

Lasabuda, A.P.E., Johansen, N.S., Laberg, J.S., Faleide, J.I., Senger, K., Rydningen, T.A., Patton, H., Knutsen, S.-M., and Hanssen, A., 2021. Cenozoic uplift and erosion of the Norwegian Barents Shelf – a review. Earth-Science Reviews, 217:103609. **https://doi.org/10.1016/j.earscirev.2021.103609**

Lenton, T.M., Rockström, J., Gaffney, O., Rahmstorf, S., Richardson, K., Steffen, W., and Schellnhuber H.J., 2019. Climate tipping points — too risky to bet against. Nature, 575:592–595. **https://doi.org/10.1038/d41586-019-03595-0**

Levy, R.H., Meyers, S.R., Naish, T.R., Golledge, N.R., McKay, R.M., Crampton, J.S., DeConto, R.M., De Santis, L., Florindo, F., Gasson, E.G.W., Harwood, D.M., Luyendyk, B.P., Powell, R.D., Clowes, C., and Kulhanek, D.K., 2019. Antarctic ice-sheet sensitivity to obliquity forcing enhanced through ocean connections. Nature Geoscience, 12(2):132–137. **https://doi.org/10.1038/s41561-018-0284-4**

Lisiecki, L.E., and Raymo, M.E., 2005. A Pliocene-Pleistocene stack of 57 globally distributed benthic $\delta^{18}O$ records. Paleoceanography, 20(1):PA1003. **https://doi.org/10.1029/2004PA001071**

Lucchi, R.G., Camerlenghi, A., Rebesco, M., Colmenero-Hidalgo, E., Sierro, F.J., Sagnotti, L., Urgeles, R., Melis, R., Morigi, C., Bárcena, M.A., Giorgetti, G., Villa, G., Persico, D., Flores, J.A., Rigual-Hernández, A.S., Pedrosa, M.T., Macri, P., and Caburlotto, A., 2013. Postglacial sedimentary processes on the Storfjorden and Kveithola trough

mouth fans: significance of extreme glacimarine sedimentation. Global and Planetary Change, 111:309–326. **https://doi.org/10.1016/j.gloplacha.2013.10.008**

Lucchi, R., Kovacevic, V., Aliani, S., Caburlotto, A., Celussi, M., Corgnati, L., Cosoli, S., Ersdal, E.A., Fredriksson, S., Goszczko, I., Husum, K., G, I., Laberg, J., Łącka, M., Langone, L., P, M., K, M., Morigi, C., Realdon, G., and Tirelli, V., 2014. Present and past flow regime. On contourite drifts west of Spitsbergen. EUROFLEETS-2 Cruise Summary Report R/V G.O. Sars, Cruise No. 191. **https://doi.org/10.13140/2.1.1975.3769**

Lucchi, R.G., Morigi, C., Sverre Laberg, J., Husum, K., Gamboa Sojo, V., Musco, M.E., Caricchi, C., Caffau, M., Sagnotti, L., Macrì, P., Princivalle, F., Giorgetti, G., Caburlotto, A., and Rebesco, M., 2018. The climatic significance of laminated sediments from turbid meltwaters on the NW Barents Sea continental margin (Arctic). Geophysical Research Abstracts, 20:EGU2018–3115. **https://meetingorganizer.copernicus.org/EGU2018/EGU2018-3115.pdf**

Lucchi, R.G., Pedrosa, M.T., Camerlenghi, A., Urgeles, R., De Mol, B., and Rebesco, M., 2012. Recent submarine landslides on the continental slope of Storfjorden and Kveithola Trough-Mouth Fans (North West Barents Sea). In Yamada, Y., Kawamura, K., Ikehara, K., Ogawa, Y., Urgeles, R., Mosher, D., Chaytor, J. and Strasser, M., Submarine Mass Movements and Their Consequences. Advances in Natural and Technological Hazards Research. Dordrecht (Springer Netherlands), 735–745. **https://doi.org/10.1007/978-94-007-2162-3_65**

Lucchi, R.G., Rebesco, M., Camerlenghi, A., Busetti, M., Tomadin, L., Villa, G., Persico, D., Morigi, C., Bonci, M.C., and Giorgetti, G., 2002. Mid-Late Pleistocene glacimarine sedimentary processes of a high-latitude, deep-sea sediment drift (Antarctic Peninsula Pacific margin). Marine Geology, 189(3–4):343–370. **https://doi.org/10.1016/S0025-3227(02)00470-X**

Lucchi, R.G., Sagnotti, L., Camerlenghi, A., Macrì, P., Rebesco, M., Pedrosa, M.T., and Giorgetti, G., 2015. Marine sedimentary record of Meltwater Pulse 1a along the NW Barents Sea continental margin. arktos, 1(1):7. **https://doi.org/10.1007/s41063-015-0008-6**

Lucchi, R.G., St. John, K., and Ronge, T.A., 2023. Expedition 403 Scientific Prospectus: Eastern Fram Strait Paleo-Archive (FRAME). International Ocean Discovery Program. **https://doi.org/10.14379/iodp.sp.403.2023**

Lucchi, R.G., St. John, K.E.K., Ronge, T.A., Barcena, M.A., De Schepper, S., Duxbury, L.C., Gebhardt, A.C., Gonzalez-Lanchas, A., Goss, G., Greco, N.M., Gruetzner, J., Haygood, L., Husum, K., Iizuka, M., Kapuge, A.K.I.U., Lam, A.R., Libman-Roshal, O., Liu, Y., Monito, L.R., Reilly, B.T., Rosenthal, Y., Sakai, Y., Sijinkumar, A.V., Suganuma, Y., and Zhong, Y., 2026a. Site U1618. In Lucchi, R.G., St. John, K.E.K., Ronge, T.A., and the Expedition 403 Scientists, Eastern Fram Strait Paleo-Archive. Proceedings of the International Ocean Discovery Program, 403: College Station, TX (International Ocean Discovery Program). **https://doi.org/10.14379/iodp.proc.403.103.2026**

Lucchi, R.G., St. John, K.E.K., Ronge, T.A., Barcena, M.A., De Schepper, S., Duxbury, L.C., Gebhardt, A.C., Gonzalez-Lanchas, A., Goss, G., Greco, N.M., Gruetzner, J., Haygood, L., Husum, K., Iizuka, M., Kapuge, A.K.I.U., Lam, A.R., Libman-Roshal, O., Liu, Y., Monito, L.R., Reilly, B.T., Rosenthal, Y., Sakai, Y., Sijinkumar, A.V., Suganuma, Y., and Zhong, Y., 2026b. Site U1624. In Lucchi, R.G., St. John, K.E.K., Ronge, T.A., and the Expedition 403 Scientists, Eastern Fram Strait Paleo-Archive. Proceedings of the International Ocean Discovery Program, 403: College Station, TX (International Ocean Discovery Program). **https://doi.org/10.14379/iodp.proc.403.107.2026**

Lucchi, R.G., St. John, K.E.K., Ronge, T.A., Barcena, M.A., De Schepper, S., Duxbury, L.C., Gebhardt, A.C., Gonzalez-Lanchas, A., Goss, G., Greco, N.M., Gruetzner, J., Haygood, L., Husum, K., Iizuka, M., Kapuge, A.K.I.U., Lam, A.R., Libman-Roshal, O., Liu, Y., Monito, L.R., Reilly, B.T., Rosenthal, Y., Sakai, Y., Sijinkumar, A.V., Suganuma, Y., and Zhong, Y., 2026c. Sites U1621–U1623. In Lucchi, R.G., St. John, K.E.K., Ronge, T.A., and the Expedition 403 Scientists, Eastern Fram Strait Paleo-Archive. Proceedings of the International Ocean Discovery Program, 403: College Station, TX (International Ocean Discovery Program). **https://doi.org/10.14379/iodp.proc.403.106.2026**

Lunt, D.J., Valdes, P.J., Haywood, A., and Rutt, I.C., 2008. Closure of the Panama Seaway during the Pliocene: implications for climate and Northern Hemisphere glaciation. Climate Dynamics, 30(1):1–18. **https://doi.org/10.1007/s00382-007-0265-6**

MacFarling Meure, C., Etheridge, D., Trudinger, C., Steele, P., Langenfelds, R., van Ommen, T., Smith, A., and Elkins, J., 2006. Law Dome CO_2, CH_4 and N_2O ice core records extended to 2000 years BP. Geophysical Research Letters, 33(14). **https://doi.org/10.1029/2006GL026152**

Mahajan, S., Zhang, R., and Delworth, T.L., 2011. Impact of the Atlantic Meridional Overturning Circulation (AMOC) on Arctic surface air temperature and sea ice variability. Journal of Climate, 24(24):6573–6581. **https://doi.org/10.1175/2011JCLI4002.1**

Marcott, S.A., Bauska, T.K., Buizert, C., Steig, E.J., Rosen, J.L., Cuffey, K.M., Fudge, T.J., Severinghaus, J.P., Ahn, J., Kalk, M.L., McConnell, J.R., Sowers, T., Taylor, K.C., White, J.W.C., and Brook, E.J., 2014. Centennial-scale changes in the global carbon cycle during the last deglaciation. Nature, 514(7524):616–619. **https://doi.org/10.1038/nature13799**

Marnela, M., Rudels, B., Houssais, M.N., Beszczynska-Möller, A., and Eriksson, P.B., 2013. Recirculation in the Fram Strait and transports of water in and north of the Fram Strait derived from CTD data. Ocean Sci., 9(3):499–519. **https://doi.org/10.5194/os-9-499-2013**

Martínez-Botí, M.A., Foster, G.L., Chalk, T.B., Rohling, E.J., Sexton, P.F., Lunt, D.J., Pancost, R.D., Badger, M.P.S., and Schmidt, D.N., 2015. Plio-Pleistocene climate sensitivity evaluated using high-resolution CO_2 records. Nature, 518(7537):49–54. **https://doi.org/10.1038/nature14145**

Martini, E., 1971. Standard Tertiary and Quaternary calcareous nannoplankton zonation. Proceedings of the Second Planktonic Conference, Roma, 1970:739–785.

Mattingsdal, R., Knies, J., Andreassen, K., Fabian, K., Husum, K., Grøsfjeld, K., and De Schepper, S., 2014. A new 6 Myr stratigraphic framework for the Atlantic–Arctic gateway. Quaternary Science Reviews, 92:170–178. **https://doi.org/10.1016/j.quascirev.2013.08.022**

Mejía, L.M., Méndez-Vicente, A., Abrevaya, L., Lawrence, K.T., Ladlow, C., Bolton, C., Cacho, I., and Stoll, H., 2017. A diatom record of CO_2 decline since the Late Miocene. Earth and Planetary Science Letters, 479:18–33. **https://doi.org/10.1016/j.epsl.2017.08.034**

Minakov, A., 2018. Late Cenozoic lithosphere dynamics in Svalbard: interplay of glaciation, seafloor spreading and mantle convection. Journal of Geodynamics, 122:1–16. **https://doi.org/10.1016/j.jog.2018.09.009**

Monnin, E., Indermühle, A., Dällenbach, A., Flückiger, J., Stauffer, B., Stocker, T.F., Raynaud, D., and Barnola, J.-M., 2001. Atmospheric CO_2 concentrations over the Last Glacial Termination. Science, 291(5501):112–114. **https://doi.org/10.1126/science.291.5501.112**

Monnin, E., Steig, E.J., Siegenthaler, U., Kawamura, K., Schwander, J., Stauffer, B., Stocker, T.F., Morse, D.L., Barnola, J.-M., Bellier, B., Raynaud, D., and Fischer, H., 2004. Evidence for substantial accumulation rate variability in Antarctica during the Holocene, through synchronization of CO_2 in the Taylor Dome, Dome C and DML ice cores. Earth and Planetary Science Letters, 224(1):45–54. **https://doi.org/10.1016/j.epsl.2004.05.007**

Montes, C., Cardona, A., Jaramillo, C., Pardo, A., Silva, J.C., Valencia, V., Ayala, C., Pérez-Angel, L.C., Rodriguez-Parra, L.A., Ramirez, V., and Niño, H., 2015. Middle Miocene closure of the Central American Seaway. Science, 348(6231):226–229. **https://doi.org/10.1126/science.aaa2815**

Morono, Y., Ito, M., Hoshino, T., Terada, T., Hori, T., Ikehara, M., D'Hondt, S., and Inagaki, F., 2020. Aerobic microbial life persists in oxic marine sediment as old as 101.5 million years. Nature Communications, 11(1):3626. **https://doi.org/10.1038/s41467-020-17330-1**

Müller, J., and Stein, R., 2014. High-resolution record of late glacial and deglacial sea ice changes in Fram Strait corroborates ice–ocean interactions during abrupt climate shifts. Earth and Planetary Science Letters, 403:446–455. **https://doi.org/10.1016/j.epsl.2014.07.016**

Myhre, A.M., Eldholm, O., and Sundvor, E., 1982. The margin between Senja and Spitsbergen fracture zones: implications from plate tectonics. Tectonophysics, 89(1–3):33–50. **https://doi.org/10.1016/0040-1951(82)90033-6**

Myhre, A.M., Thiede, J., Firth, J.V., et al., 1995. Proceedings of the Ocean Drilling Program, Initial Reports, 151: College Station, TX (Ocean Drilling Program). **https://doi.org/10.2973/odp.proc.ir.151.1995**

Naughten, K.A., Holland, P.R., and De Rydt, J., 2023. Unavoidable future increase in West Antarctic ice-shelf melting over the twenty-first century. Nature Climate Change, 13(11):1222–1228. **https://doi.org/10.1038/s41558-023-01818-x**

Nilsen, F., Skogseth, R., Vaardal-Lunde, J., and Inall, M., 2016. A simple shelf circulation model: intrusion of Atlantic Water on the West Spitsbergen shelf. Journal of Physical Oceanography, 46(4):1209–1230. **https://doi.org/10.1175/JPO-D-15-0058.1**

North Greenland Ice Core Project Members, 2004. High-resolution record of Northern Hemisphere climate extending into the last interglacial period. Nature, 431(7005):147–151. **https://doi.org/10.1038/nature02805**

Norwegian Polar Institute, 2022. Salinity in the core of the West-Spitsbergen current. Environmental monitoring of Svalbard and Jan Mayen (MOSJ). **https://mosj.no/en/climate/ocean/temperature-salinity-fram-strait.html**

Not, C., and Hillaire-Marcel, C., 2012. Enhanced sea-ice export from the Arctic during the Younger Dryas. Nature Communications, 3(1):647. **https://doi.org/10.1038/ncomms1658**

Nyman, K.H.M., and Ditlevsen, P.D., 2019. The middle Pleistocene transition by frequency locking and slow ramping of internal period. Climate Dynamics, 53(5):3023–3038. **https://doi.org/10.1007/s00382-019-04679-3**

O'Dea, A., Lessios, H.A., Coates, A.G., Eytan, R.I., Restrepo-Moreno, S.A., Cione, A.L., Collins, L.S., de Queiroz, A., Farris, D.W., Norris, R.D., Stallard, R.F., Woodburne, M.O., Aguilera, O., Aubry, M.-P., Berggren, W.A., Budd, A.F., Cozzuol, M.A., Coppard, S.E., Duque-Caro, H., Finnegan, S., Gasparini, G.M., Grossman, E.L., Johnson, K.G., Keigwin, L.D., Knowlton, N., Leigh, E.G., Leonard-Pingel, J.S., Marko, P.B., Pyenson, N.D., Rachello-Dolmen, P.G., Soibelzon, E., Soibelzon, L., Todd, J.A., Vermeij, G.J., and Jackson, J.B.C., 2016. Formation of the Isthmus of Panama. Science Advances, 2(8):e1600883. **https://doi.org/10.1126/sciadv.1600883**

Orsi, W.D., 2018. Ecology and evolution of seafloor and subseafloor microbial communities. Nature Reviews Microbiology, 16(11):671–683. **https://doi.org/10.1038/s41579-018-0046-8**

Orsi, W.D., Coolen, M.J.L., Wuchter, C., He, L., More, K.D., Irigoien, X., Chust, G., Johnson, C., Hemingway, J.D., Lee, M., Galy, V., and Giosan, L., 2017. Climate oscillations reflected within the microbiome of Arabian Sea sediments. Scientific Reports, 7(1):6040. **https://doi.org/10.1038/s41598-017-05590-9**

Overland, J.E., Wood, K.R., and Wang, M., 2011. Warm Arctic - cold continents: climate impacts of the newly open Arctic Sea. Polar Research. **https://doi.org/10.3402/polar.v30i0.15787**

Panieri, G., Knies, J., Vadakkepuliyambatta, S., Lee, A.L., and Schubert, C.J., 2023. Evidence of Arctic methane emissions across the mid-Pleistocene. Communications Earth & Environment, 4(1):109. **https://doi.org/10.1038/s43247-023-00772-y**

Pape, T., Bünz, S., Hong, W.-L., Torres, M.E., Riedel, M., Panieri, G., Lepland, A., Hsu, C.-W., Wintersteller, P., Wallmann, K., Schmidt, C., Yao, H., and Bohrmann, G., 2020. Origin and transformation of light hydrocarbons ascending at an active pockmark on Vestnesa Ridge, Arctic Ocean. Journal of Geophysical Research: Solid Earth, 125(1):e2018JB016679. **https://doi.org/10.1029/2018JB016679**

Patton, H., Alexandropoulou, N., Lasabuda, A.P.E., Knies, J., Andreassen, K., Winsborrow, M., Laberg, J.S., and Hubbard, A., 2024. Glacial erosion and Quaternary landscape development of the Eurasian Arctic. Earth-Science Reviews, 258:104936. **https://doi.org/10.1016/j.earscirev.2024.104936**

Patton, H., Hubbard, A., Heyman, J., Alexandropoulou, N., Lasabuda, A.P.E., Stroeven, A.P., Hall, A.M., Winsborrow, M., Sugden, D.E., Kleman, J., and Andreassen, K., 2022. The extreme yet transient nature of glacial erosion. Nature Communications, 13(1):7377. **https://doi.org/10.1038/s41467-022-35072-0**

Petit, J.R., Jouzel, J., Raynaud, D., Barkov, N.I., Barnola, J.M., Basile, I., Bender, M., Chappellaz, J., Davis, M., Delaygue, G., Delmotte, M., Kotlyakov, V.M., Legrand, M., Lipenkov, V.Y., Lorius, C., PÉpin, L., Ritz, C., Saltzman, E., and

Stievenard, M., 1999. Climate and atmospheric history of the past 420,000 years from the Vostok ice core, Antarctica. Nature, 399(6735):429–436. **https://doi.org/10.1038/20859**

Petrini, M., Colleoni, F., Kirchner, N., Hughes, A.L.C., Camerlenghi, A., Rebesco, M., Lucchi, R.G., Forte, E., Colucci, R.R., and Noormets, R., 2018. Interplay of grounding-line dynamics and sub-shelf melting during retreat of the Bjørnøyrenna Ice Stream. Scientific Reports, 8(1):7196. **https://doi.org/10.1038/s41598-018-25664-6**

Petrini, M., Colleoni, F., Kirchner, N., Hughes, A.L.C., Camerlenghi, A., Rebesco, M., Lucchi, R.G., Forte, E., Colucci, R.R., Noormets, R., and Mangerud, J., 2020. Simulated last deglaciation of the Barents Sea Ice Sheet primarily driven by oceanic conditions. Quaternary Science Reviews, 238:106314. **https://doi.org/10.1016/j.quascirev.2020.106314**

Pimmel, A., and Claypool, G., 2001. Technical Note 30: Introduction to shipboard organic geochemistry on the JOIDES Resolution. Ocean Drilling Program. **https://doi.org/10.2973/odp.tn.30.2001**

Pisias, N.G., and Moore, T.C., 1981. The evolution of Pleistocene climate: a time series approach. Earth and Planetary Science Letters, 52(2):450–458. **https://doi.org/10.1016/0012-821X(81)90197-7**

Plaza-Faverola, A., Sultan, N., Lucchi, R.G., El bani Altuna, N., Ramachandran, H., Singhroha, S., Cooke, F., Vadakkepuliyambatta, S., Ezat, M.M., and Rasmussen, T.L., 2023. Spatial changes in gas transport and sediment stiffness influenced by regional stress: observations from piezometer data along Vestnesa Ridge, eastern Fram Strait. Journal of Geophysical Research: Solid Earth, 128(5):e2022JB025868. **https://doi.org/10.1029/2022JB025868**

Plaza-Faverola, A., Bünz, S., Johnson, J.E., Chand, S., Knies, J., Mienert, J., and Franek, P., 2015. Role of tectonic stress in seepage evolution along the gas hydrate-charged Vestnesa Ridge, Fram Strait. Geophysical Research Letters, 42(3):733–742. **https://doi.org/10.1002/2014GL062474**

Poirier, A., and Hillaire-Marcel, C., 2011. Improved Os-isotope stratigraphy of the Arctic Ocean. Geophysical Research Letters, 38(14):L14607. **https://doi.org/10.1029/2011GL047953**

Quadfasel, D., Rudels, B., and Kurz, K., 1988. Outflow of dense water from a Svalbard fjord into the Fram Strait. Deep Sea Research, Part A. Oceanographic Research Papers, 35(7):1143–1150. **https://doi.org/10.1016/0198-0149(88)90006-4**

Quadfasel, D., Rudels, B., and Selchow, S., 1992. The Central Bank vortex in the Barents Sea: water mass transformation and circulation. ICES Marine Science Symposia, 195:40–51. **https://doi.org/10.17895/ices.pub.19270622**

Rae, J.W.B., Zhang, Y.G., Liu, X., Foster, G.L., Stoll, H.M., and Whiteford, R.D.M., 2021. Atmospheric CO_2 over the past 66 million years from marine archives. Annual Review of Earth and Planetary Sciences, 49(Volume 49, 2021):609–641. **https://doi.org/10.1146/annurev-earth-082420-063026**

Rahmstorf, S., Box, J.E., Feulner, G., Mann, M.E., Robinson, A., Rutherford, S., and Schaffernicht, E.J., 2015. Exceptional twentieth-century slowdown in Atlantic Ocean overturning circulation. Nature Climate Change, 5(5):475–480. **https://doi.org/10.1038/nclimate2554**

Rantanen, M., Karpechko, A.Y., Lipponen, A., Nordling, K., Hyvärinen, O., Ruosteenoja, K., Vihma, T., and Laaksonen, A., 2022. The Arctic has warmed nearly four times faster than the globe since 1979. Communications Earth & Environment, 3(1):168. **https://doi.org/10.1038/s43247-022-00498-3**

Rasmussen, T.L., and Nielsen, T., 2024. Glacial-interglacial sedimentation control on gas seepage exemplified by Vestnesa Ridge off NW Svalbard margin. Frontiers in Earth Science, 12:1356341. **https://doi.org/10.3389/feart.2024.1356341**

Rasmussen, T.L., Thomsen, E., Ślubowska, M.A., Jessen, S., Solheim, A., and Koç, N., 2007. Paleoceanographic evolution of the SW Svalbard margin (76°N) since 20,000 14C yr BP. Quaternary Research, 67(1):100–114. **https://doi.org/10.1016/j.yqres.2006.07.002**

Raymo, M.E., Jansen, E., Blum, P., and Herbert, T.D. (Eds.), 1999. Proceedings of the Ocean Drilling Program, Scientific Results, 162: College Station, TX (Ocean Drilling Program). **https://doi.org/10.2973/odp.proc.sr.162.1999**

Raymo, M.E., and Nisancioglu, K.H., 2003. The 41 kyr world: Milankovitch's other unsolved mystery. Paleoceanography, 18(1):1011. **https://doi.org/10.1029/2002PA000791**

Razmjooei, M.J., Henderiks, J., Coxall, H.K., Baumann, K.-H., Vermassen, F., Jakobsson, M., Niessen, F., and O'Regan, M., 2023. Revision of the Quaternary calcareous nannofossil biochronology of Arctic Ocean sediments. Quaternary Science Reviews, 321:108382. **https://doi.org/10.1016/j.quascirev.2023.108382**

Rebesco, M., Hernández-Molina, F.J., Van Rooij, D., and Wåhlin, A., 2014a. Contourites and associated sediments controlled by deep-water circulation processes: state-of-the-art and future considerations. Marine Geology, 352:111–154. **https://doi.org/10.1016/j.margeo.2014.03.011**

Rebesco, M., Laberg, J.S., Pedrosa, M.T., Camerlenghi, A., Lucchi, R.G., Zgur, F., and Wardell, N., 2014b. Onset and growth of Trough-Mouth Fans on the North-Western Barents Sea margin – implications for the evolution of the Barents Sea/Svalbard Ice Sheet. Quaternary Science Reviews, 92:227–234. **https://doi.org/10.1016/j.quascirev.2013.08.015**

Rebesco, M., Wåhlin, A., Laberg, J.S., Schauer, U., Beszczynska-Möller, A., Lucchi, R.G., Noormets, R., Accettella, D., Zarayskaya, Y., and Diviacco, P., 2013. Quaternary contourite drifts of the Western Spitsbergen margin. Deep Sea Research, Part I: Oceanographic Research Papers, 79:156–168. **https://doi.org/10.1016/j.dsr.2013.05.013**

Rial, J.A., Oh, J., and Reischmann, E., 2013. Synchronization of the climate system to eccentricity forcing and the 100,000-year problem. Nature Geoscience, 6(4):289–293. **https://doi.org/10.1038/ngeo1756**

Rørvik, K.L., Laberg, J.S., Hald, M., Ravna, E.K., and Vorren, T.O., 2010. Behavior of the northwestern part of the Fennoscandian Ice Sheet during the Last Glacial Maximum – a response to external forcing. Quaternary Science Reviews, 29(17):2224–2237. **https://doi.org/10.1016/j.quascirev.2010.05.022**

Røy, H., Kallmeyer, J., Adhikari, R.R., Pockalny, R., Jørgensen, B.B., and D'Hondt, S., 2012. Aerobic microbial respiration in 86-million-year-old deep-sea red clay. Science, 336(6083):922–925. **https://doi.org/10.1126/science.1219424**

Rubino, M., Etheridge, D.M., Trudinger, C.M., Allison, C.E., Battle, M.O., Langenfelds, R.L., Steele, L.P., Curran, M., Bender, M., White, J.W.C., Jenk, T.M., Blunier, T., and Francey, R.J., 2013. A revised 1000year atmospheric $\delta^{13}C$-CO_2 record from Law Dome and South Pole, Antarctica. Journal of Geophysical Research: Atmospheres, 118(15):8482–8499. **https://doi.org/10.1002/jgrd.50668**

Rudels, B., Meyer, R., Fahrbach, E., Ivanov, V.V., Østerhus, S., Quadfasel, D., Schauer, U., Tverberg, V., and Woodgate, R.A., 2000. Water mass distribution in Fram Strait and over the Yermak Plateau in summer 1997. Annales Geophysicae, 18(6):687–705. **https://doi.org/10.1007/s00585-000-0687-5**

Saloranta, T.M., and Haugan, P.M., 2004. Northward cooling and freshening of the warm core of the West Spitsbergen Current. Polar Research, 23(1):79–88. **https://doi.org/10.3402/polar.v23i1.6268**

Schauer, U., 1995. The release of brine-enriched shelf water from Storfjord into the Norwegian Sea. Journal of Geophysical Research: Oceans, 100(C8):16015–16028. **https://doi.org/10.1029/95JC01184**

Schauer, U., Fahrbach, E., Osterhus, S., and Rohardt, G., 2004. Arctic warming through the Fram Strait: Oceanic heat transport from 3 years of measurements. Journal of Geophysical Research: Oceans, 109(C6):C06026. **https://doi.org/10.1029/2003JC001823**

Schmidt, D., 2007. The closure history of the Panama Isthmus: evidence from isotopes and fossils to models and molecules. In Williams, M., Haywood, A.M., Gregory, F.J., and Schmidt, D.N. (Eds.) Deep-Time Perspectives on Climate Change: Marrying the Signal from Computer Models and Biological Proxies. Special Publication - Geological Society of London: 429–444. **https://doi.org/10.1144/TMS002.19**

Schneider, A., Panieri, G., Lepland, A., Consolaro, C., Crémière, A., Forwick, M., Johnson, J.E., Plaza-Faverola, A., Sauer, S., and Knies, J., 2018. Methane seepage at Vestnesa Ridge (NW Svalbard) since the Last Glacial Maximum. Quaternary Science Reviews, 193:98–117. **https://doi.org/10.1016/j.quascirev.2018.06.006**

Schneider, R., Schmitt, J., Köhler, P., Joos, F., and Fischer, H., 2013. A reconstruction of atmospheric carbon dioxide and its stable carbon isotopic composition from the penultimate glacial maximum to the last glacial inception. Clim. Past, 9(6):2507–2523. **https://doi.org/10.5194/cp-9-2507-2013**

Sejrup, H.P., Hjelstuen, B.O., Patton, H., Esteves, M., Winsborrow, M., Rasmussen, T.L., Andreassen, K., and Hubbard, A., 2022. The role of ocean and atmospheric dynamics in the marine-based collapse of the last Eurasian Ice Sheet. Communications Earth & Environment, 3(1):119. **https://doi.org/10.1038/s43247-022-00447-0**

Seki, O., Foster, G.L., Schmidt, D.N., Mackensen, A., Kawamura, K., and Pancost, R.D., 2010. Alkenone and boron-based Pliocene pCO_2 records. Earth and Planetary Science Letters, 292(1–2):201–211. **https://doi.org/10.1016/j.epsl.2010.01.037**

Shackleton, C.S., Winsborrow, M.C.M., Andreassen, K., Lucchi, R.G., and Bjarnadóttir, L.R., 2020. Ice-margin retreat and grounding-zone dynamics during initial deglaciation of the Storfjordrenna Ice Stream, western Barents Sea. Boreas, 49(1):38–51. **https://doi.org/10.1111/bor.12420**

Shackleton, N.J., 2000. The 100,000-year ice-age cycle identified and found to lag temperature, carbon dioxide, and orbital eccentricity. Science, 289(5486):1897–1902. **https://doi.org/10.1126/science.289.5486.1897**

Siegenthaler, U., Stocker, T.F., Monnin, E., Lüthi, D., Schwander, J., Stauffer, B., Raynaud, D., Barnola, J.-M., Fischer, H., Masson-Delmotte, V., and Jouzel, J., 2005. Stable carbon cycle climate relationship during the Late Pleistocene. Science, 310(5752):1313–1317. **https://doi.org/10.1126/science.1120130**

Skogseth, R., Haugan, P.M., and Jakobsson, M., 2005. Watermass transformations in Storfjorden. Continental Shelf Research, 25(5–6):667–695. **https://doi.org/10.1016/j.csr.2004.10.005**

Smith, A.J., Mienert, J., Bünz, S., and Greinert, J., 2014. Thermogenic methane injection via bubble transport into the upper Arctic Ocean from the hydrate-charged Vestnesa Ridge, Svalbard. Geochemistry, Geophysics, Geosystems, 15(5):1945–1959. **https://doi.org/10.1002/2013GC005179**

Solheim, A., Andersen, E.S., Elverhøi, A., and Fiedler, A., 1996. Late Cenozoic depositional history of the western Svalbard continental shelf, controlled by subsidence and climate. Global and Planetary Change, 12(1–4):135–148. **https://doi.org/10.1016/0921-8181(95)00016-X**

Sosdian, S.M., Greenop, R., Hain, M.P., Foster, G.L., Pearson, P.N., and Lear, C.H., 2018. Constraining the evolution of Neogene ocean carbonate chemistry using the boron isotope pH proxy. Earth and Planetary Science Letters, 498:362–376. **https://doi.org/10.1016/j.epsl.2018.06.017**

St. John, K., 2008. Cenozoic ice-rafting history of the central Arctic Ocean: terrigenous sands on the Lomonosov Ridge. Paleoceanography and Paleoclimatology, 23(1):PA1S05. **https://doi.org/10.1029/2007PA001483**

St. John, K.E.K., and Krissek, L.A., 2002. The Late Miocene to Pleistocene ice-rafting history of southeast Greenland. Boreas, 31(1):28–35. **https://doi.org/10.1111/j.1502-3885.2002.tb01053.x**

St. John, K.E.K., Lucchi, R.G., Ronge, T.A., Barcena, M.A., De Schepper, S., Duxbury, L.C., Gebhardt, A.C., Gonzalez-Lanchas, A., Goss, G., Greco, N.M., Gruetzner, J., Haygood, L., Husum, K., Iizuka, M., Kapuge, A.K.I.U., Lam, A.R., Libman-Roshal, O., Liu, Y., Monito, L.R., Reilly, B.T., Rosenthal, Y., Sakai, Y., Sijinkumar, A.V., Suganuma, Y., and Zhong, Y., 2026a. Site U1619. In Lucchi, R.G., St. John, K.E.K., Ronge, T.A., and the Expedition 403 Scientists, Eastern Fram Strait Paleo-Archive. Proceedings of the International Ocean Discovery Program, 403: College Station, TX (International Ocean Discovery Program). **https://doi.org/10.14379/iodp.proc.403.104.2026**

St. John, K.E.K., Lucchi, R.G., Ronge, T.A., Barcena, M.A., De Schepper, S., Duxbury, L.C., Gebhardt, A.C., Gonzalez-Lanchas, A., Goss, G., Greco, N.M., Gruetzner, J., Haygood, L., Husum, K., Iizuka, M., Kapuge, A.K.I.U., Lam, A.R., Libman-Roshal, O., Liu, Y., Monito, L.R., Reilly, B.T., Rosenthal, Y., Sakai, Y., Sijinkumar, A.V., Suganuma, Y., and Zhong, Y., 2026b. Site U1620. In Lucchi, R.G., St. John, K.E.K., Ronge, T.A., and the Expedition 403 Scientists, Eastern Fram Strait Paleo-Archive. Proceedings of the International Ocean Discovery Program, 403: College Station, TX (International Ocean Discovery Program). **https://doi.org/10.14379/iodp.proc.403.105.2026**

Stärz, M., Jokat, W., Knorr, G., and Lohmann, G., 2017. Threshold in North Atlantic-Arctic Ocean circulation controlled by the subsidence of the Greenland-Scotland Ridge. Nature Communications, 8(1):15681. **https://doi.org/10.1038/ncomms15681**

Stein, R., and Fahl, K., 2013. Biomarker proxy shows potential for studying the entire Quaternary Arctic sea ice history. Organic Geochemistry, 55:98–102. **https://doi.org/10.1016/j.orggeochem.2012.11.005**

Stein, R., Fahl, K., Schreck, M., Knorr, G., Niessen, F., Forwick, M., Gebhardt, C., Jensen, L., Kaminski, M., Kopf, A., Matthiessen, J., Jokat, W., and Lohmann, G., 2016. Evidence for ice-free summers in the late Miocene central Arctic Ocean. Nature Communications, 7(1):11148. **https://doi.org/10.1038/ncomms11148**

Stevenson, R., Poirier, A., Véron, A., Carignan, J., and Hillaire-Marcel, C., 2015. Late Eocene to present isotopic (Sr-Nd-Pb) and geochemical evolution of sediments from the Lomonosov Ridge, Arctic Ocean: implications for continental sources and linkage with the North Atlantic Ocean. Comptes Rendus Geoscience, 347(5–6):227–135. **https://doi.org/10.1016/j.crte.2015.02.008**

Stocker, T.F., and Johnsen, S.J., 2003. A minimum thermodynamic model for the bipolar seesaw. Paleoceanography and Paleoclimatology, 18(4):1087. **https://doi.org/10.1029/2003PA000920**

Stocker, T.F., Qin, D., Plattner, G.-K., Tignor, M., Allen, S.K., Boschung, J., Nauels, A., Xia, Y., Bex, V., and Midgley, P.M. (Eds.), 2013. Climate Change 2013: The Physical Science Basis. Contribution of Working Group I to the Fifth Assessment Report of the Intergovernmental Panel on Climate Change.: New York (Cambridge University Press). **https://doi.org/10.1017/CBO9781107415324**

Stow, D.A.V., Kahler, G., and Reeder, M., 2002. Fossil contourites: type example from an Oligocene palaeoslope system, Cyprus. In Stow, D.A.V., Pudsey, C.J., Howe, J.A., Faugères, J.-C., and Viana, A.R. (Eds.), Deep-Water Contourite Systems: Modern Drifts and Ancient Series, Seismic and Sedimentary Characteristics. Geological Society, London, Memoirs, 22: 443–455. **https://doi.org/10.1144/GSL.MEM.2002.022.01.31**

Sultan, N., Plaza-Faverola, A., Vadakkepuliyambatta, S., Buenz, S., and Knies, J., 2020. Impact of tides and sea-level on deep-sea Arctic methane emissions. Nature Communications, 11(1):5087. **https://doi.org/10.1038/s41467-020-18899-3**

Swift, J.H., and Koltermann, K.P., 1988. The origin of Norwegian Sea Deep Water. Journal of Geophysical Research: Oceans, 93(C4):3563–3569. **https://doi.org/10.1029/JC093iC04p03563**

Sztybor, K., and Rasmussen, T., 2017a. Diagenetic disturbances of marine sedimentary records from methane-influenced environments in the Fram Strait as indications of variation in seep intensity during the last 35 000 years. Boreas, 46(2):212–228. **https://doi.org/10.1111/bor.12202**

Sztybor, K., and Rasmussen, T., 2017b. Late glacial and deglacial palaeoceanographic changes at Vestnesa Ridge, Fram Strait: methane seep versus non-seep environments. Palaeogeography, Palaeoclimatology, Palaeoecology, 476:77–89. **https://doi.org/10.1016/j.palaeo.2017.04.001**

Tan, N., Ramstein, G., Dumas, C., Contoux, C., Ladant, J.-B., Sepulchre, P., Zhang, Z., and De Schepper, S., 2017. Exploring the MIS M2 glaciation occurring during a warm and high atmospheric CO_2 Pliocene background climate. Earth and Planetary Science Letters, 472:266–276. **https://doi.org/10.1016/j.epsl.2017.04.050**

Tanner, T., Hernández-Almeida, I., Drury, A.J., Guitián, J., and Stoll, H., 2020. Decreasing atmospheric CO_2 during the Late Miocene cooling. Paleoceanography and Paleoclimatology, 35(12):e2020PA003925. **https://doi.org/10.1029/2020PA003925**

Teigen, S.H., Nilsen, F., and Gjevik, B., 2010. Barotropic instability in the West Spitsbergen Current. Journal of Geophysical Research: Oceans, 115(C7). **https://doi.org/10.1029/2009JC005996**

Tesi, T., Muschitiello, F., Mollenhauer, G., Miserocchi, S., Langone, L., Ceccarelli, C., Panieri, G., Chiggiato, J., Nogarotto, A., Hefter, J., Ingrosso, G., Giglio, F., Giordano, P., and Capotondi, L., 2021. Rapid Atlantification along the Fram Strait at the beginning of the 20th century. Science Advances, 7(48):eabj2946. **https://doi.org/10.1126/sciadv.abj2946**

The Cenozoic CO_2 Proxy Integration Project (CenCO2PIP) Consortium, 2023. Toward a Cenozoic history of atmospheric CO_2. Science, 382(6675):eadi5177. **https://doi.org/10.1126/science.adi5177**

Thiede, J., and Myhre, A.M., 1996. The paleoceanographic history of the North Atlantic-Arctic gateways: synthesis of the Leg 151 drilling results. In Thiede, J., Myhre, A.M., Firth, J.V., Johnson, G.L., and Ruddiman, W.F. (Eds.), Proceedings of the Ocean Drilling Program, Scientific Results. 151: College Station, TX (Ocean Drilling Program), 645–658. **https://doi.org/10.2973/odp.proc.sr.151.147.1996**

Thompson, B., Jakobsson, M., Nilsson, J., Nycander, J., and Döös, K., 2012. A model study of the first ventilated regime of the Arctic Ocean during the early Miocene. Polar Research, 31(4):267–273. **https://doi.org/10.3402/polar.v31i0.10859**

Tian, J., Ma, X., Zhou, J., Jiang, X., Lyle, M., Shackford, J., and Wilkens, R., 2018. Paleoceanography of the east equatorial Pacific over the past 16 Myr and Pacific–Atlantic comparison: High resolution benthic foraminiferal $\delta^{18}O$ and $\delta^{13}C$ records at IODP Site U1337. Earth and Planetary Science Letters, 499:185–196. **https://doi.org/10.1016/j.epsl.2018.07.025**

Torricella, F., Gamboa Sojo, V.M., Gariboldi, K., Douss, N., Musco, M.E., Caricchi, C., Lucchi, R.G., Carbonara, K., and Morigi, C., 2022. Multiproxy investigation of the last 2,000 years BP marine paleoenvironmental record along the western Spitsbergen margin. Arctic, Antarctic, and Alpine Research, 54(1):562–583. **https://doi.org/10.1080/15230430.2022.2123859**

Torricella, F., Morigi, C., Gamboa-Sojo, V., Carbonara, K., Bronzo, L., and Lucchi, R.G., 2025. Paleoceanographic changes along the western Spitsbergen margin, evidence from planktic microfossil during the last 10 kyr BP. Palaeogeography, Palaeoclimatology, Palaeoecology, 670:112940. **https://doi.org/10.1016/j.palaeo.2025.112940**

Tripati, A., and Darby, D., 2018. Evidence for ephemeral middle Eocene to early Oligocene Greenland glacial ice and pan-Arctic sea ice. Nature Communications, 9(1):1038. **https://doi.org/10.1038/s41467-018-03180-5**

Tsubouchi, T., Bacon, S., Aksenov, Y., Naveira Garabato, A.C., Beszczynska-Möller, A., Hansen, E., de Steur, L., Curry, B., and Lee, C.M., 2018. The Arctic Ocean seasonal cycles of heat and freshwater fluxes: observation-based inverse estimates. Journal of Physical Oceanography, 48(9):2029–2055. **https://doi.org/10.1175/JPO-D-17-0239.1**

Turney, C.S.M., Fogwill, C.J., Golledge, N.R., McKay, N.P., van Sebille, E., Jones, R.T., Etheridge, D., Rubino, M., Thornton, D.P., Davies, S.M., Ramsey, C.B., Thomas, Z.A., Bird, M.I., Munksgaard, N.C., Kohno, M., Woodward, J., Winter, K., Weyrich, L.S., Rootes, C.M., Millman, H., Albert, P.G., Rivera, A., van Ommen, T., Curran, M., Moy, A., Rahmstorf, S., Kawamura, K., Hillenbrand, C.-D., Weber, M.E., Manning, C.J., Young, J., and Cooper, A., 2020. Early Last Interglacial ocean warming drove substantial ice mass loss from Antarctica. Proceedings of the National Academy of Sciences of the United States of America, 117(8):3996–4006. **https://doi.org/10.1073/pnas.1902469117**

Tzedakis, P.C., Raynaud, D., McManus, J.F., Berger, A., Brovkin, V., and Kiefer, T., 2009. Interglacial diversity. Nature Geoscience, 2(11):751–755. **https://doi.org/10.1038/ngeo660**

Vanneste, M., Berndt, C., Sverre Laberg, J., and Mienert, J., 2007. On the origin of large shelf embayments on glaciated margins—effects of lateral ice flux variations and glacio-dynamics west of Svalbard. Quaternary Science Reviews, 26(19):2406–2419. **https://doi.org/10.1016/j.quascirev.2007.05.005**

von Appen, W.-J., Schauer, U., Hattermann, T., and Beszczynska-Möller, A., 2016. Seasonal cycle of mesoscale instability of the West Spitsbergen Current. Journal of Physical Oceanography, 46(4):1231–1254. **https://doi.org/10.1175/JPO-D-15-0184.1**

Vorren, T.O., and Laberg, J.S., 1997. Trough mouth fans — palaeoclimate and ice-sheet monitors. Quaternary Science Reviews, 16(8):865–881. **https://doi.org/10.1016/S0277-3791(97)00003-6**

Waghorn, K.A., Bünz, S., Plaza-Faverola, A., and Johnson, J.E., 2018. 3-D seismic investigation of a gas hydrate and fluid flow system on an active mid-ocean ridge; Svyatogor Ridge, Fram Strait. Geochemistry, Geophysics, Geosystems, 19(8):2325–2341. **https://doi.org/10.1029/2018GC007482**

Waghorn, K.A., Vadakkepuliyambatta, S., Plaza-Faverola, A., Johnson, J.E., Bünz, S., and Waage, M., 2020. Crustal processes sustain Arctic abiotic gas hydrate and fluid flow systems. Scientific Reports, 10(1):10679. **https://doi.org/10.1038/s41598-020-67426-3**

Weijer, W., Haine, W.N., Siddiqui, A.H., Cheng, W., Veneziani, M., and Kurtakoti, P., 2022. Interactions between the Arctic Mediterranean and the Atlantic Meridional Overturning Circulation: a review. Oceanography, 35(3–4):118–127. **https://doi.org/10.5670/oceanog.2022.130**

Westerhold, T., Marwan, N., Drury, A.J., Liebrand, D., Agnini, C., Anagnostou, E., Barnet, J.S.K., Bohaty, S.M., De Vleeschouwer, D., Florindo, F., Frederichs, T., Hodell, D.A., Holbourn, A.E., Kroon, D., Lauretano, V., Littler, K., Lourens, L.J., Lyle, M., Pälike, H., Röhl, U., Tian, J., Wilkens, R.H., Wilson, P.A., and Zachos, J.C., 2020. An astronomically dated record of Earth's climate and its predictability over the last 66 million years. Science, 369(6509):1383–1387. **https://doi.org/10.1126/science.aba6853**

Wilkens, R.H., Westerhold, T., Drury, A.J., Lyle, M., Gorgas, T., and Tian, J., 2017. Revisiting the Ceara Rise, equatorial Atlantic Ocean: isotope stratigraphy of ODP Leg 154 from 0 to 5 Ma. Climate of the Past, 13(7):779–793. **https://doi.org/10.5194/cp-13-779-2017**

Wolf, T.C.W., and Thiede, J., 1991. History of terrigenous sedimentation during the past 10 m.y. in the North Atlantic (ODP Legs 104 and 105 and DSDP Leg 81). Marine Geology, 101(1–4):83–102. **https://doi.org/10.1016/0025-3227(91)90064-B**

Wolf-Welling, T.C.W., Thiede, J., Myhre, A.M., and Leg 151 Shipboard Scientific Party, 1995. Bulk sediment parameter and coarse fraction analysis: paleoceanographic implications of Fram Strait Sites 908 and 909, ODP Leg 151 (NAAG). Eos, Transactions of the American Geophysical Union, 76:166.

Wright, J.D., 1998. The role of the Greenland-Scotland ridge in Neogene climate changes. Oxford Monographs on Geology and Geophysics, 39:192–211. **https://doi.org/10.1093/oso/9780195112450.003.0009**

Zachos, J.C., Dickens, G.R., and Zeebe, R.E., 2008. An early Cenozoic perspective on greenhouse warming and carbon-cycle dynamics. Nature, 451(7176):279–283. **https://doi.org/10.1038/nature06588**

Zhang, Y.G., Henderiks, J., and Liu, X., 2020. Refining the alkenone-pCO_2 method II: towards resolving the physiological parameter 'b'. Geochimica et Cosmochimica Acta, 281:118–134. **https://doi.org/10.1016/j.gca.2020.05.002**

Zhang, Y.G., Pagani, M., Henderiks, J., and Ren, H., 2017. A long history of equatorial deep-water upwelling in the Pacific Ocean. Earth and Planetary Science Letters, 467:1–9. **https://doi.org/10.1016/j.epsl.2017.03.016**

Zhang, Y.G., Pearson, A., Benthien, A., Dong, L., Huybers, P., Liu, X., and Pagani, M., 2019. Refining the alkenone-pCO_2 method I: lessons from the Quaternary glacial cycles. Geochimica et Cosmochimica Acta, 260:177–191. **https://doi.org/10.1016/j.gca.2019.06.032**

Zhang, Z.S., Nisancioglu, K.H., Chandler, M.A., Haywood, A.M., Otto-Bliesner, B.L., Ramstein, G., Stepanek, C., Abe-Ouchi, A., Chan, W.L., Bragg, F.J., Contoux, C., Dolan, A.M., Hill, D.J., Jost, A., Kamae, Y., Lohmann, G., Lunt, D.J., Rosenbloom, N.A., Sohl, L.E., and Ueda, H., 2013. Mid-pliocene Atlantic meridional overturning circulation not unlike modern. Climate of the Past, 9(4):1495–1504. **https://doi.org/10.5194/cp-9-1495-2013**

Zhao, R., Hannisdal, B., Mogollon, J.M., and Jørgensen, S.L., 2019. Nitrifier abundance and diversity peak at deep redox transition zones. Scientific Reports, 9(1):8633. **https://doi.org/10.1038/s41598-019-44585-6**

Zieba, K.J., Omosanya, K.d.O., and Knies, J., 2017. A flexural isostasy model for the Pleistocene evolution of the Barents Sea bathymetry. Norwegian Journal of Geology, 97(1):1–19. **https://doi.org/10.17850/njg97-1-01**